الجمهوريــة الجزائريــة الديمقراطيــة الشعبيــة

People's Democratic Republic of Algeria

وزارة التعليم العالي و البحث العلمي

Ministry of Higher Education and Scientific Research

20 août 1955- University Skikda

Faculty of Science

Department of Physics

جامعة 20 اوت 1955 سكيكدة

كلية العلوم

قسم الفيزياء

THESIS

Submitted to obtain the degree of DOCTORAT

In Energy Physics and Renewable Energies

Presented by:

Maissa Bouselsal

Theme:

Thermo-Convective Study of a Hybrid Nanofluid with Entropy Generation

Supported by: 16/ 09 /2025 before a jury composed of:

Chairman:	Mr. D. Omeiri	Professor	20 août 1955- University Skikda
Reporter:	Mr. F. Mebarek-Oudina	Professor	20 août 1955- University Skikda
Examiner:	Mr. M. Kadja	Professor	Mentouri university - constantine
	Mr. Y. Kabar	Professor	National polytechnic school-constantine
	Mr. S. Benissad	Professor	Mentouri university - constantine

University year : 2024/2025

الجمهوريــة الجزائريــة الديمقراطيــة الشعبيــة

People's Democratic Republic of Algeria

وزارة التعليم العالي و البحث العلمي

Ministry of Higher Education and Scientific Research

جامعة 20 اوت 1955 سكيكدة
جامعة 02 اوت 1955 سكيكدة كلية
كلية العلوم
العلوم
قسم الفيزياء
قسم الفيزياء

20 août 1955- University
Skikda
Faculty of Science
Department of Physics

THESIS
Submitted to obtain the degree of DOCTORAT

In Energy Physics and Renewable Energies

Presented by:

Maissa Bouselsal

Email: maissabou8@gmail.com

m.bouselsal@univ-skikda.dz

Theme:

Thermo-Convective Study of a Hybrid Nanofluid with Entropy Generation

Abstract

In this paper, forced convection and entropy generation in a shell/tube heat exchanger are studied numerically. We ran the computations for various hybrid nanofluids. The finite element method has been used to solve the equations governing the flow and heat transfer. To compute the flow and temperature fields, the Nusselt number, and the entropy production, a COMSOL Multiphysics algorithm has been built. In-depth research is done on the effects of Rayleigh and Reynolds numbers, the nanofluid type and volume percentage, the various tube radius effects, the average Nusselt number, and entropy generation. The findings demonstrate that the application of nanofluids enhances heat transmission while lowering entropy production. Lastly, a numerical analysis in three dimensions of laminar forced convection in a shell/tube heat exchanger containing various nanofluids is showcased.

Keywords: Forced convection, Shell/tube heat exchanger, Entropy generation, Nanofluid.

Résumé

Le but de cette étude est d'analyser numériquement la convection forcée et la production d'entropie dans un échangeur de chaleur à calandre/tube. Les calculs ont été effectués pour différents nanofluides hybrides. On a résolu les équations de l'écoulement et du transfert de chaleur en utilisant la méthode des éléments finis. Un code commercial dans COMSOL Multiphysics a été utilisé pour calculer les champs d'écoulement et de température, le nombre de Nusselt et la production d'entropie. Les effets des nombres de Rayleigh et de Reynolds, de la fraction volumique du nanofluide, du type de nanofluide, des différents effets de rayon du tube, du nombre de Nusselt moyen, et de la production d'entropie sont étudiés en détail. Les résultats montrent que l'utilisation de nanofluides améliore le transfert de chaleur et réduit la production d'entropie. Enfin, L'analyse numérique de la convection forcée laminaire dans une étude tridimensionnelle un échangeur de chaleur tube / calandre rempli de différents nanofluides est présenté.

Mots-clés : Convection forcée, échangeur de chaleur tube / calandre, Génération d'entropie, Nanofluide.

ملخص

الهدف من هذا العمل هو الدراسة العددية للحمل الحراري القسري وتوليد الانتروبيا في المبادل الحراري الصدفي/ الأنبوبي. تم إجراء الحسابات لسوائل نانوية هجينة مختلفة. تم حل المعادلات التي تحكم التدفق وانتقال الحرارة باستخدام طريقة العناصر المحدودة. تم تطوير كود في كومسول ميلتي فيزيك لحساب مجالات التدفق ودرجة الحرارة، وعدد نوسيلت، وتوليد الإنتروبي. تمت دراسة تأثيرات أعداد رايلي ورينولدز، والجزء الحجمي للسائل النانوي، ونوع السائل النانوي، وتأثير نصف قطر الأنبوب المنتشر، ومتوسط عدد نوسيلت، وتوليد الإنتروبيا بالتفصيل. تُظهر النتائج أن استخدام الموائع النانوية يحسّن من انتقال الحرارة ويقلل من توليد الإنتروبيا. أخيرًا، تم تقديم دراسة عددية ثلاثية الأبعاد للحمل الحراري القسري الصفحي في مبادل حراري غلاف/أنبوب مملوء بسوائل نانوية مختلفة.

كلمات البحث : الحمل الحراري القسري، مبادل حراري صدفي وأنبوبي، توليد الإنتروبي، مائع نانوي

Acknowledgements

First of all, I thank our God for giving me the courage, strength, and patience to carry out this modest work.

My sincere thanks and gratitude go firstly to my supervisor, **Mr. Mebarek-Oudina Fateh**, professor at the University of Skikda, for having followed and directed me during the completion of this thesis. I would like to thank him warmly for his help and availability.

I would like to thank Mr D. Omeiri, Professor at the University of Skikda, for agreeing to chair the defense jury. I also thank Mr. M. Kadja professor at the University of Constantine, Mr Y. Kabar professor at the national polytechnic school constantine, Mr S. Benissad professor at the University of Constantine for having accepted to evaluate my modest work.

My deepest thanks go to my parents and all my family.

Finally, I would like to thank all those who helped and supported me during the completion of this work.

Dedication

Finally, I take my hat off to the years of study that have passed.

First of all, praise be to God Almighty. I dedicate my graduation and the fruits of my success to my parents ... and to my brothers and sisters who were my support and consolation.

Maissa

Contents

CHAPTER II: BIBLIOGRAPHIC SYNTHESIS

CHAPTER III: MATHEMATICAL MODEL AND NUMERICAL PROCEDURE

CHAPTER Ⅳ:RESULTS AND DISCUSSION

Nomenclature

List of symbols

g	Acceleration due to gravitational ($m \cdot s^{-2}$)
x,y	Cartesian coordinates (m)
u,v	Components of velocity (ms^{-1})
Q	Contains heat sources other than viscous dissipation (W/m^3)
ε	Efficiency
H	Heat exchanger height (m)
q	Heat flux by conduction (W/m^2)
q_r	Heat flux by radiation (W/m^2)
$\dot{q}$	Heat generation per unit volume (volumetric heat density)
C_{min}	Minimum heat capacity rate
Nu	Nusselt number (average)
U	Overall heat transfer coefficient, W/m^2K
Pr	Prandtl number
p	Pressure (Pa)
Ra	Rayleigh number
Re	Reynolds number
Ri	Richardson number

C_p	Specific heatc apacity at Constant pressure (J/(kg·K))
T	Temperature (K)
k	Thermal conductivity ($W.m^{-1}.K^{-1}$)
t	Time (s)
A	Total heat transfer surface area of heat exchanger
R	Tube radius
N	Undulation number

Greeksymbols

β	Coefficient of thermal expansion (K^{-1})
∇	Del operator
ψ	Dimensionless stream function
μ	Dynamic viscosity ($Kg\ m^{-1}\cdot s^{-1}$)
σ	Electrical conductivity ($s.m^{-1}$)
ρ	Fluid density ($kg\ m^{-3}$)
φ	Hybrid nanoparticles volume fraction (%)
I	Identity matrix
ν	Kinematic viscosity ($m^2\cdot s^{-1}$)
α	Thermal diffusivity ($m^2\cdot s^{-1}$)
τ	Viscous stress tensor (Pa)

Subscript

avg	Average
c	Cold
f	Fluid (base fluid)
h	Hot
hnf	Hybrid nanofluid
nf	Nanofluid
np	Nanoparticles

List of Figures

List of Tables

GENERAL INTRODUCTION

GENERAL INTRODUCTION

These days, solar energy is the energy of the future and the only way for the underprivileged to substitute petroleum-based goods. Heat exchangers find widespread use in several applications, including solar thermal energy storage systems, water heating systems, solar collectors, and other small heat exchanger uses. Materials like aluminum, iron, copper, steel, bronze, ceramic and glass PTFE, and graphite, as well as non-metallic materials, are related to heat exchanger efficiency. The coefficient of heat transfer varies among different materials. when a result, when the heat transfer coefficient rises, so does the heat exchange capacity.

This is accomplished by modifying the geometric shape of the heat exchangers. With rising demand, the value of heat exchangers varies from field to field; their use is intended to lower costs and save energy. The heat exchanger is consequently a crucial component of all energy management plans, which in turn protects the environment. A heat exchanger is a crucial tool for thermal engineers and is necessary for energy management since a significant portion of the energy utilized in the various sectors flows through it at least once [1,2]. Heat exchangers [3] are typically used to accomplish heat exchange between the two fluids, and they have a varied application in a variety of industries for both heating and cooling [4]. The essential demand for natural energy sources has made energy guidance a prominent aim for scientists as research and technology have advanced. Regenerative heat exchangers are becoming a weapon of the times, used by factories and companies to rationalize energy consumption and save massive quantities of wasted energy. Its ability to absorb waste heat allows it to warm up cold gasses that are often heated in thermal furnaces and motors that burn fossil fuels for fuel. As a result, these motors utilize less energy and precious fossil fuel. Utilizing geothermal heat from the earth, subsurface heat exchangers have also been utilized to cool and heat fluids for use in agriculture, industry, and residential settings. The researchers carried out numerical and experimental tests regarding the characteristics of the fluids involved (physico-chemical properties) and the nature of the systems in which they occur in order to enhance the heat transfer utilizing convection as a cooling strategy. There are various kinds of heat exchangers, therefore choosing the appropriate one for a given process is crucial because a bad choice can cause the equipment to malfunction or the system to operate improperly. The tube and shell varieties of heat exchangers are the most widely utilized in a number of process industries [3,5] among the various forms [6]. This is because high-pressure

applications are made possible and these parts are simple to replace and clean. It is utilized in numerous industries, including feed water heaters, condensing units, chemical processing, oil refineries, and the electrical sector. Consequently, depending on the application, there is a constant need for the creation of small heat exchangers. Researchers are constantly keeping an eye on advancements in heat exchange efficacy in order to meet these needs. In addition to altering the geometry of the heat transfer surfaces or units, including single- or multi-type nanoparticles into the heat transfer fluids is a strategy that shows promise for increasing heat transfer efficiency. The phrase "nanofluid" or "hybrid nanofluid" refers to the combination of these nanoparticles and heat transfer fluid. Research has demonstrated that, in comparison to a pure assembled fluid, the addition of nanoparticles to a carrier liquid matrix can enhance heat transmission.

In the present work, we devoted the first chapter to the generalization of nanofluids.

we have devoted the second chapter to a bibliographic synthesis of previous work on nanofluids and natural, forced, and mixed convection in cavities, as well as entropy generation. This chapter also presents a study listing the thermophysical parameters encountered during the study of nanofluids in order to better specify the different quantities associated with a nanofluid.

The third chapter then presents the mathematical formulation that leads to the solution of the forced and natural convection issue in the given configuration (Shell/ Tube Heat Exchanger), under the scenario where the nanofluid is assimilated into an incompressible fluid with specific thermophysical properties. Then, for the two cases two-dimensional (2-D) and three-dimensional (3-D). we detail the boundary conditions used, the numerical resolution technique used, and the convergence criteria.

The fourth chapter is devoted to presenting and discussing the results obtained (Isotherms, Streamlines and Entropy), and four applications have been launched.

this chapter is devoted to the presentation of the results obtained in configuration (2-D) of convection flow in heat exchangers, filled with nanofluid, and of entropy generation. After the first validation step, focusing on the impact of certain parameters such as Rayleigh and Reynolds numbers, the solid volume fraction of the nanofluid, and the type of the nanofluids. also, presentation of the results obtained the laminar flow of hybrid nanofluid (MgO-

SWCNT/water) in a 2D zigzag cavity. The results of the numerical simulation allowed us to make several observations on the effects of the presence of nanoparticles in the base fluid.

And devoted to the presentation of the results obtained in configuration (3D) of convection flow in heat exchangers, filled with nanofluid, and of entropy generation. Following the initial validation stage, attention is paid to the effects of certain factors, including the kind of nanofluid, the solid volume percentage, and the Rayleigh and Reynolds numbers.

Finally, we will conclude with a general conclusion that will be accompanied by a set of perspectives for future developments.

CHAPTER I:

GENERALITIES

CHAPTER I: GENERALITIES

I.1. INTRODUCTION:

One of the most significant industrial processes is heat transfer. Heat must be effectively handled in all industrial systems by adding, removing, or shifting heat in the appropriate places. Because of their inadequate thermal performance, conventional heat transfer fluids, including water, ethylene glycol (EG), pump oil, etc., have not proven to have enough capacity for cooling applications. It has previously been demonstrated that the thermal performance of these conventional fluids could be enhanced by the addition of solid particles. For high-tech applications like microelectronics, data centers, and microchannels, these solutions with particles larger than a micrometer are ineffective. Consequently, the cooling industries have made the development of highly effective heat transfer fluids a top priority in order to overcome the drawbacks of conventional fluids. The introduction of nanofluids over the past ten years by nanoscience and nanotechnology has provided a new solution by enhancing the performance of heat transfer fluids, especially in high-tech applications.

This chapter presents general information on nanofluids. to the study of natural, forced, and mixed convection in cavities, as well as a study of entropy generation in different enclosures.

I.2. BASIC CONCEPTS:

Convection characterizes the propagation of heat in a fluid, gas, or liquid whose molecules are in motion. Two types of convection are distinguished below. In natural convection, the movement of fluid particles is caused by differences in density induced by an imposed temperature gradient in the presence of a gravitational field.

In forced convection, the movement of fluid particles is triggered by a mechanical process (pump, fan, etc.) that is independent of thermal phenomena, i.e., an external pressure gradient.

Mixed convection corresponds to the coupling of the two preceding phenomena (natural and forced convection) when the fictitious flow velocities due to the two types of convection are considered separately and of the same order of magnitude.

I.3. GENERALITIES ABOUT NANOFLUIDS:

I.3.1. Definition:

Colloidal solutions made up of particles the size of nanometers suspended in a fluid are called nanofluids. These particles are called nanoparticles. Ever since its unique thermal properties were discovered, this kind of solution has generated a lot of interest.
The term "nanoparticle" is used when the particle has at least one of its dimensions less than 100 nm. Since the typical radius of an atom is about 0.1 nm, a nanoparticle can consist of a few dozen to several hundred atoms. For example, the most famous nanoparticles, fullerenes, are made up of only 60 or 70 carbon atoms. Their very small size gives nanoparticles very significant, specific surfaces [7].

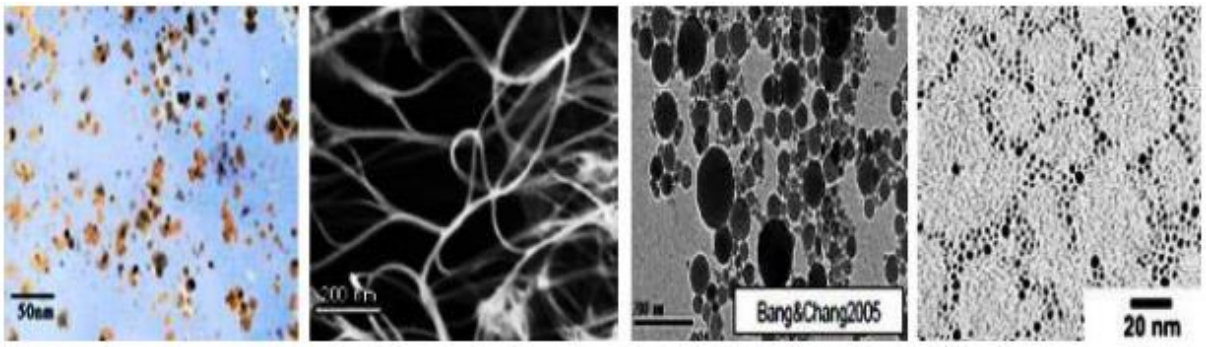

Figure (I. 1): Nanofluids seen through an electron microscope: ethylene glycol + 0.5% copper; water + alumina; water + gold 2 nm, [8]

I.3.2. Classification of nanofluids:

The classification of nanofluids depends essentially on the classification of nanoparticles in suspension. Nanoparticles can be classified according to various criteria, the most common of which are listed below:

I.3.2.1. **Nanoparticle size classification:**

Based on the dimensions of nanoparticles, Buzea et al. [9] proposed to classify them into three distinct classes:

- Class 1: This class includes thin films and surface coatings smaller than 100 nm.
- Class 2: Thick coatings and nanoporous filters.

- Class 3: Nanoparticles in compact form with a polyhedral or spheroid structure. This structure may be simple, such as a free nanoparticle, or more complex, forming aggregates (agglomerates of nanoparticles). Nanoparticles generally have a crystalline structure and are often spherical in shape.

I.3.2.2. Classification according to the chemical nature of nanoparticles:

From a chemical point of view, two main categories of nanoparticles can be distinguished:

- Organic nanoparticles: These include nanoparticles based on carbon atoms, such as carbon nanotubes, fullerenes, carbon black, graphene nanosheets, carbon nanofibers, and carbon nanofoams.

- Inorganic nanoparticles: A distinction is made between metallic nanoparticles (Au, Ag, Al, Zn, Fe, Cu), metal oxide nanoparticles (CuO, TiO_2, ZnO, SiO_2, Al_2O_3), and quantum dots. [10]

I.3.3. Preparation of nanofluids :

There are several ways to create nanofluids, including first-stage, second-stage, and other methods. A surfactant can be added to stop the sedimentation of nanoparticles while the device is operating. The process starts with the preparation of the nanofluid. Because of this, researchers ought to concentrate more on attaining a high degree of stability. According to colloid theory, sedimentation in suspensions stops when particle size falls below a critical radius because Brownian forces balance the gravitational forces. For some uses, smaller nanoparticles might be more appropriate. Their large surface area, however, causes agglomerates to grow between them [11, 12]. As a result, scientists view the creation of a stable nanofluid with ideal particle diameter and concentration as a significant task. There are two popular processes for creating nanofluids: the two-step

I.3.3.1. One-step method:

The one-step process combines the synthesis of nanofluids with the manufacture of nanoparticles, wherein the nanoparticles are directly created using either the liquid chemical method or the physical vapor deposition (PVD) technique. In this method, the processes of

storage via desiccation, transit, and discrete distribution of nanoparticles are prevented, such that nanoparticle accumulation is decreased and the stability of the fluids is increased.
In a single step, the synthesis and dispersion of nanoparticles in the base fluid happen concurrently. As an illustration, Argonne has created a one-step method for producing nanofluids that allows nanoscale vapor from a metallic source material to be distributed in fluids at low vapor pressure [13]. This novel one-step procedure was created to generate stable Cu nanoparticle suspensions devoid of dispersants by overcoming the van der Waals forces between nanoparticles.

The one-step chemical technique is evolving quickly since the one-step physical method is not appropriate for large-scale nanofluid synthesis and is very expensive. To create stable metal nanofluides. Zhu et al. [14] and Liu et al. [15] employed chemical reduction techniques in one step. Phuoc and colleagues [16] have also produced water-soluble nanoparticles on Ag by employing optical ablation as a step in a liquid. The main benefit of the step-by-step process is that the nanoparticles are more uniformly sized and relatively pure. Also, there are a few drawbacks to the method in stages. The most crucial aspect is that residual reactive substances remain in nanofluids due to incomplete stabilization or a reaction. Moreover, this process is only compatible with fluids with a base at low steam pressure.

I.3.3.2. Two-step method:

In a two-step procedure, inert gas condensation and chemical vapor deposition are two examples of physical or chemical techniques used to initially create nanoparticles in dry powder form. The synthesis of ultrafine metal particles has made extensive use of inert gas evaporation-condensation technology since the 1930s (nanoparticles are created by the evaporation of a metal source in an inert gas). Furthermore, the fundamental chemical process for creating nanoparticles involves combining a molecule usually a halide that contains a metal atom with a reducing agent to extract the remaining components of the complex. This is followed by the dispersion of the powder in the liquid. The primary benefit of the two-step approach is that it allows for the low-cost mass production of nanoparticles since they may be made independently in an industrial manner. Rather than metal nanoparticles, oxide nanoparticles are a good fit for this technique. The two-step procedure's main issue is the aggregation of nanoparticles. Particles aggregated strongly both before and after dispersion in ethylene glycol with nine hours of sonication, as demonstrated by Kwak and Kim [17]. The

majority of researchers purchase powdered nanoparticles and combine them with a liquid base. These nanofluids are not stable, though pH can be adjusted and surfactant can be added to boost stability. A few researchers buy commercially produced nanofluids. However, these nanofluids are tainted with contaminants and contain nanoparticles that are not the exact size specified by the provider.

I.3.3.3. Other methods:

In order to produce nanofluids with comparatively high features and increased stability, several researchers are developing new techniques. Wei et al. [18] have developed a method for making copper nanofluids. This method can be created by further converting the precursors with microwave and ultrasonic irradiation [19]. Chen et al. [20] created monodisperse noble metal colloids using phase transfer. Aqueous-organic phase transfer was employed by Feng et al. [21] to create water-soluble nanoparticles of platinum, silver, and gold. Stable kerosene-based Fe_3O_4 nanofluids are also made by the phase transfer technique [22]. As mentioned before, research has shown that the chemical solution method can produce nanofluids with higher conductivity and higher stability [23].

I.3.4. Nanofluid Types:

The term "nanofluids" refers to fluids that contain particles dispersed on a nanometric scale. These can include single-element nanoparticles (Cu, Fe, and Ag), single-element oxides (CuO, Cu_2O, Al_2O_3, and T_iO_2), alloys (Cu-Zn, Fe-Ni, and Ag-Cu), multi-element oxides ($CuZnFe_4O_4$, $NiFe_2O_4$, and $ZnFe_2O_4$), metal carbides (SiC, B_4C, and ZrC), metal nitrides (SiN, TiN, and AlN), and carbon particles (graphite, carbon nanotubes, and diamond) suspended in water, ethanol, EG, oil, and coolants. They fall into two primary categories: hybrid nanofluids and monomaterial nanofluids. [24, 25, 26]

I.3.4.1. Single material nanofluids:

This kind of nanofluid was first proposed by Choi in 1995 [27] This is regarded as the traditional sort of nanofluid utilized, in which a single kind of nanoparticle is employed to create the suspension by various techniques of production. Numerous writers have noted that because these nanofluids thermophysical characteristics are far better than those of their base fluid, they perform better.

I.3.4.2. Hybrid nanofluids:

An advanced class of nanofluids called hybrid nanofluids is made up of multiple types of nanoparticles suspended in a base fluid.The goal of Jana et al. [28] experimental investigation into this kind of fluid was to increase its thermal conductivity over that of a typical nanofluid made of a single substance. They investigated Cu, Au, and carbon nanotube (CNT) nanoparticles dispersed in water, as well as the hybrids of these particles (CNT - Cu / H_2O and CNT - Au / H_2O). The findings demonstrated that Cu / H_2O nanofluids had the highest thermal conductivity of all the samples examined and that this conductivity rose linearly as particle concentration increased. However, compared to other forms of nanofluid, the stability of the CNT – Cu / H_2O nanofluid has led to a longer stabilizing time. As a result, the fluid's thermal conductivity can be maintained for a significantly longer time before declining. [29,30]

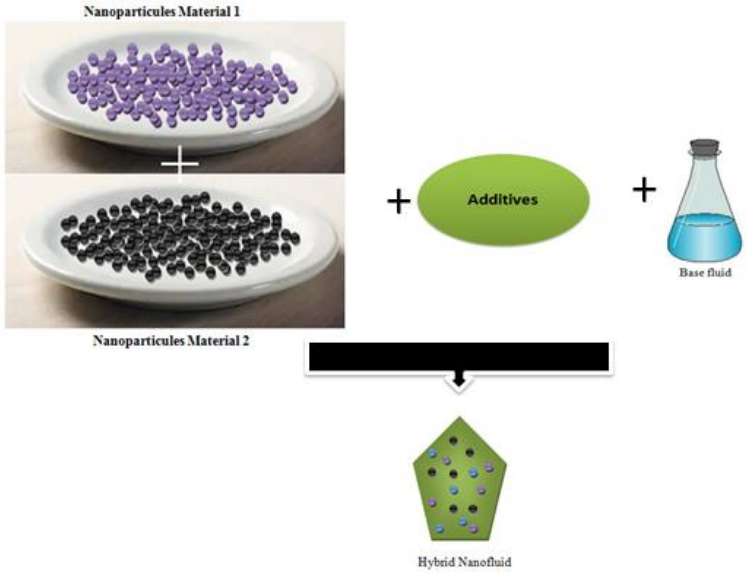

Figure (I. 2): Graphical representation of Hybrid nanofluid.

I.3.4.3. Tri Hybrid Nanofluids:

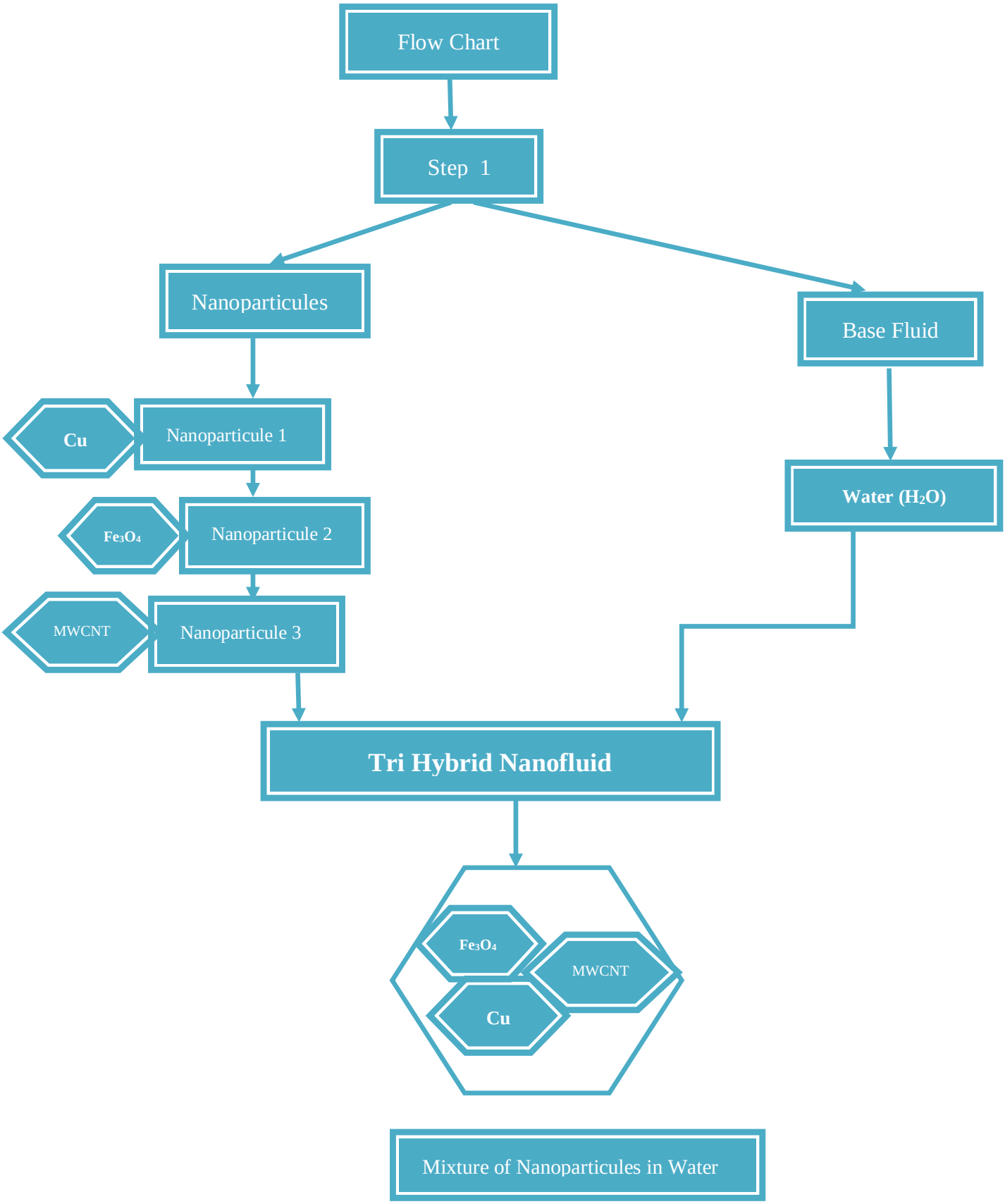

Figure (I. 3): The preparation method for Tri Hybrid Nanofluid

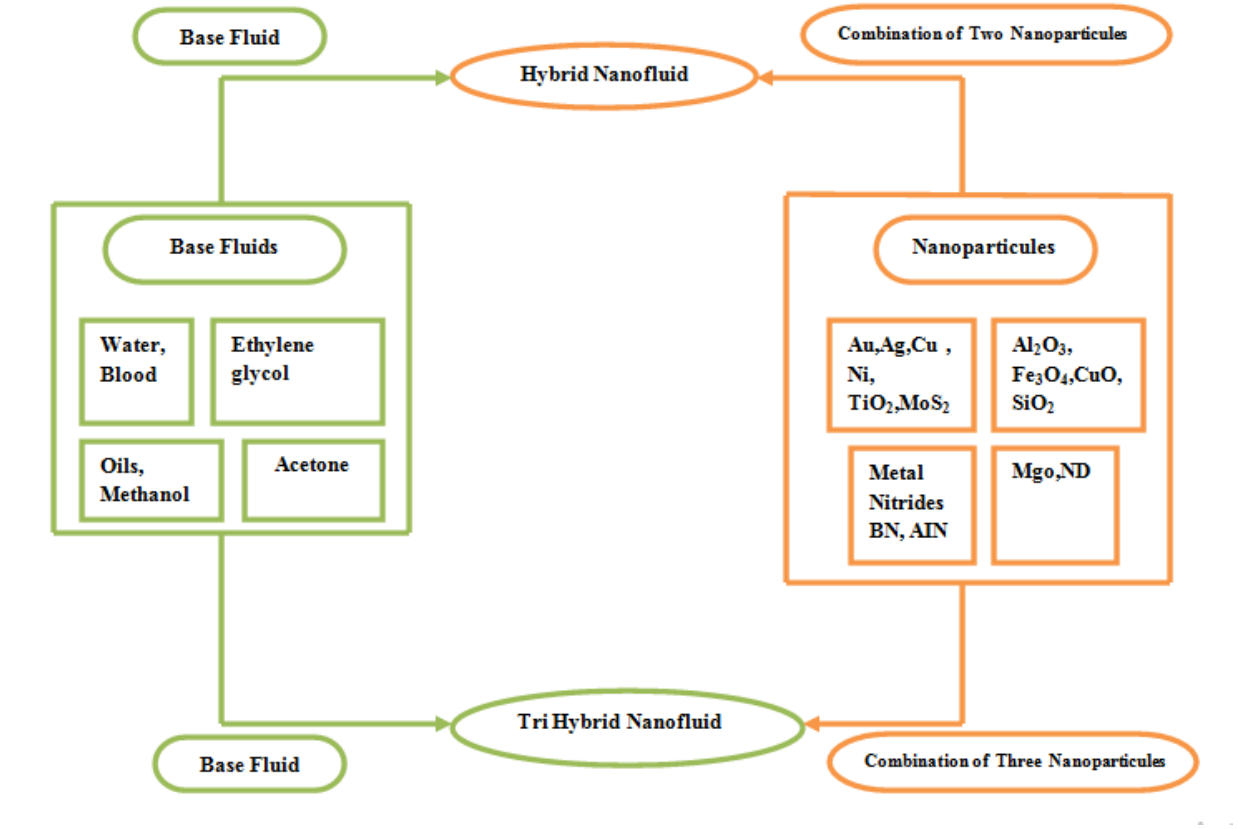

Figure (I. 4): Flow chart of Tri Hybrid Nanofluid and Hybrid Nanofluid

I.3.5. Nanofluid applications:

The various applications of nanofluids are presented as follows: transport (cooling management/heat engine vehicle), electronic cooling, space, nuclear systems cooling, heat exchangers, biomedicine, solar water heating, domestic refrigerators, drilling, lubricants, thermal storage, etc.

I.3.6. Advantages of Nanofluids:

It's undeniable that a good nanofluid boosts the efficiency of any liquid cooling system without making more noise or consuming more energy. On the contrary, since overall efficiency has improved, you might think of reducing ventilation or getting a less powerful pump while keeping the same level of performance if quiet operation is the priority. However, nanofluids offer the following advantages:

- A large surface area for heat transmission between particles and fluids due to its high specific surface area.
- Strong dispersion stability characterized by a predominately Brownian particle motion.
- less pumping power needed to obtain an equivalent intensification of heat transfer when compared to a pure liquid.
- less particle clogging than with traditional slurries, which allowed for system downsizing.
- Variable particle concentrations can be used to achieve adjustable qualities, such as surface wettability and thermal conductivity, to suit various applications.

I.3.7. Disadvantages:

Surface erosion and sedimentation are effects that can be neglected with a nanofluid. Corrosion remains a point to be checked, but if it's well chosen by taking something inert or adapting it to your circuit, then there won't be any worries. But it does have a number of disadvantages :

- Stability of nanoparticle dispersion.
- Greater pumping power and pressure drop.
- Lower specific heat and higher viscosity.
- High cost of nanofluids.
- Challenges within the manufacturing procedure.

I.5. CONCLUSION:

In this chapter, a presentation of generalities and basic notions on natural, forced, and mixed convection, as well as a general description of nanofluids, has been carried out. Analysis of these studies has enabled us to identify the various parameters that can influence the thermal behavior of nanofluids.

CHAPTER II:

BIBLIOGRAPHIC SYNTHESIS

II.1. INTRODUCTION:

The conductivity and thermal capacity of the heat transfer fluids are the primary determinants of heat transfer intensity. The nanofluid is a novel class of fluid that has been developing in recent years. Nanofluids are heat-transfer fluids, like water, glycol water, or oil, that have had metallic or non-metallic oxides (SiO_2, Al_2O_3, TiO_2) or metal nanoparticles (Al, Cu, Ag, etc.) added to them. By drastically changing the carrier fluid's thermal conductivity, these nanofluids may enhance heat transmission in comparatively modest amounts as compared to traditional fluids. The performance of different heat exchangers can be enhanced thanks to this improvement in heat transmission, which makes nanofluids a viable new heat transfer technology.

The scientific literature on the study of Hybrid nanofluid in various enclosures including natural, forced, and mixed convection is reviewed in this chapter. A lot of theoretical and experimental work has been done on the study of natural, forced, and mixed convection in Heat exchangers and cavities because of its implications for many industrial phenomena, including metallurgy, building insulation (in the case of double glazing), cooling electrical circuits and nuclear reactors, etc.

II.2. BIBLIOGRAPHIC SYNTHESIS:

Given the significance of nanofluids, a number of investigations into their thermal behavior and physical attributes, including dynamic viscosity and heat transfer coefficient, have demonstrated how distinct nanofluids are from base fluids in terms of thermophysical properties and improved heat transfer. In their early research, Choi [27] discovered that adding a tiny quantity of nanoparticles (volume concentration ranging from 1% to 5% Al_2O_3) increased thermal conductivity in carbon nanotubes by 20%.

Hybrid nanofluids have unique chemical and physical characteristics, such as strong thermal conductivity [31–35]. In-person experiments and their analysis are typically costly and time-consuming. Wide variations are therefore also inappropriate for the parametric analysis of the prototypes [36-37]. Therefore, in order to provide a clear study of these thermal devices, computational analysis is preferred. The literature on heat exchangers and heat transfer improvement analysis is extensive [38]. A heat exchanger's accurate modeling was examined

by Zaversky et al. [39]. In order to increase the Nusselt number and the convective coefficient of heat transfer, Shahdad and Fazel [40] discussed the use of perforated fins as an alternative to simple fins. The improved heat transmission employing honeycomb tubes over smooth tubes was studied by Xie et al. [41]. The heat transmission of circular and elliptical tubes (12 numbers) under varied Re values was compared by Matos et al. [42, 43]. Nouri-Borujerdi and Lavasani [44,45] investigated the thermo-fluid flow properties of basic conduits with a cam form. A 2D study was conducted in an elliptical circular tube heat exchanger by Mohanty et al. [46]. The magnetic dipole effect on a radiative ferromagnetic liquid was explored numerically by Dharmaiah et al. [47]. Li et al.'s study [48] examined the heat transmission and frictional losses in a heat exchanger with an elliptical tube.An elliptical tube-based heat exchanger's frictional losses were examined by Bouris et al. [49], who discovered that a larger heat transfer area results in a greater pressure drop. An experimental study on forced convective heat transfer across a spiral tube-based heat exchanger's surface was carried out by Moawed [50]. Reduced temperature differences improve heat exchanger performance, according to research by Rosen and Dincer [51]. According to Khan et al.'s analysis [52] of the forced convective processes in elliptical-shaped tubes, heat transfers more readily as the air-water flow increases. The impact of the angle of attack on the total thermal performance of a heat exchanger with an elliptical tube was investigated by Harris and Goldschmidt [53]. An elliptical-shaped tube finned heat exchanger was numerically investigated by Teo et al. [54]. Thirty percent more heat transfer was detected than with circular tubes. Thermal behavior was calculated by Li et al. [55] using elliptical-shaped tubes that had axial ratios of 0.3, 0.5, and 0.8. Experimental work on tube and shell heat exchangers with split baffles at varying angular orientations of the baffles 0◦, 15◦, 30◦, and 45◦ from the horizontal was carried out by Kumar and Jhinge [56]. Raj and Ganne [57] looked into the effects of three different baffle tilt angles 0, 10, and 20 with a deflector cut of 36% on the heat transmission properties of a tube/shell heat exchanger. A simulation of a shell/tube heat exchanger with overlapping non-continuous intermediate helical baffles (30, 40, and 50 helix angles) was carried out by Zhang et al. [58]. A numerical simulation of a continuous spiral baffle tube/shell heat exchanger was carried out by Sivarajan et al. [59]; the results showed that the spiral baffle tube/shell heat exchanger has better flow performance and better heat transfer than the conventional shell and tube baffle heat exchanger. Kwon et al. [60] demonstrated that the use of ZnO nanoparticles and Al_2O_3 leads to an increase in the coefficient of heat transfer to 30% at a concentration of 6% Al_2O_3.

Albadretal. [61] investigated heat transfer through a heat exchanger using the nanofluid Al_2O_3 at different concentrations. The forced convection heat transfer coefficient is slight higher than that of the base liquid at the same inlet temperatures and mass flow rate. Asadi et al. [62] conducted an experimental investigation on the heat transfer capabilities of an oil-based hybrid nanofluid, Al_2O_3-MWCNT, and discovered improved heat transmission. Using Al_2O_3 nanoparticles, Ghazanfari et al. [63] conducted a numerical analysis of the overall performance of a twisted-tube-based shell-type heat exchanger. They discovered a 20% increase in heat transfer and a 40% increase in pressure drop. Refers [64–66] provide a thorough analysis of the performance enhancement in heat exchangers.

On the other hand, In the presence of an external magnetic field, Mebarek-Oudina et al. [67] quantitatively studied free convection in a grooved porous enclosure filled with MgO – Ag / H_2O hybrid nano-liquid. Using the Galerkin finite element method, the problem's governing equations are solved. They found: Convective heat transfer coefficient increases with increasing Rayleigh number; the fluid flow force accelerates significantly with increasing Rayleigh number and decelerates with increasing magnetic field strength; and the maximum and minimum values of the flux function increase with increasing Rayleigh number value.

Heat transmission and stable magneto-hydrodynamic natural convection in a cold corrugated thin-walled porous enclosure with a hot elliptical inner cylinder populated by a Fe_3O_4 - MWCNT / H_2O hybrid nanofluid have been statistically studied by Mourad et al. [68].
The Galerkin finite element method (GFEM) is used to verify the governing equations. The researchers discovered that: the intensity of nanofluid flow circulation increases with increasing amplitude or number of corrugations; maximal heat transfer constraint occurs at high concentrations and high Rayleigh numbers.

Heat transmission by natural convection in the limited annular region between two homocentric cylinders was quantitatively investigated by Mebarek-Oudina et al. [69]. A titanium nanofluid consisting of water and ethylene glycol was poured into the annular gap. Using the TDMA and SIMPLER algorithms in conjunction with the finite volume method yields the numerical solution. They discovered that for the nanofluid (φ = 3%), the values of the flow function increase when the volume ratio of EG in the base fluid increases. The use of TiO_2-ethylene glycol/water nanofluid improves natural convection inside the annular space

better than the pure ethylene glycol/water mixture. In contrast, a different pattern of behavior is evident for ($\varphi = 0\%$).

The effects of the hybrid nanofluid MWCNT - Fe_3O_4 / H_2O and the variable magnetic field on an exponentially contracting porous sheet with sliding boundary conditions were investigated by Swain et al. [70]. They found: Schmidt number and chemical reaction parameters increase mass transfer rate, while Prandtl number and radiation parameter increase heat transfer rate; hybridity improves temperature profiles as well as concentration profiles.

Titanium nanofluids filled in a cylindrical ring have been the subject of hydrodynamic and thermal properties studied numerically by Mebarek-Oudina [71]. Using the SIMPLER algorithm in conjunction with the finite volume method yields the numerical solution. Water, motor oil, and ethylene glycol are the basis fluids. It is found: Rayleigh number and nanoparticle volume fraction affect thermal efficiency; Impact of TiO_2 nanofluids on heat transmission is correlated with base fluid types; For a small Rayleigh number, the nanoparticle effect appears clearly on heat transfer; heat transfer growth rate with nanoparticle volume fraction and Rayleigh number; The average Nusselt number depends on the base fluid change.

Abu-Libdeh et al. [72] have investigated a novel type of cavity filled with Ag - MgO / H_2O nanofluids and porous media that are compatible with total entropy and natural convection under a continuous magnetic field. The problem is expressed in the dimensionless form of the governing equations and is solved by the finite element method. They discovered that when the Hartmann number increases, the rate of heat transfer decreases, and the magnetic field may be employed as a superb heat transfer controller.

Mebarek-Oudina et al. [73] studied the laminar flow of a nanofluid in a trapezoidal cavity and also measured the convective exchanges taking place within it. The cavity is geometrically trapezoidal at right angles, containing a Cu - Al_2O_3 / H_2O hybrid nanofluid. They found: when free convection is minimal, the impact of raising the hybrid nanofluid's volume fraction becomes noteworthy; compared to a nano liquid, a hybrid nano-fluid collected from equal amounts of Al_2O_3 and Cu suspended in a H_2O-based liquid has no significant improvement on the average Nusselt number; Convective heat transport is decreased and conductive heat transport is increased when internal heat generating rate is raised.

CHAPTER II: BIBLIOGRAPHIC SYNTHESIS

The effects of the volume percentage of Cu - H_2O nanoparticles and the Hartmann number caused by an inclined magnetic field on heat transport and irreversibility in a porous medium with a saturable nanofluid Darcy-Brinkman-Forchheimer couvercle have been studied by Marzougui et al. [74] They discovered: For all Hartman numbers, the generation of thermal entropie decreases almost linearly through the volume fraction of nanoparticules; the angles at which the generation of magnetic entropie is minimal correspond to the angles at which the generation of thermal entropie is maximal, and vice versa. As the volume percentage of nanoparticles increases, the irreversibility of heat decreases, and the generation of magnetic entropy increases at a constant angle of the magnetic field.

Mebarek-Oudina and Bessaïh [75] studied numerically the heat transfer by natural convection of Cu - H_2O nanofluid in a vertical cylindrical annular enclosure with two discrete heat sources of different lengths. Using the SIMPLER algorithm in conjunction with the finite volume method yields the numerical solution. They found: The volume percentage of nanoparticles increases with heat transmission; maximum temperature decreases with increasing nanoparticle volume fraction; Heat transfer and heating element temperature depend on Rayleigh number, nanoparticle volume fraction, and heating element length. For all Rayleigh numbers, Nanoparticles have an impact on heat transmission. Heating element size has a significant influence on heat transfer rate.

Stable laminar mixed convection inside a square cavity loaded with various kinds of nanoparticles was statistically investigated by Zaydan et al. [76]. They found: the presence of nanoparticles always increases heat transfer, irrespective of the type of nanoparticles or the type of base fluid; an improvement in heat transfer using spherical nanoparticles compared with cylindrical nanoparticles.

The impact of MoS_2 molybdenum disulfide nanoparticles on the MHD flow of a nanofluid channel with increasing walls was investigated by Raza et al. [77]. They discovered that: increasing the solid volume percentage improved the heat transfer rate; spherical nanoparticles raised the local Nusselt number more than other nanoparticles taken into consideration.

Mourad et al. [78] studied the stable laminar natural convective flow and heat transfer of a Cu - H_2O nanofluid between a cold corrugated porous enclosure and a hot elliptical cylinder.

They found: It was observed that whenever a high-volume fraction of nanoparticles was associated with a high level of Rayleigh number, maximum heat transfer enhancements took place; convective thermal energy flux increased with increasing Rayleigh and Darcy volume fractions.

The buoyant convective flow and heat transport increase of Cu - H_2O nanofluid in a differentially heated vertical ring with a thin baffle were studied statistically by Pushpa et al. [79]. They discovered that when the volume proportion of nanofluid and Rayleigh increases, heat transmission also increases. Heat transfer for nanofluids is superior to that of base fluids at low Rayleigh; the rate of heat transport rises as the volume fraction of nanofluids increases; and the flow circulation rate of nanofluids is superior to that of the base fluid.

Double-diffusive transport and entropy generation in a wavy cylindrical enclosure containing a Cu-H_2O Casson nanofluid under the effects of thermal radiation and a magnetic field were statistically investigated by Alomari et al. [80]. The finite element approach with a Galerkin formulation was used to numerically solve the governing equations. They discovered that the Rayleigh number (Ra) had a major impact on mass and heat transmission. As Ra rose from 10^3 to 10^6, the Nusselt number increased by around 60%, suggesting improved convective transport.

The Entropy Generation (EG) caused by buoyant Al_2O_3-H_2O nanofluid convective flow in a square shape with a fin was investigated by Bouchoucha et al. [81]. The bottom border is maintained at a higher temperature (T_H), the top wall of the closed space is kept at a cool thermal condition (T_C), and the remainder of the area is subject to adiabatic limitations, treating it as conductive. A handmade computer code is used to discretize the model equations from the finite volume approach. They discovered that at higher Ra (Ra = 10^5), the NPs significantly contribute to the lowering of entropy by improving thermal transport from the heater to the cold boundary and creating a uniform thermal distribution within the enclosure, which lowers the formation of total entropy.

Mebarek-Oudina et al [82] investigated the effects of geometrical factors on free convective heat transfer in a hollow with zigzag walls that contained a hybrid nanofluid made of water-suspended single-walled carbon nanotubes (SWCNT) and magnesium oxide (MgO). Applying multiphysics software that has been tested and is based on the Galerkin finite element method to calculate. They found that A balance between efficiency and irreversibility

is shown by higher nanoparticle volume fractions, which raise thermal irreversibility and the average Nusselt number; Heat transmission efficiency is significantly impacted by both Ra and the volume fraction of nanoparticles; differences result in observable changes in performance.

Mixed convection motion was examined by Rashidi et al. [83] in a heated container that was subjected to a horizontal magnetic field and had a lid saturated with a hybrid Al_2O_3 –Cu / H_2O nanosuspension. They discovered that while the addition of Cu nanoparticles to the nanofluid at a lower Ri was very successful and had no discernible effect at a higher Ri, the inclusion of Al_2O_3 nanoparticles increased energy transfer performance for all Ri and Ha examined. The application of hybrid nanoparticles did not always result in an increase in the rate of heat transfer; thus, the existence of hybrid nanoparticles may depend on other factors, such as the Richardson number.

Asogwa et al. [84] examined the Al_2O_3 – CuO / H_2O hybrid nanofluid via an exponentially accelerating Riga plate. They found: with increasing nanoparticle volume fraction, the higher density of cupric nano-fluid is improved over alumina through a decrease in velocity distribution; with an exponential increase in radiation, CuO nanofluid behaves better than Al_2O_3, since CuO nanofluid is a better heat conductor and non-acidic.

Said et al. [85] Numerical analysis was performed on mixed convection in a two-dimensional enclosure filled with a nanoliquid Cu/H_2O through a porous medium. The Brinkman-Forchheimer model is used to designate the nanoliquid flow. While the other walls are thermally insulated, the top and bottom horizontal walls are regarded as hot (T_h) and cold (T_c), respectively. They found that Heat transmission was noticeably improved by raising the Reynolds number to $Re \geq 250$; The heat transmission of NFs was strongly impacted by the Ha number; higher Ha values caused the immobilization of nanoparticles as a result of Lorentz forces, which in turn affected Nusselt number plots and highlighted the significance of the magnetic field in changing heat transport.

Natural convection in a hollow filled with an electrically conductive Cu / H_2O nanofluid controlled by a periodic temperature profile along the vertical wall was quantitatively explored by Hussam et al. [86]. They found that the maximum Nusselt number increased as

the hot wall forcing amplitude increased, indicating a significant improvement in heat transfer for larger amplitudes.

Alhashash and H. Saleh [87] studied the natural convection of a hybrid NEPCM nanofluid in a corrugated enclosure caused by a thermal difference between a cold and a warm corrugated wall. The finite element approach was used to solve the equations. They found that overall heat transfer improved further by adjourning the NEPCM particle volume fraction, and latent heat modification of corrugated surface temperatures enhanced NEPCM success in terms of improved thermal performance.

Asmadi et al. [88] examined the performance of an alumina-copper/water hybrid nanofluid in buoyancy-driven heat transfer of a U-shaped cavity with a heated wavy wall. A three-node triangular finite element method is used to solve the system by considering the Galerkin weighted residual algorithm. They found that copper-alumina/water hybrid nanofluid enhances the ther- mal performance within a U-shaped lid compared to pure water up to 16% for all cases; In the Cu-Al_2O_3/pure water hybrid nanofluid, the ratio of 1:9 between Cu and Al_2O_3 yields the largest gain in thermal performance rate when compared to other ratios.

Fares et al. [89] numerically studied the flow of an Ag / H_2O nanoliquid within a porous square enclosure under the action of an external magnetic field with different inclination angles and different nanoparticle volume fractions. The Lorentz force law emerges to frame the magnetic field efficiency, while the Darcy-Forchheimer model provides a mathematical formulation of the porosity issues. They found: cavity thermal efficiency is enhanced by increasing fluid inertia; inserted nanoparticles generally increase heat transfer; The average Nusselt number rises sharply as the volume percentage of nanoparticles rises; Thermal performance falls with rising Hartmann number and rises with increasing Rayleigh number and volume fraction.

Al_2O_3 and TiO_2 nanoparticles in EG fluid flowed unsteadily through a saturated porous medium confined by two vertical surfaces with heat generation and no-slip boundary conditions, according to research by Hazarika et al. [90]. They found: Al_2O_3 and TiO_2 nanoparticles are generated with increasing volume fraction values; all nanoparticle velocity profiles are very high for TiO_2 nanoparticles compared to Al_2O_3; and nanoparticle velocities and temperatures are strongly depressed with high heat generation compared to no heat generation.

Heat transfer and entropy formation in Cu-Al_2O_3/water hybrid nanofluid flow generated by an elastic curved surface were investigated by Afridi et al. [91]. They found: As the volume fraction grows, so does the development of entropy; When flowing on a flat surface as opposed to a curved surface, the rate of entropy generation is lower; and less entropy is generated in the regular nanofluid flow compared to the hybrid nanofluid.

Shah et al. [92] examined the effects of a constant heat source and magnetic field on a porous cylinder with a free convective Fe_3O_4 –MWCNT /H_2O Magnetized non-darcy nanofluid. They found that the hybrid nanofluid's rising inter-particle collision causes the hot wall temperature to rise with a bigger Hartmann number. At lower Darcy numbers, this temperature increase with higher Hartmann numbers is more pronounced.

Abu Bakar et al. [93] investigated the flow and heat transfer behavior of mired convection with the appearance of Ag -TiO_2 /H_2O hybrid nanofluid in a porous medium, heat generation, surtion/injection, thermal radiation, and magneto-hydrodynamics. They found: The hybrid of two different nanoparticles between Ag and TiO_2 exhibits greater boundary layer flow performance than the impact of mono-titanium dioxide TiO_2 nanoparticles; friction coefficient factor and velocity profile improve positively alongside hybrid nanofluid nanoparticles.

Wahid et al. [94] studied the magneto-hydrodynamic radiative flow of a hybrid nanofluid Al_2O_3 – Cu /H_2O in front of a permeable vertical plate with mixed convection. They found: It has been observed that physical quantities of interest decrease and boundary layer separation speeds up with volume increases and copper concentration; For the feasible solution, the mixed convection parameter globally reduced friction and increased the specific heat transfer rate.

Wahid et al. [95] numerically investigated a three-dimensional radiative flow of Cu -Al_2O_3 /H_2O hybrid nanofluid in front of a permeable shrink plate. They found: heat transfer rate is increased with intensification of the thermal radiation parameter and reduced with intensification of the volumetric copper concentration parameter; intensification of the volumetric copper concentration slowed boundary layer separation; Skin friction coefficients can be improved with an intensification of the volumetric copper concentration. The temperature profile is intensified with an increment in the volumetric copper concentration parameter but reduced with an intensification of the suction and thermal radiation parameters.

Khashi'Ie et al. [96] investigated the conventional flow and heat transfer characteristics of an Al_2O_3 – Cu /H_2O hybrid nanofluid in front of a stretch/shrink foil. They found that hybrid nanofluids with an appropriate combination of nanoparticles have the best heat transfer performance compared to traditional nanofluids; For bigger values of the shrinkage parameter, the heat transfer rate increases as d increases; for all values of the stretch parameter, the opposite outcome is obtained.

The magneto-hydrodynamic natural convection and entropy formation of a Cu/H_2O nanofluid in a porous ring between a heated Koch snowflake and a lower-temperature corrugated cylinder have been studied numerically by Mourad et al. [97]. The numerical algorithm relies on the finite element method developed by Galerkin. They found that Increasing the Rayleigh number causes the flow in the ring to become more intense, which increases the enclosure's free convective flow and speeds up heat transfer and irreversibility because of fluid friction.
Gul et al. [98]. investigated the Cu-Al_2O_3/H_2O nanofluid's natural convections into a permeability chamber. The control volume method has been used to approach the analysis numerically, and the magnetic field is also performed on the fow feld. Numerous metrics of hybrid nanofluid fractions, Rayleigh numbers, Hartmann numbers, and porosity factor were added to the research of hybrid nanofluid heat in terms of the transfer flux. They found that Fluid (Cu + Al_2O_3/H_2O) velocity diminishes significantly around the center of the channel due to a strengthening of Ra, Ha, and φ, according to the explanations; In comparison to traditional fluids, the hybrid nanofluid's temperature profile appears to be consistently higher.

Saeed et al. [99] have numerically investigated the Darcy-Forchheimer flow solution for TiO_2 -Al_2O_3 /H_2O hybrid nanofluid using slip conditions. To regulate the heat transfer of the flow system, a swirling disk creates the fluid flow, which is then subjected to thermal stratification and nonlinear thermal radiation. They found: Nusselt number parameters have the potential to improve mass transfer rate in magnitude, while nanofluid factors have the opposite result; heat transfer rate amplitude increases with R factors while it decreases with Prandtl and Nusselt factors.

Ahmadian et al. [100] studied a three-dimensional (3D) numerical solution of an unsteady Ag – MgO /H_2O hybrid nanofluid flow with heat and mass transfer caused by the up/down motion of a corrugated rotating disk. They found that the use of hybrid nanofluid is more

effective in overcoming low energy transmission, and the up/down motion of the rotating corrugated disk positively affects fluid temperature and velocity.

The Ag-MgO/H_2O hybrid nanofluid flow over the conical space between the disk and the cone has been examined by Alrabaiah et al. [101]. The method used is parametric continuation (PCM). They found: fluid velocity increases with increasing amounts of nanoparticles (Ag and MgO); The magnetic impact significantly enhanced the thermal energy profile; addition of nanoparticles to the base fluid.

The Falkner-Skan problem has been studied by Dinarvand et al. [102]. The two-dimensional laminar incompressible boundary layer flow of a hybrid nanofluid of TiO_2-CuO/H_2O on a stationary or moving wedge was explored semi-analytically.

They found: Skin friction and the hybrid nanofluid's local heat transfer rate both improve with an increase in the mass of the first and second nanoparticles; In comparison to other nanoparticle shapes, a spherical nanoparticle will have a small local Nusselt number.

Gul et al. [103] examined and compared the heat transfer effect in single Cu /H_2O and Cu - Al_2O_3 /H_2O hybrid nanofluids, which were permitted to move over a foil spreading surface. They found: As with the addition of nanoparticles, concentration of the volume fraction increases the temperature field while viscosity reduces the velocity field; the heat transfer effect in the hybrid Cu - Al_2O_3 /H_2O nanofluid is more effective than the single Cu /H_2O nanofluid.

Tlili et al. [104] numerically investigated the flow of 3D nonlinear radiative CuO -MgO /Methanol nanofluid through an irregularly dimensioned sheet with the slip effect. They discovered that compared to CuO –MgO / Methanol hybrid nanofluid, CuO / Methanol nanofluid had superior convective properties; The combination of CuO, MgO, and methanol has an insulating property.

Waini et al. [105] examined flow from the stagnation point to a stretching/shrinking cylinder in hybrid Cu -Al_2O_3 /H_2O nanofluids. They found: Increased heat transfer rate when hybrid nanofluids were present; As Reynolds number climbed, so did the Nusselt number; The Reynolds number effect was more dominant for the stretching surface case.

On a three-dimensional stretched foil, Abid et al. [106] investigated the comparative impact study of two distinct nanoparticles: copper Cu and copper oxide CuO. The fluid flows

analyzed were magneto fluid, partly ionized water, and kerosene mixed with copper or copper oxide. They found: When it comes to the temperature of the partially ionized nanofluid, copper nanoparticles have a stronger effect than copper oxide nanoparticles; The CuO-water nanofluid has a partially ionized fluid velocity that is higher than that of the other nanofluids when velocity increases, and the Cu-kerosene oil nanofluid exhibits a dramatic fall in fluid velocity whenever velocity decreases; In comparison to the other three partially ionized nanofluids, the temperature is highest when copper nanoparticles are disseminated in the partially ionized water-based fluid under the influence of major parameters.

Ramzan et al. [107] studied the hydrodynamic and thermal characteristics of two hybrid nanofluids: grapheme -Ag/H_2O and grapheme –CuO /H_2O with different particle shapes in a porous medium. They found that the entropy profile improves as the Brinkman number reaches higher and higher levels. The amount of heat released in grapheme –Ag /H_2O is greater than in grapheme –CuO /H_2O. Due to the increased irreversibility of grapheme –Ag /H_2O, it will be inefficient in solar thermal systems; grapheme –Ag /H_2O is important for temperature enhancement.

Jawad et al. [108] studied the magnetohydrodynamic flow of Al_2O_3 –Cu /H_2O hybrid nanofluid to an extension/shrinkage foil with thermal radiation. They found that increases in the fluid's thermal efficiency are due to increases in the volume percentage of nanoparticles, when compared to conventional fluids, and hybrid nanofluids are the most successful at raising the thermal conductivity of second-grade fluids.

Bilal et al. [109] examined the heat and flow characteristics of the magneto-hydrodynamic hybrid nanofluid CNT -Fe_3O_4 /H_2O flowing in a horizontal parallel channel with heat radiation through squeezing and expanding porous walls. They found: Though a contrary result is observed for single- and multiwall CNT, increasing the volume fraction of Fe_3O_4 nanoparticles can accelerate heat transmission to the walls; When the thermal radiation parameter is large, the local heat flux drops. For ferro-nanofluids, it is greater, while for hybrid nanofluids, its values are lower.

Saeed et al. [110] studied irreversibility analysis for the flow of torque-stressed hybrid nanofluid passed over a stretching surface. The hybrid nanofluid was prepared by suspending solid nanoparticles of SWCNT and MWCNT in pure human blood. They found an increase in the rate of heat transmission with a higher volume fraction of nanoparticles; The result

demonstrates that the most effective way to raise the flow's rate of heat transfer is through hybrid nanofluids.

In order to find an effective heat transfer fluid to replace conventional fluids and cutting-edge nanofluids, Jamshed et al. [111] investigated a novel hybrid nanofluid.
utilizing a hybrid hyperbolic tangent combination of nanofluids, consisting of a blend of titanium dioxide (TiO_2) and non-Newtonian ethylene glycol (EG) as the basis fluid.
They performed collective numerical calculations of parametric analysis employing governing equivalencies, utilizing the Keller-Box approach. They discovered that the progressive kind of nanofluid shown a promising improvement in the thermophysical and hydrodynamic properties associated with heat transmission.
Riaz et al. [112] studied a new model of entropy generation effects measured in the Cu-blood nano-fluid flow under the effect of ciliary-oriented motion. They discovered that when there is a viscous dissipation term, the nanofluid performs at a faster rate of heat transfer.

Albqmi and Sivanandam [113] have investigated the impact of thermal radiation and entropy generation on the magneto-hydrodynamic nanofluid Al_2O_3 /H_2O in a porous Darcy-Forchheimer medium with variable heat flux when subjected to an electric field. The resulting dimensionless model is solved numerically in Matlab using the bvp4 command. They found: This study is salutary to thermal science applications because it discusses the factors that lead to functioning hybrid nanoliquid thermal enhancement; the study can be extended with different nanoparticles and base fluids to explore enhancement techniques.

Alhashash [114] numerically investigated convective heat transfer in two composite enclosures. Both enclosures switch to nanofluid-clear Al_2O_3 /H_2O enclosures. A finite difference method that is iterative is used to obtain numerical solutions. It is found that heat transfer improvement is indicated with higher thermal conductivity ratios; an increase in NuI values is obtained when the nanoparticle concentration is increased.

The convective heat transfer performance of Al_2O_3/H_2O nanofluid through the shell/tube heat exchanger was numerically studied by Barik et al. [115]. They found that Alumina nanoparticles had a very high intrinsic thermal conductivity, which increased the heat transfer coefficient overall; As flux mass decreases, the overall coefficient of heat transfer also

decreases; These investigations demonstrated that when the Reynolds number rises, the Nusselt number also rises and achieves its maximum value.

In a porous enclosure filled with a Cu-Al_2O_3/water hybrid nanofluid and featuring a corrugated wall heated from below, Kadhima et al. [116] investigated buoyancy-driven flow. The Galerkin finite element method is used to solve the equations for non-dimensional fluid flow and heat transfer. They found: When compared to pure fluid, the usage of Cu-Al_2O_3/water hybrid nanofluid enhances temperature gradients, which in turn leads to enhanced heat transfer rates; Heat transfer and fluid flow are impacted differently by the number of corrugations; with N = 4, the best heat transfer performance is attained.

Alsabery et al. [117] numerically studied natural convection inside a porous cavity partially layered with a heated corrugated solid wall. Al_2O_3 -water nanofluid is deposited in the cavity. The finite element approach is used to solve the problem, which is stated in the dimensionless form of the governing equations. They discovered that corrugation of the solid wall reduces the total entropy generation rate and raises the average Nusselt number.

The influence of many parameters on heat transfer rate, flow behavior, and entropy generation in a MoS_2-GO/water hybrid nanofluid inhabiting a porous trapezoidal enclosure with a revolving inner tube was quantitatively examined by Maneengam et al. [118].
Using COMSOL Multiphysics, the governing equations were discretized and solved using the finite element method. They found: Fluid thermal conductivity rises with increasing concentration of nanoparticles; Fluid fluidity is related to entropy formation caused by fluid friction. It rises in proportion to the amount of nanoparticles.

Gumir et al. [119] have numerically analyzed heat transfer by natural convection in a square porous cavity with a solid corrugated finite wall filled with Fe_3O_4 –MWCNT /water hybrid nanofluid. The governing equations were solved using COMSOL Multiphysics modeling software and the Galerkin finite element method.

They found: Since the addition of nanoparticles raises the fluid's dynamic viscosity, the flow function drops as φ increases; The mean Nusselt number is influenced by nanoparticle concentration and rises with concentration; The flux function's maximum values fall as wave amplitude increases, while its minimum values increase.

Barman and Rao [120] have numerically investigated natural convection performed on the flow of different types of nanofluids (Al_2O_3 -H_2O, Cu -H_2O, and TiO_2 -H_2O) and buoyancy heat transfer through porous media packed inside a corrugated cavity. The finite difference approach is used to solve the dimensionless governing equations for nanofluid flow via the Darcian porous medium iteratively. They discovered that the convection process can be regulated by the presence of nanoparticles. It seems that the wall's corrugation was a regulating factor in the convection process.

Khan et al [121] have numerically analyzed the mixed convection of Al_2O_3 –Cu /H_2O hybrid nanofluide inside a trapezoïdale cavity with a fendu couvercle. A cold barrier in the shape of a triangle is positioned inside the cavity. This system, which has physical boundary constraints, is digitally resolved using Galerkin's method of final elements. They found that Reynolds and Richardson's formula for calculating the Nusselt number is the percentage of solid nanoparticle volume; the highest local Nusselt number is found at the level of the obstacle's living arêtes.

Mohd Hashim et al. [122] have numerically investigated the effect of hybrid nano-fluid Al_2O_3 –Cu /H_2O in a trapezoidal cavity with a heated left wall and a cold right wall for heat transfer. An inclined wall, a high Rayleigh number, and high concentration Al_2O_3 –Cu nanoparticles are effective in enhancing the heat transfer rate. Additionally, they created a new association between the Rayleigh number, viscosity, angle, effective thermal conductivity, and average Nusselt number.

By utilizing the Lattice Boltzmann technique, Ferhi et al. [123] statistically studied magnetized conjugate heat transport in a split L-shaped heat exchanger (HE) filled with eco-nanofluid, which is functionalized graphene nanoplatelets (GnPs) dispersed in water. They found that increasing temperature increases heat transport and entropy production in HE. Increasing temperature increases the rate of heat transport and reduces Sgen.

The flow and heat transfer properties of an Al_2O_3-SiO_2/water hybrid nanofluid in a partially heated square porous cavity have been studied by Aneja and Sharma [124].

The dimensionless nonlinear coupled partial differential equations of the flow issue are solved by the finite element method with a penalty parameter. They found that 1% and 2% of the hybrid nanoparticle volume fraction are relevant for the intensity of isothermal profiles and

contours; Little change is seen when the volume percentage of nanoparticles in streamlines and isotherms is increased further; As the hybrid nanofluids' volume fraction, Rayleigh number, and Darcy number increase, so does their average Nusselt number.

The formation of thermodynamic irreversibility and thermal convection for a double-lid flow in a partially porous laminated hexagonal enclosure was studied by Ahlawat et al. [125]. A micropolar Ag –MgO / water hybrid nanofluid was filled in the hexagonal cavity.
The finite difference method (FDM) in conjunction with successive over-relaxation (SOR), successive under-relaxation (SUR), and Gauss-Seidel iteration strategies was used to solve the dimensionless system of equations. The necessary results were generated using a problem-specific program in the MATLAB code. They found: the thermal conductivity of the base fluid is improved when φ hybrid nanofluid, leading to an increase in Nu avg and S Total; an increase in pressure directly increases wall velocity, which has a positive impact on heat convection and entropy generation processes.
Taking into consideration the Brownian effect of nanoparticles, Islam et al. [126] investigated the effects of heat generation or absorption on free convective flow and temperature transport in a triangular corrugated enclosure filled with Cu -H_2O nanofluid.
Dimensionless nonlinear PDEs are performed numerically using Galerkin's weighted residual type finite element technique. They found that, through increases in Rayleigh number and nanoparticle volume, both fluid flow and temperature flow change remarkably; The greater Rayleigh number and lower Hartmann number correspond to convective heat transfer; A major factor in thermal transport is the small size of nanoparticles; The rate of heat transport increases as nanoparticle diameter decreases.

Kadhim et al. [127] have numerically investigated buoyancy-driven flow in a porous enclosure with a corrugated wall heated from the bottom and filled with Cu -Al_2O_3 /water hybrid nanofluid. The Galerkin finite element method is used to solve the equations for non-dimensional fluid flow and heat transfer. They found: The usage of Cu -Al_2O_3 /water hybrid nanofluid enhances temperature gradients, resulting to higher heat transfer rates than pure fluid.

Alsabery et al. [128] studied a heated corrugated solid wall enclosed in a partially stratified porous cavity through natural convection; Compact heat exchangers come into contact with

the geometry. Alumina nanoparticles are put in the water to increase the heat exchange process.Results are computed numerically using Galerkin's weighted residual element technique. They found: nanofluid volume fraction increases the mean Nusselt number and decreases the overall rate of entropy generation; while confounding circulations within the porous layer, solid wall corrugation increases the mean Nusselt number and minimizes the overall rate of entropy generation.

Islam et al. [129] have numerically analyzed heat transfer in a closed cavity using magnetohydrodynamic natural convection. heat transfer consequences based on hybrid nanofluid (Cu -TiO_2 /H_2O) natural convective hexagonal heat exchangers. The infinite Galerkin element method is utilized to construct a numerical solution that encompasses the complex phenomenon. The statistical methodology called RSM is used to study the sensitivity of the output function for a thorough evaluation of the heat transport mechanism. They found that the results of the sensitivity study indicate that whereas Ha has a detrimental impact on heat transfer from heated surfaces, Ra and φ have a positive impact on Nu avg.

Convection flow of a cross fluid with water and carboxymethyl cellulose over a stretching sheet with convection heating was investigated by Ali et al. [130]. It uses a cross nanofluid with Al_2O_3, Cu nanoparticles, and CMC water as its base fluid. The present analysis considers minimizing of entropy generation. With the right conversion, the system of PDEs is changed into a collection of ODEs. They found that entropy generation and Bejan number of Cu, Al_2O_3, and Cu+Al_2O_3 are quite similar trends for We and δ; Temperature distribution, entropy generation, and Bejan number Cu, Al_2O_3, and Cu+Al_2O_3 are enhanced as increases the value of thermal radiation Rd.

Tayebi and Chamkha [131] have examined the natural convection of the Al_2O_3 -Cu /water hybrid nanofluid in a cavity with a corrugated conductive cylinder centered under a constant horizontal magnetic field. The finite volume discretization approach is used to solve the fundamental equations in their non-dimensional form numerically. They found that enhancing the free convective flux in this configuration with suspended copper and alumina nanoparticles in water is more effective when dominating the convection mechanism.

Soleimani et al. [132] numerically investigated boiling in a highly subcooled flow of HFE-7100 with various alumina nanoparticle concentrations in a microchannel heat sink by computational fluid dynamics simulations in three dimensions.

They found the application of nanofluids at a volumetric concentration of 4% increased the overall heat transfer coefficient by 3%, They concluded that the enhancement in heat transfer brought about by the use of nanofluids pales in comparison to the enhancement brought about by the use of two-phase flow.

Islama et al. [133] examined natural convection phenomenon in what is regarded as a mechanical chamber, a triangle cage. The flow is unstable, and the bottom of the triangle has a sinusoidal heat source that is filled with nanofluid CNT-water. The Galerkin finite element method (GFEM) is used to verify the governing equations. They found the thermal and fluid acts of the fluid, such as temperature gradients, pressure gradient amplitude, overall temperature, mean fluid temperature, and velocity amplitude, all increase significantly as Ra increases.

Hamida and Hatami [134] have examined a finned microchannel's geometry and made it more numerically applicable for nanofluid LED cooling. Al_2O_3-water was selected as the working fluid and employed as the nanofluid cooling flow in the commercial code COMSOL-Multiphysics. numerically utilizing the finite element method (GFEM) of Galerkine-weighted residual. They found fin length had the greatest effect on the number of Nusselt nanoparticles, and Al_2O_3 with $\varphi = 0.05$ reported the greatest heat transfer value; The temperature of the nanofluid increased by up to 6.5% as a result of various fin device designs, improving the LED cooling process.

Ishak et al. [135] used the finite element method to quantitatively analyze mixed convection and entropy generation in a trapezoidal cavity containing an Al_2O_3-water nanofluid with a localized solid cylinder.They found Increasing Richardson and Reynolds numbers increase the heat transfer rate as well as the nanoparticle volume fraction due to increased buoyancy and viscous forces; maximum mean Nusselt values are obtained for high R values.

Hamzah et al. [136] investigated, in a magnetic field, mixed convection with entropy formation in a porous corrugated lid enclosure filled with CNT-water nanofluid. using the Galerkin finite element method, or GFEM. They found that Because of the natural convection

effect, raising the Ri greatly raises the Nu number; Additionally, a higher Darcy number results in a more porous effect on heat transport, which raises the Nu number; Heat transfer is reinforced by the presence of a corrugated wall, which raises the Nusselt number. This reinforcement rises as the number and amplitude of corrugations increase.

Khan et al. [137] have numerically calculated stable hybrid alloy nanoparticles AA7075 and AA7072 whose Boundary layer flow is considered towards a thinly moving needle under Dufour and Soret limitations and severe radiation consequences. The MATLAB software's built-in function, bvp4c, is used to solve the converted ordinary differential equations numerically. They found a Nusselt number increase in the presence of hybrid nanoparticles.

The convection of carbon nanotube-water nanofluid in a three-dimensional cavity under a magnetic field has been numerically explored by Gal et al. [138].
The finite element approach is applied to solve the three-dimensional governing equations. It is based on Galerkin's weighted residue methodology. They found the use of nanoparticles can improve the heat transfer rate by 100% and increase entropy production by 30%; Viscous entropy is reduced when the fin angle is increased, while thermal and magnetic entropies are increased; The temperature and flux fields alter significantly when the fins angle is increased.

Karagiannakis et al. [139] have numerically examined the natural laminar and convective flow of a nanometer of Al_2O_3 -water in a rectangular porous container with a magnetic field present.Darcy-Brinkman momentum equations with buoyancy and advective inertia are applied in the suggested model. They found that magnetic field strength is important for temperature and temperature distributions; Under certain circumstances, the presence of nanoparticles reduces the efficiency of heat transfer.

Munawar et al. [140] discussed the mixed convection of Ag -MgO /water hybrid nanofluid under a uniform magnetic field in a square enclosure with a circular heater. The governing equations are normalized using an appropriate set of variables and solved with the finite element method. We find: Increasing concentrations of nanoscopic hybrid particles lead to an increase in Nuavg at the central heater for mixed convection; heat transport increases as the percentage volume fraction of nanoscopic hybrid particles improves in the case of forced convection, but there is no sign of free convection.

Lu et al. [141] studied the heat flux, entropy production, and heat transfer properties of a dissipative Fe_3O_4–CuO /H_2O nanofluid in the presence of boundary transpiration effects. The problem is mathematically modeled using the concept of Tiwari and Dass. We find: The solid volume fraction (φ) and the Eckert number are intimately correlated with the entropy generation number; Entropy generation by non-conservative forces is higher in the Fe_3O_4 - H_2O nanoliquid than in the CuO -H_2O nanoliquid; the velocity of the CuO -H_2O nanofluid is greater than that of the Fe_3O_4 -H_2O nanofluid; Compared to the CuO-H_2O nanoliquid, the Fe_3O_4-H_2O nanoliquid has a wider thermal boundary layer.

Mukherjee et al. [142] studied Heat transfer by turbulent forced convection and formation of entropy in an Al_2O_3-glycol (EG) nanofluid in a circular tube with a constant wall temperature. The main goal of the study is to create an analytical framework for simulating the properties of nanofluids in the thermal system in question using mathematical models. We find: Increasing nanoparticle addition increases entropy generation; by increasing Re, entropy generation increased.

Islam et al. [143] numerically studied the uneven free convective heat transfer between copper and water in a square container where the non-uniform horizontal periodic magnetic effect predominates. The Galerkina-type FEP model was used in monetary analyses of nonlinear PDEs. They found The nanoparticle size significantly improves the heat transfer rate; The stability of the nanoparticle is significantly influenced by its diameter; The heat transfer rate is greater for smaller nanoparticle sizes.;The highest heat transfer is obtained for Fe_3O_4-water and Cu-water nanofuids compared to nano-water nanofuids.

Asmadi et al. [144] have numerically investigated the buoyancy heat transfer of Cu -Al_2O_3 /water hybrid nanofluid in a U-shaped housing under the influence of cavity tilt. The problem is calculated and solved using Galerkin's weighted residual approach in conjunction with the finite element method. The Newton-Raphson method is used as the convergence criterion for each iteration. They found the replacement of some metal oxide nanoparticles by metal nanoparticles increases the heat transfer performance inside the enclosure; The enclosure's internal heat transmission rate is enhanced by the hybrid nanofluid.

Barhoi et al. [145] have numerically investigated the natural convection method of heat transport in a square enclosure filled with nanofluid. The enclosure's inside is designed to

mimic natural convection using the nanofluids Cu-water, Al_2O_3-water, and TiO_2-water. This numerical issue was solved using the commercial CFD program ANSYS-FLUENT, with the governing differential equations discretized using a control volume technique. They found that with a Heat transmission rate increases as flow rate increases due to an increased volume fraction of nanoparticles; the flow patterns are nearly identical with a constant Rayleigh number and an increasing volume fraction; however, the Nusselt number rises.

Islam et al. [146] studied A Cu-H_2O nanofluid-loaded right-angled triangular cavity with two-dimensional time-independent free convective flow and temperature flow. Galerkin's weighted residual finite element method's robust PDE solver was utilized to numerically solve the dimensionless nonlinear PDEs. With the weighted residual finite element analysis of Galerkin. They found that additional nanoparticles significantly enhance the temperature flux; the Rayleigh number has a major impact on the flow field and temperature transfer value.

Ali et al. [147] numerically studied mixed convection in a rectangular cavity with a lid filled with Al_2O_3 –Cu /Water hybrid nanofluid utilizing the SIMPLE algorithm and the finite volume approach. They found that heat transfer is higher in nano-fluids than in pure water and is maximal in the case of Al_2O_3 -Cu / Water hybrid nanofluids; Heat transfer is increased when the volume fraction is raised; increasing the Reynolds number increases heat transfer.

Transient forced HNF flow and heat transfer in a three-dimensional annulus with hot and cold rods were studied by Goldanlou et al. [148]. via symmetry simulation. The study's primary objective is to model the geometry using a symmetry scheme and investigate how the thermal and hydraulic properties are affected by different Reynolds numbers, emissivity coefficients, and nanoparticle volume fractions. They found that for the model at Re = 3000 and $\varphi_1 = 0.05$, all studied cases with different base fluids have similar behavior. For all studied cases, the total Nu_{ave} reduces firstly by an increment of the volume concentrations of Cu nanoparticles until φ_2 = 0.01 or 0.02 and then, the total Nu_{ave} rises by an increment of the volume concentrations of Cu nanoparticles; By increment of Reynolds numbers, the Nu_{ave} augments.

Al-Farhany et al. [149] numerically investigated natural convection in a square enclosure with a vertical baffle fixed to the bottom wall and nanofluid Cu-water subjected to sinusoidal temperature on the vertical walls. They found Because of the enhanced buoyant strength and thermal conductivity caused by the higher Rayleigh number and nanofluid concentration, the

Nusselt number increased; At large Rayleigh numbers, the circulation cores corresponding to nanofluids exhibited greater strength than those of pure water; Because of the strong heat transfer via the baffle, which could be transported to the cavity without the baffle's influence, the Nusselt number grew as the thermal conductivity ratio increased.

II.3. Conclusion:

We provide a review of recent works that are available in the literature in this chapter. in order to comprehend the study of forced, mixed, and natural convection with hybrid nanofluid. We have been able to determine the different parameters that can affect the thermal behavior of heat transfer by analyzing these investigations, and the inclusion of nanoparticules within heat transfer fluids has shown an appreciable improvement in heat transfer.

CHAPTER III:

MATHEMATICAL MODEL AND NUMERICAL PROCEDURE

III.1. INTRODUCTION:

Despite the long history of research on convection heat transfer, this form of heat transfer is still the most popular due to its numerous industrial uses. However, because of their elegant thermal characteristics, nanofluids are gaining a lot of attention for their application as heat transfer fluids.

To evaluate the potential for enhancing heat transfer in such thermal conditions, a full scientific knowledge of the mechanisms involved in temperature gradient-induced flows in confined spaces in the presence of nanofluids is therefore necessary. The dependency of the dynamic and thermal fields on the confinement effect and the thermodynamic parameters of the nanofluid make these flows appear simple, but they are actually very complex. It takes the application of numerical instruments designed for the study of such events to master these intricate flows.

The first part, we present a two-dimensional (2-D) (Heat Exchanger) investigation with COMSOL Multiphysics in this chapter. We first discuss the general forms of the equations regulating the flow. Then, creating the required mesh, and selecting the proper boundary conditions.

The second part describes the steps involved in creating a (3-D) geometric model (Shell/ Tube Heat Exchanger), creating the required mesh, and selecting the proper boundary conditions. It also describes the finite element method that the "COMSOL Multiphysics" software utilized to resolve the equation system. This software was used to do a three-dimensional numerical simulation.

III.2. BASIC MATHEMATICS:

Differential equations, which serve as models for physical phenomena, are frequently used to formulate any given physical phenomenon. The behavior of a phenomenon in space must be expressed in a model. These equations are based on the concepts of mass conservation, momentum conservation (Navier-Stokes equations), energy conservation, and entropy generation.

III.2.1. Continuity equation:

This equation expresses the mass conservation principle. Tensorily, it can be expressed as follows: [150]

$$\frac{\partial(\rho u_j)}{\partial x_j} = 0 \qquad \text{III.1}$$

III.2.2. Equation of momentum:

The principle of conservation of momentum establishes the relationship between the characteristics of the fluid as it moves and the causes that produce it. It asserts that the total of all external forces acting on the control volume equals the rate of change of momentum in the control volume. It can be written in tensor form as follows: [150]

$$\frac{\partial(\rho u_i v_j)}{\partial x_j} = \rho g_i - \frac{\partial p}{\partial x_i} + \frac{\partial}{\partial x_j}\left(\mu \frac{\partial u_i}{\partial x_j}\right) \qquad \text{III.2}$$

$\frac{\partial(\rho u_i v_j)}{\partial x_j}$: Represents the net rate of momentum transport in direction i per fluid movement.

ρg_i : Represents volume forces in the i direction.

$\frac{\partial p}{\partial x_i}$: Represents forces due to pressure.

$\frac{\partial}{\partial x_j}\left(\mu \frac{\partial u_i}{\partial x_j}\right)$: Represents net viscosity forces

(j : indice de somme, = 1∼3).

(i : indice de direction, = 1∼3).

III.2.3. Energy equation:

The fundamental principle of thermodynamics yields the equation for energy conservation for an incompressible Newtonian fluid [150]. This is how the energy equation is represented:

$$\rho c_p \frac{\partial (u_j T)}{\partial x_j} = \frac{\partial}{\partial x_j}\left(k \frac{\partial T}{\partial x_j}\right) + \dot{q} + \mu\Phi \qquad \text{III.3}$$

$\boldsymbol{k}$: Thermal conductivity

C_p: Heat capacity
ρ: Fluid density
$\dot{q}$: Volumetric heat density
μ: Dynamic viscosity
Φ: Viscous dissipation

III.3. NUMERICAL METHODOLOGY:

This section describes the numerical method used to investigate the constrained natural convection problem, in which a nanofluid serves as the energy vector. The primary goal of numerical CFD (computational fluid dynamics) simulations of flow and heat transfer has been to measure the rate at which nanofluids promote heat transfer. The simulation is implemented via the COMSOL Multiphysics calculation code, which offers a wide range of options for setting up the cases to be studied (calculation and post-processing).

Using the Galerkin finite element method, the conservation equations are discretized across the computation domain (FEM). The domain of computing is divided into a suitable smaller mesh structure. By using piecewise cubic polynomials in the function space, the computational domain is discretized. All of the relevant hydrothermal boundary layers that are closer to the walls are accurately represented since the necessary mesh components are placed in this way. The mesh independence research is used to choose the element size.

The iterative method of computing the elemental equations yields a final solution with a convergence criterion of 10^{-8}. The solved data is then stored for post-processing, which creates the local and global data.

III.3.1. Finite element method (FEM):

One of the best techniques for the numerical solution of partial differential equations is the Finite Element Method (FEM). The majority of real-world issues, whether they are stationary or time-dependent, linear or non-linear, are described in a complicated geometric domain, and regardless of the operational circumstances, they can be addressed by it. As seen in the graphic below, the finite element method discretizes space using basic geometric elements, such as triangles or quadrangles in general. Next, the equations' strong form is swapped out for their weak form, where the unknowns are represented by a linear combination of basis functions whose support is one of the elements [151–153].

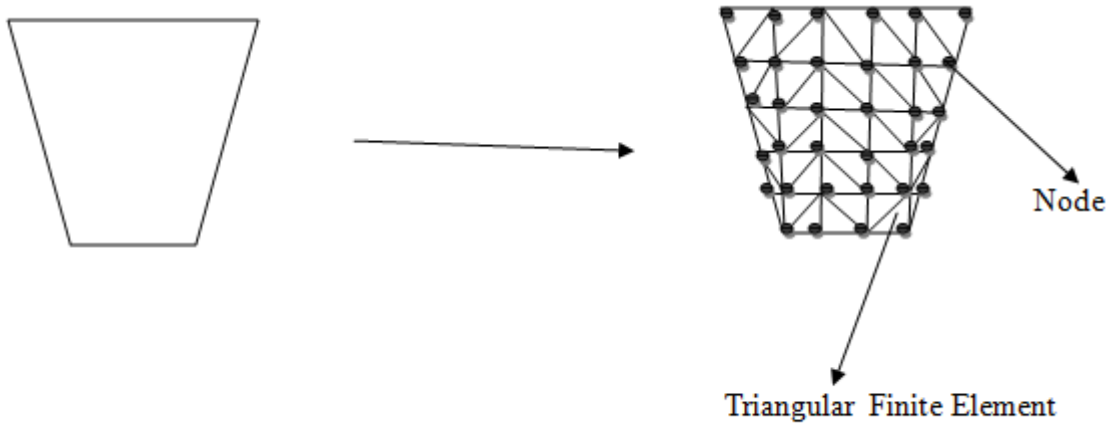

Figure (III.1): Discretization and calculation elements using the finite element method

III.3.2. Advantages and disadvantages:

Even in complex geometries and in real working conditions, the finite element method is a powerful tool for solving partial differential equations. Using simple geometric elements (triangles or quadrangles in general), the finite element technique discretizes space. Then, the weak form of the equations replaces the strong form, and the unknowns are approximated by a linear combination of functions, one of which is the support. This method's delicate implementation is its drawback [154].

III.3.3. Synthesis:

Fortunately, advancements in computer science have corresponded with the growth of numerical techniques (finite differences, finite volumes, finite elements, boundary integrals, etc.). Programs that once needed sophisticated, costly computers can now be run on

inexpensive PCs. This has made software development easier. In this work, there was a temptation to use COMSOL Multiphysics software to solve the partial differential equations using the finite element method because the global problem resolution is very complex due to the interactions between different phenomena occurring within the aqueous electrolyte to be desalinated. This software's multiphysics capability was built in from the ground up, enabling the user to quickly and simply mix models that depict various physical phenomena however they see fit. In certain situations, the user will need to model and integrate his program into the basic software, but in other situations, this can be accomplished by utilizing the built-in features of the program [154].

III.4. CONFIGURATION 2-D:

III.4.1. Case 1: 2D Shell / Tube Heat Exchanger

III.4.1.1. Geometry 1:

Figure (II.2) depicts a schematic representation of a two-dimensional typical tube/shell heat exchanger. The real perspective of a tube/shell heat exchanger part from RA2K SONATRACH Skikda, Algeria is depicted in Figures (III.3) and (III.4). Figure (III.3) also displays an expanded image of a tube together with its several modified shapes (circular, square, rectangular, and diamond). The fundamental form, which is circular, is used to compare any improvements in heat transport that may have occurred. A quarter of the two tubes and half of a tube bundle make up the computational domain. The tube bundles are thought to be made of aluminum. The water-based Al_2O_3-MWCNT hybrid nanofluid transfers heat from the heated fluid passing through the variously shaped tubes by passing through the spaces between the tube bundles. The goal of this work is to use the hybrid nanofluid Al_2O_3-MWCNT to model a shell and tube heat exchanger in order to enhance the cooling fluid's heat transfer.

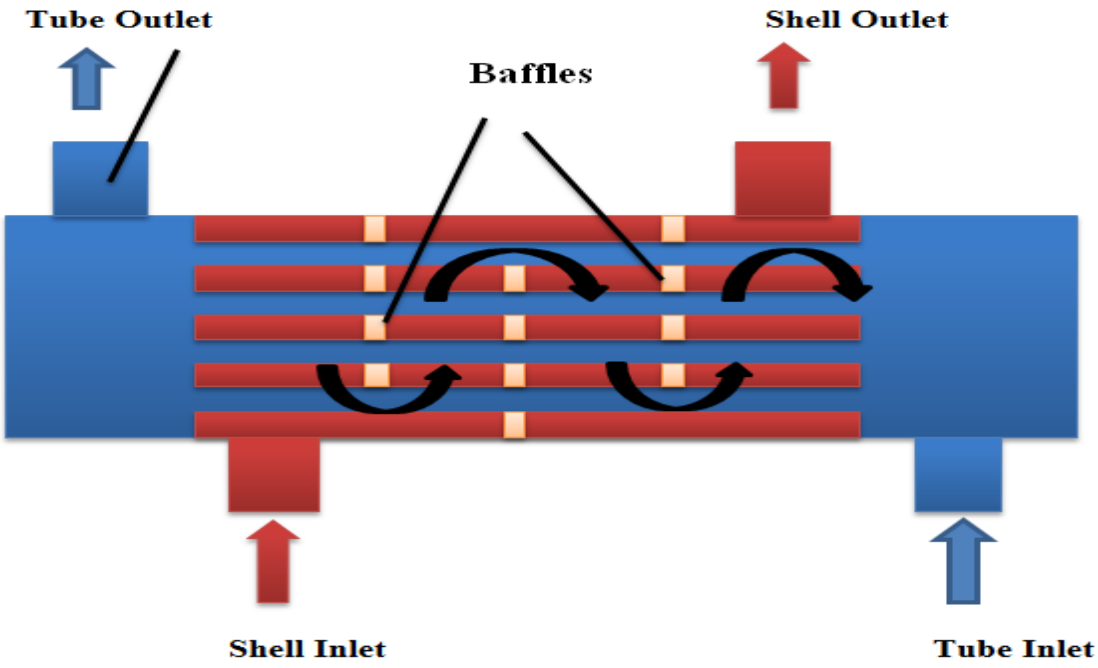

Figure (III.2): Schematic representation of a conventional tube/shell heat exchanger.

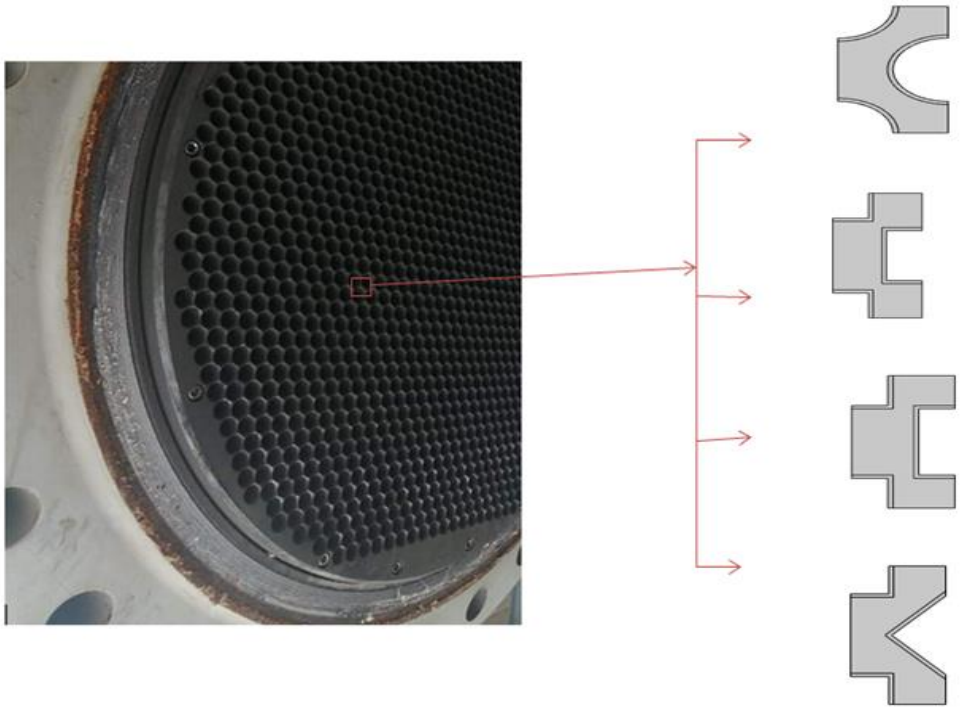

Figure (III.3): Tube/shell heat exchanger section from Refinery 2 Sonatrach Skikda RA_2K

Figure (III.4): Tube/shell heat exchanger from Refinery 2 Sonatrach Skikda RA_2K

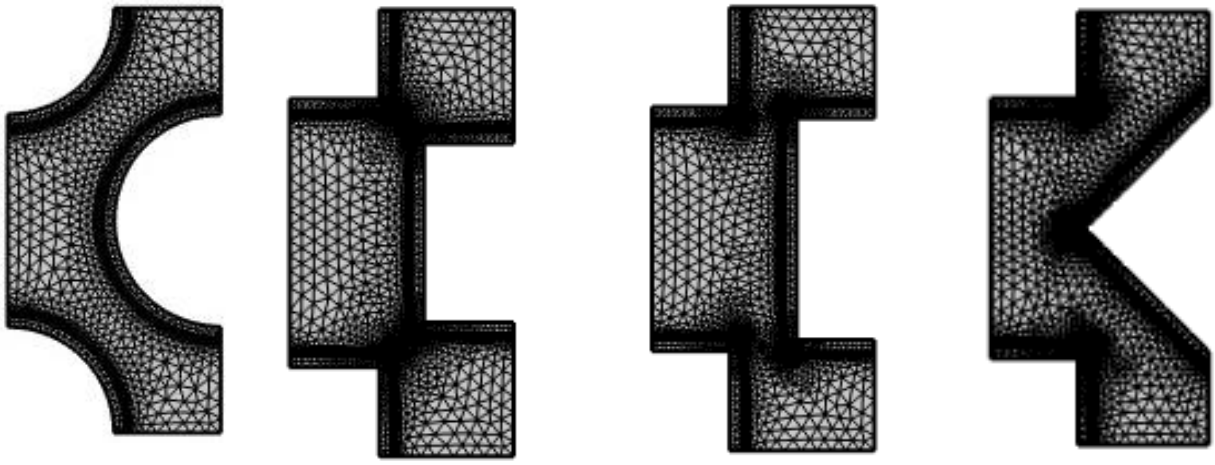

Circular tube **Square tube** **Rectangular tube** **Diamond tube**

Figure (III.5): Mesh of a Tube/Shell Heat Exchanger with Different Shapes of Manufacturing Tubes

III.4.1.2. Geometry 2:

In this work, a Shell / Tube Heat Exchanger filled with a Cu-Fe_3O_4-MWCNT/Water Tri hybrid nanofluid was studied numerically for heat transmission and regular turbulent forced convection. The governing equations are checked using Galerkin's finite element method (GFEM).

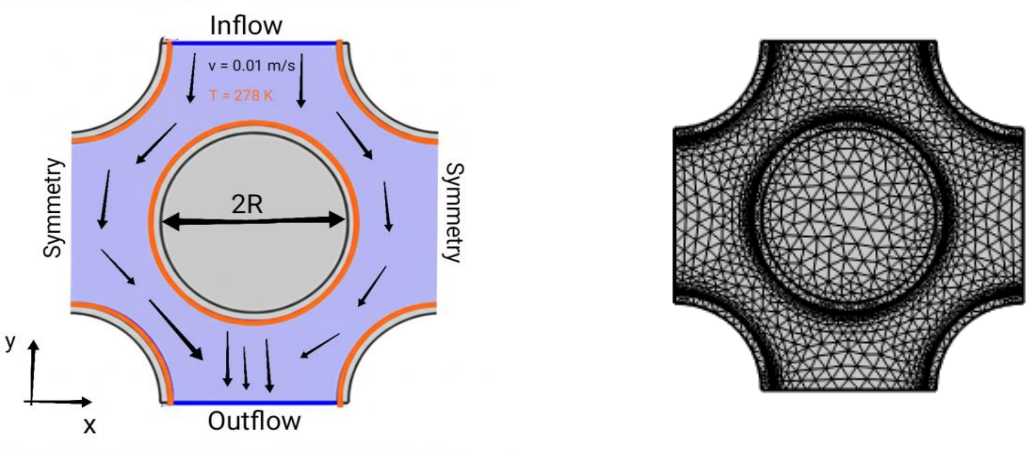

(a) (b)

Figure (III.6): The computational domain (a) 2D view of the geometry, (b) grid mesh.

III.4.1.3. Mathematical model and equations:

Numerical solutions are found for the leading equations pertaining to continuity, momentum, and energy. This mathematical model is solved using the k-ε turbulent flow model [155–156], and the expression is as follows:

$$\frac{\partial u}{\partial t} + \rho(u.\nabla)u = \nabla.[-pI + K] + F \qquad \text{III.4}$$

$$\frac{\partial \rho}{\partial t} + \nabla.(\rho u) = 0 \qquad \text{III.5}$$

where:

$$K = \left(\mu + \mu_T\right)(\nabla u + (\nabla u)^T) - \frac{2}{3}\left(\mu + \mu_T\right)(\nabla . u)I - \frac{2}{3}\rho k I \quad \text{III.6}$$

$$\rho c_p \left(\frac{\partial T}{\partial t} + u\,.\ \nabla T\right) + \nabla.(q + q_r) = \beta T \left(\frac{\partial p}{\partial t} + u\,.\ \nabla p\right) + \tau : \nabla u + Q \quad \text{III.7}$$

$$\beta = -\frac{1}{\rho}\frac{\partial \rho}{\partial T} \quad \text{III.8}$$

$$Q_p = \beta T \left(\frac{\partial p}{\partial t} + u\,.\ \nabla p\right) \quad \text{III.9}$$

The fluid's viscous dissipation is represented by the second term:

$$Q_{vd} = \tau : \nabla u \quad \text{III.10}$$

We can write the following for the turbulent kinetic energy:

$$\rho \frac{\partial k}{\partial t} + \rho(u.\nabla)k = \nabla.\left[\left(\mu + \frac{\mu_T}{\sigma_k}\right)\nabla k\right] + p_k - \rho\mathcal{E} \quad \text{III.11}$$

For dissipation:

$$\rho \frac{\partial \mathcal{E}}{\partial t} + \rho(u.\nabla)\mathcal{E} = \nabla.\left[\left(\mu + \frac{\mu_T}{\sigma_\mathcal{E}}\right)\nabla \mathcal{E}\right] + C_{\mathcal{E}1}\frac{\mathcal{E}}{k}p_K - C_{\mathcal{E}2}\rho\frac{\mathcal{E}^2}{k} \quad \text{III.12}$$

where: $\mathcal{E} = ep$

For turbulent viscosity:

$$\boldsymbol{\mu_T} = \rho C_\mu \frac{k^2}{\mathcal{E}} \quad \text{III.13}$$

Les constates utilisées dans les équations de viscosité turbulente, d'énergie cinétique turbulente, et de dissipation sont fixé :$C_{\mathcal{E}1} = 1.44, C_{\mathcal{E}2} = 1.92, \delta_k = 1, C_\mu = 0.09, \delta_\mathcal{E} = 1.3$

La production d'énergie cinétique turbulente peut être exprimée comme suit :

The following are fixed coefficients for turbulent kinetic energy, dissipation, and viscosity:

$$C_{\varepsilon 1} = 1.44, C_{\varepsilon 2} = 1.92, \delta_k = 1, C_\mu = 0.09, \delta_\varepsilon = 1.3$$

The turbulent kinetic energy output can be stated as:

$$P_K = \boldsymbol{\mu_T}\left[\nabla u : (\nabla u + (\nabla u)^T) - \frac{2}{3}(\nabla . u)^2\right] - \frac{2}{3}\rho k \nabla . u \quad \text{III.14}$$

The Reynolds number is used to nondimensionalize the flowing fluid's velocity:

$$Re = \frac{\rho u D}{\mu} \quad \text{III.15}$$

Both local and global heat transfer are used to assess the heat transfer properties using the Nusselt number (Nu):

$$Nu_{loc} = \frac{k_{hnf}}{k_{bf}}\frac{\partial T}{\partial y} \quad \text{III.16}$$

$$Nu_{avg} = \frac{1}{L}\int_0^L Nu_{loc} dL \quad \text{III.17}$$

III.4.1.4. Modeling of hybrid nanofluid:

The working fluid used in this study (Geometries 1) is an Al_2O_3-MWCNT hybrid nanofluid, which is essentially a suspension of MWCNT and Al_2O_3 nanoparticles in water, the base fluid, in accordance with the mixture rules [156]. For the current thermal-hydrodynamic study, a hybrid nanoparticle mixture consisting of MWCNT and Al_2O_3 has been used.

Overall, Al_2O_3 exhibits lower thermal and electrical conductivities in comparison to MWCNT. However, Al_2O_3 has lower conductivities than MWCNT. As a result, greater conductivities much higher than the base liquid are produced through the combination (hybrid) production of MWCNT and Al_2O_3 nanoparticles. In this regard, it's important to note that the flow of hybrid nanofluids in heat exchanger devices is a relatively new field; as such, further study can provide a deeper comprehension of it, which is necessary for practical implementations [156]. The thermo-physical characteristics of the base fluid (water) and the Al_2O_3 and MWCNT nanoparticles are listed in Table (III.1). However, a number of recent studies have examined MWCNT-Al_2O_3-water hybrid nanofluid, suggesting a broad range of its potential uses and dependability. It encourages us to select MWCNT-Al_2O_3-water hybrid nanofluid as the study's working fluid. The volume fraction of the hybrid nanoparticles is

represented by the sign φ. The standard correlations, which can be written as follows, are used to estimate the parameters of the hybrid nanofluid:

$$\varphi = \varphi_{Al_2O_3} + \varphi_{MWCNT}$$

$$\rho_{np} = \frac{\varphi_{Al_2O_3}\rho_{Al_2O_3} + \varphi_{MWCNT}\rho_{MWCNT}}{\varphi}$$

$$\left(C_p\right)_{np} = \frac{\varphi_{Al_2O_3}\left(C_p\right)_{Al_2O_3} + \varphi_{MWCNT}\left(C_p\right)_{MWCNT}}{\varphi} \quad \text{III.18}$$

$$\beta_{np} = \frac{\varphi_{Al_2O_3}\beta_{Al_2O_3} + \varphi_{MWCNT}\beta_{MWCNT}}{\varphi}$$

$$k_{np} = \frac{\varphi_{Al_2O_3}k_{Al_2O_3} + \varphi_{MWCNT}k_{MWCNT}}{\varphi}$$

$$\sigma_{\boldsymbol{np}} = \frac{\varphi_{Al_2O_3}\sigma_{Al_2O_3} + \varphi_{MWCNT}\sigma_{MWCNT}}{\varphi}$$

Hybrid Nanofluid :

$$\sigma_{hnf} = (1-\varphi)\sigma_{bf} + \varphi\sigma_{np}$$

$$\rho_{hnf} = (1-\varphi)\rho_{bf} + \varphi\rho_{np}$$

$$(\rho\beta)_{hnf} = (1-\varphi)(\rho\beta)_{bf} + \varphi(\rho\beta)_{np}$$

$$\left(\rho C_p\right)_{hnf} = (1-\ \varphi)\left(\rho C_p\right)_{bf} + \varphi\left(\rho C_p\right)_{np}$$

$$\alpha_{hnf} = \frac{k_{hnf}}{\left(\rho C_p\right)_{hnf}}(12)$$

$$\frac{k_{hnf}}{k_{bf}} = \frac{k_{np} + (n-1)k_{bf} - (n-1)\left(k_{bf} - k_{np}\right)\varphi}{k_{np} + (n-1)k_{bf} + \left(k_{bf} - k_{np}\right)\varphi}$$

$$\mu_{hnf} = \frac{\mu_{bf}}{(1-\varphi)^{2.5}}$$

$$\frac{\sigma_{hnf}}{\sigma_{bf}} = 1 + \frac{3(\sigma_{np} - \sigma_{bf})\varphi}{(\sigma_{np} + 2\sigma_{bf}) - (\sigma_{np} - \sigma_{bf})\varphi}$$

Tri hybrid nanofluid:

$$\rho_{thnf} = (1-\varphi_1)\{(1-\varphi_2)[(1-\varphi_3)\rho_f + \rho_3\varphi_3] + \rho_2\varphi_2\} + \rho_1\varphi_1$$

$$\mu_{thnf} = \frac{\mu_f}{(1-\varphi_1)^{2.5}(1-\varphi_2)^{2.5}(1-\varphi_3)^{2.5}}$$

$$\frac{k_{thnf}}{k_{hnf}} = \frac{k_1 + 2k_{hnf} - 2\varphi_1(k_{hnf} - k_1)}{k_1 + 2k_{hnf} + \varphi_1(k_{hnf} - k_1)}$$

Where:

$$\frac{k_{hnf}}{k_{nf}} = \frac{k_2 + 2k_{nf} - 2\varphi_2(k_{nf} - k_2)}{k_2 + 2k_{nf} + \varphi_2(k_{nf} - k_2)}$$

And:

$$\frac{k_{nf}}{k_f} = \frac{k_3 + 2k_f - 2\varphi_3(k_f - k_3)}{k_3 + 2k_f + \varphi_3(k_f - k_3)}$$

$$(\rho C_p)_{thnf} = (1-\varphi_3)\left\{(1-\varphi_2)\left[(1-\varphi_1)(\rho C_p)_f + \varphi_1(\rho C_p)_{S1}\right] + \varphi_2(\rho C_p)_{S2}\right\} + \varphi_3(\rho C_p)_{S3}$$

Table (III.1): Thermo-physical proprieties of the Al_2O_3-MWCNT/water Hybrid nanofluid [157-158].

	ρ (kg/m^3)	k (W/m k)	C_p (J/kg k)	σ(s/m)
$Water$	997.1	0.613	4179	5.5*10^-6
$MWCNT$	2100	3000	711	10^-7
Al_2O_3	3950	36.96	785.02	

We looked at the heat transfer characteristics of the hybrid nanofluid (Cu-Fe_3O_4-MWCNT/water) in the Shell/Tube Heat Exchanger (Geometries 2). Heat transport was examined in relation to various characteristics, including Rayleigh number and volume fraction. We also looked at isotherms, rationalities, and the mean Nusselt number. Table (III.2) reports the thermo-physical properties of the Cu+Fe_3O_4 + MWCNT nanoparticles and the base fluid (water).

Table (III.2): Thermo-physical properties of Nanoparticules Ag-Cu-Fe_3O_4-MWCNT/Water [159,160]

	ρ(kg/m^3)	k (W/m k)	C_p (J/kg k)	σ(s/m)
Water	997.1	0.613	4179	5.5*10^-6
$MWCNT$	2100	3000	711	10^-7
Fe_3O_4	5180	9.6	670	25,000
Cu	8954	400	385	59.6*10^-6
Ag	10500	429	235	

III.4.1.5. The Total Entropy and Efficiency:

The entropy generation technique integrates the ideas of thermodynamics, the fundamental laws of heat transfer, and fluid mechanics. Entropy generation, a measure of a system's imperfections, is defined as a combination of the entropy produced by viscous fluid effects and that produced by thermal effects.

$$S_{tot} = \frac{k}{(T_{avg})^2}\left[\left(\frac{\partial\theta}{\partial x}\right)^2 + \left(\frac{\partial\theta}{\partial y}\right)^2\right] + \frac{\mu_{nf}}{T_{avg}}\left[\frac{\varepsilon_p}{k}(u^2+v^2) + 2\left(\frac{\partial u}{\partial x}\right)^2 + 2\left(\frac{\partial v}{\partial y}\right)^2 + \left(\frac{\partial u}{\partial y}+\frac{\partial v}{\partial x}\right)^2\right] + \frac{\sigma_{nf}}{T_{avg}}\beta^2 v \quad \text{III.19}$$

$$T_{avg} = \frac{T_{inlet} + T_{tube}}{2}$$

$$\mathcal{E} = \frac{q}{q_{max}} = \frac{q}{C_{min}(T_{inlet} - T_{tube})} \quad \text{III.20}$$

$$q = UA\Delta T_{ml} \quad \text{III.21}$$

$$\Delta T_{ml} = \frac{\Delta T_1 - \Delta T_2}{ln(\Delta T_1 / \Delta T_2)}$$

$$\boldsymbol{\Delta T_1 = T_{hot,in} - T_{cold,out}} \qquad \boldsymbol{\Delta T_2 = T_{hot,out} - T_{cold,in}}$$

III.4.1.6. Simplifying hypotheses:

In order to establish the simplified mathematical model governing natural convection in a nanofluid, we have adopted the following assumptions:

1: Nanofluid flow is assumed to be time dependent, turbulent, and two-dimensional.

2: The nanofluid is assimilated into an incompressible Non-Newtonian fluid.

III.4.1.7. Boundary conditions:

The following are the boundary conditions used in this study:

- Symmetry (insulation against heat) at the boundaries of the area.
- Fixed inlet temperature T = 285 K with speed *v* = 0.01 m/s.
- T=278K, the set temperature at the tube's inner surfaces.
- Convection dominated movement at the exit.
- Tube material: aluminum

III.4.2. Case 2: Zigzage walled cavity

III.4.2.1. Geometry 3:

In this work, natural convection heat transport has been studied numerically in a zigzag-walled enclosure with a cylinder occupied by a MgO-SWCNT/water hybrid nanofluid.

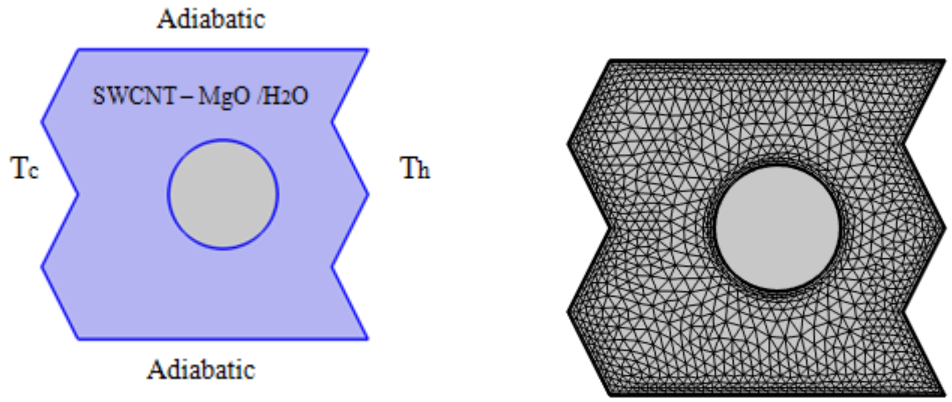

(a) (b)

Figure (III.7): The computational domain (a) 2D view of the geometry, (b) grid mesh.

III.4.2.2. Simplifying hypotheses:

In order to establish the simplified mathematical model governing natural convection in a nanofluid, we have adopted the following assumptions:

1: It is considered that the flow of nanofluids is two-dimensional, laminar, and stationary.

2: The nanofluid is assimilated into an incompressible Non-Newtonian fluid.

III.4.2.3. Mathematical model and equations:

Continuity equation:

$$\frac{\partial u}{\partial x} + \frac{\partial v}{\partial y} = 0 \qquad \text{III.22}$$

X-momentum:

$$\rho_{nf}\left(u\frac{\partial u}{\partial x}+v\frac{\partial u}{\partial y}\right)=-\frac{\partial P}{\partial x}+\mu_{nf}\left(\frac{\partial^2 u}{\partial x^2}+\frac{\partial^2 u}{\partial y^2}\right) \quad \text{III.23}$$

Y-momentum:

$$\rho_{nf}\left(u\frac{\partial v}{\partial x}+v\frac{\partial u}{\partial y}\right)=-\frac{\partial P}{\partial y}+\mu_{nf}\left(\frac{\partial^2 v}{\partial x^2}+\frac{\partial^2 v}{\partial y^2}\right)+\rho_{nf}\beta_{nf}g(T-T_c)-\delta_{nf}B^2 v \quad \text{III.24}$$

Energy equation:

$$(\rho C_p)_{nf}\left(u\frac{\partial T}{\partial x}+v\frac{\partial T}{\partial y}\right)=k_{nf}\left(\frac{\partial^2 T}{\partial x^2}+\frac{\partial^2 T}{\partial y^2}\right) \quad \text{III.25}$$

$$X=\frac{x}{L}\ ;Y=\frac{y}{L}\ ;U=\frac{u}{U_0}\ ;V=\frac{v}{U_0}\ ;P=\frac{p}{\rho_{nf}U_0^2}\ ;p_r=\frac{\upsilon_{bf}}{\alpha_{bf}}$$

$$Ra=\frac{\beta_{bf}g(T_h-T_c)L^3}{\alpha_{bf}\upsilon_{bf}} \quad \text{III.26}$$

$$Nu_{loc}=\frac{k_{hnf}}{k_{bf}}\frac{\partial T}{\partial y} \quad \text{III.27}$$

$$Nu_{avg}=\frac{1}{L}\int_0^L Nu_{loc}dL \quad \text{III.28}$$

Nanofluid:

$$\varphi=\varphi_{MgO}+\varphi_{SWCNT} \quad \text{III.29}$$

$$\rho_{np}=\frac{\varphi_{MgO}\rho_{MgO}+\varphi_{SWCNT}\rho_{SWCNT}}{\varphi}$$

$$(C_p)_{np}=\frac{\varphi_{MgO}(C_p)_{MgO}+\varphi_{SWCNT}(C_p)_{SWCNT}}{\varphi}$$

$$\beta_{np}=\frac{\varphi_{MgO}\beta_{MgO}+\varphi_{SWCNT}\beta_{SWCNT}}{\varphi}$$

$$k_{np} = \frac{\varphi_{MgO} k_{MgO} + \varphi_{SWCNT} k_{SWCNT}}{\varphi}$$

$$\sigma_{\boldsymbol{np}} = \frac{\varphi_{MgO} \sigma_{MgO} + \varphi_{SWCNT} \sigma_{SWCNT}}{\varphi}$$

Hybrid nanofluid:

$$\sigma_{hnf} = (1-\varphi)\sigma_{bf} + \varphi\sigma_{np}$$

$$\rho_{hnf} = (1-\varphi)\rho_{bf} + \varphi\rho_{np}$$

$$(\rho\beta)_{hnf} = (1-\varphi)(\rho\beta)_{bf} + \varphi(\rho\beta)_{np}$$

$$\left(\rho C_p\right)_{hnf} = (1-\ \varphi)\left(\rho C_p\right)_{bf} + \varphi\left(\rho C_p\right)_{np}$$

$$\alpha_{hnf} = \frac{k_{hnf}}{\left(\rho C_p\right)_{hnf}}$$

$$\frac{k_{hnf}}{k_{bf}} = \frac{k_{np} + (n-1)k_{bf} - (n-1)\left(k_{bf} - k_{np}\right)\varphi}{k_{np} + (n-1)k_{bf} + \left(k_{bf} - k_{np}\right)\varphi}$$

$$\mu_{hnf} = \frac{\mu_{bf}}{(1-\varphi)^{2.5}}$$

$$\frac{\sigma_{hnf}}{\sigma_{bf}} = 1 + \frac{3(\sigma_{np} - \sigma_{bf})\varphi}{\left(\sigma_{np} + 2\sigma_{bf}\right) - \left(\sigma_{np} - \sigma_{bf}\right)\varphi}$$

We looked into the heat transfer characteristics of the hybrid nanofluid (MgO-SWCNT/water) in the square cavity.Heat transport was examined in relation to various characteristics, including Rayleigh number and volume fraction. We also looked at isotherms, rationalities, and the mean Nusselt number. Table (III.3) reports the thermo-physical properties of the MgO + SWCNT nanoparticles and the base fluid (water).

	ρ(kg/m^3)	k (W/m k)	C_p (J/kg k)	$\boldsymbol{\sigma}$(s/m)
Water	997.1	0.613	4179	5.5*10^-6
$SWCNT$	2600	6600	425	2.54^4
MgO	3560	45	955	5.392*10^-6

Table (III.3): Thermophysical properties of MgO-SWCNT /Water nanofluids [161,162]

III.5. CONFIGURATION 3-D:

III.5.1. Geometries:

This study's convective motion is regarded as laminar, three-dimensional, and steady.

The computational domain and related boundary conditions are depicted in Figure (III.9), which also contains media saturated with hybrid nanoliquids. The lateral sides are made of Aisi steel, and the tube material is aluminum. Ag, Fe_3O_4 and MWCNT nanoparticles are combined with water, which serves as the basis liquid for the working suspensions. Table (III.2) provides a summary of the thermo-physical properties of the fluide base and nanoparticles.

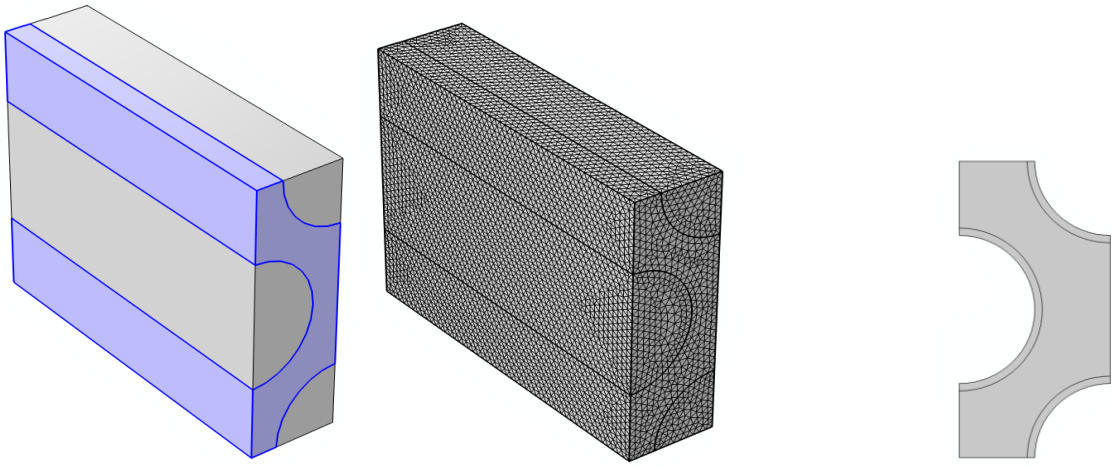

(a) (b) (c)

Figure (III.9): The computational domain (a) 3D view of the geometry, (b) grid mesh and (c) 2D view of the geometry.

III.5.2. Simplifying hypotheses:

In order to establish the simplified mathematical model governing natural convection in a nanofluid, we have adopted the following assumptions:

1: It is assumed that the flow of nanofluid is three-dimensional, Turbulent.

2: The nanofluid is assimilated into an incompressible Non-Newtonian fluid.

III.5.3. Boundary conditions:

The following are the boundary conditions used in this study:

- Symmetry (insulation against heat) at the boundaries of the area.
- Fixed inlet temperature T = 330 K with speed *v* = 0.05 m/s.
- A constant temperature of T=385K at the tube's inner surfaces.
- Convection dominated movement at the exit.
- Tube material: aluminum

III.5.4. Mathematical model and equations:

The problem was solved by applying the laminar flow model. The Navier-Stokes equations are the fundamental equations used by COMSOL Multiphysics to solve fluid flow models [164–166] in the following ways:

The equation of momentum:

$$\rho \frac{D\vec{V}}{Dt} = \Delta . \sigma + F \qquad \text{III.30}$$

$\boldsymbol{\sigma}$ the stress tensor, where F is the total of the many gravitational forces influencing the cube $\vec{V} = u\vec{\imath} + v\vec{\jmath} + w\vec{k}$ fluid velocity vector. On the other hand, the stress tensor is a symmetrical rank-two tensor, and its covariant components the shear stresses and the normal stresses, $\boldsymbol{\sigma}$ can be described mathematically as follows:

$$\sigma_{ij} = \begin{pmatrix} \sigma_{xx} & \tau_{xy} & \tau_{xz} \\ \tau_{yx} & \sigma_{yy} & \tau_{yz} \\ \tau_{zx} & \tau_{zy} & \sigma_{zz} \end{pmatrix} \qquad \text{III.31}$$

$$\sigma_{ij} = \begin{pmatrix} \sigma_{xx} & \tau_{xy} & \tau_{xz} \\ \tau_{yx} & \sigma_{yy} & \tau_{yz} \\ \tau_{zx} & \tau_{zy} & \sigma_{zz} \end{pmatrix} = -\begin{pmatrix} p & 0 & 0 \\ 0 & p & 0 \\ 0 & 0 & p \end{pmatrix} + \begin{pmatrix} \sigma_{xx} + p & \tau_{xy} & \tau_{xz} \\ \tau_{yx} & \sigma_{yy} + p & \tau_{yz} \\ \tau_{zx} & \tau_{zy} & \sigma_{zz} + p \end{pmatrix}$$

$$-\begin{pmatrix} p & 0 & 0 \\ 0 & p & 0 \\ 0 & 0 & p \end{pmatrix} + \begin{pmatrix} \sigma_{xx} + p & \tau_{xy} & \tau_{xz} \\ \tau_{yx} & \sigma_{yy} + p & \tau_{yz} \\ \tau_{zx} & \tau_{zy} & \sigma_{zz} + p \end{pmatrix} = -pI + \text{Ŧ}$$

$$p = -\frac{1}{2}(\sigma_{xx} + \sigma_{yy} + \sigma_{zz}) \quad \text{III.32}$$

$$I = \begin{pmatrix} 1 & 0 & 0 \\ 0 & 1 & 0 \\ 0 & 0 & 1 \end{pmatrix}$$

$$\text{Ŧ} = \begin{pmatrix} \sigma_{xx} + p & \tau_{xy} & \tau_{xz} \\ \tau_{yx} & \sigma_{yy} + p & \tau_{yz} \\ \tau_{zx} & \tau_{zy} & \sigma_{zz} + p \end{pmatrix}$$

Navier-Stokes equation:

$$\rho \frac{D\vec{V}}{Dt} = -\nabla p + \vec{\nabla}.\text{Ŧ} + F \quad \text{III.33}$$

demonstrates how to describe the deviatoric stress tensor Ŧ as follows:

$$\text{Ŧ} = \mu\left[\nabla\vec{V} + (\nabla\vec{V})^T\right] - \frac{2}{3}\mu(\vec{\nabla}.\vec{v}) \quad \text{III.34}$$

$$\vec{\nabla} = \frac{\partial}{\partial x}\vec{\imath} + \frac{\partial}{\partial y}\vec{\jmath} + \frac{\partial}{\partial z}\vec{k} \quad \text{III.35}$$

For the purpose of steady-state analysis, the momentum equation for fluid flow can thus be streamlined to:

$$\rho(\vec{V}.\vec{\nabla})\vec{V} = \nabla.\left\{-pI + \mu\left[\nabla\vec{V} + (\nabla\vec{V})^T\right] - \frac{2}{3}\mu(\vec{\nabla}.\vec{V})I\right\}F \quad \text{III.36}$$

The continuity equation:

The mass flow per second for the three directions, assuming that density and velocity are functions of space and time, is represented as follows in order to obtain the equation: a differential control volume of sizes , dy, dz :

$$-\frac{\partial}{\partial x}(\rho u)dydz$$

$$-\frac{\partial}{\partial y}(\rho v)dxdz \qquad \text{III.37}$$

$$-\frac{\partial}{\partial z}(\rho w)dydz$$

For the x,y and z directions respectively. According to the principle of conservation of matter, the sum of the three must be equal to the temporal rate of mass change, $\frac{\partial}{\partial t}(\rho\, dx\, dy\, dz)$. The dx, dy, dz terms can be ignored or eliminated among the other terms because a control volume is independent of time. As a result, the resultant equation can be reduced as follows:

$$\frac{\partial \rho}{\partial t}+\frac{\partial}{\partial x}(\rho u)+\frac{\partial}{\partial y}(\rho v)+\frac{\partial}{\partial z}(\rho w)=0 \qquad \text{III.38}$$

Gradient vector can be used to further simplify the aforementioned equation, making it as simple as this:

$$\frac{\partial \rho}{\partial t}+\vec{\nabla}.\rho\vec{V}=0 \qquad \text{III.39}$$

Energy equation:

$$\rho C_p u\nabla T=\vec{\nabla}.(k\nabla T)+Q \qquad \text{III.40}$$

Total entropy and efficiency:

$$S_{tot}=\frac{k}{(T_{avg})^2}\left[\left(\frac{\partial\theta}{\partial x}\right)^2+\left(\frac{\partial\theta}{\partial y}\right)^2\right]+\frac{\mu_{nf}}{T_{avg}}\left[\frac{\varepsilon_p}{k}(u^2+v^2)+2\left(\frac{\partial u}{\partial x}\right)^2+2\left(\frac{\partial v}{\partial y}\right)^2+\left(\frac{\partial u}{\partial y}+\frac{\partial v}{\partial x}\right)^2\right]+\frac{\sigma_{nf}}{T_{avg}}\beta^2 v \qquad \text{II.41}$$

$$T_{avg}=\frac{T_{inlet}+T_{tube}}{2}$$

$$\mathcal{E}_{\mathrm{p}}=\frac{\mathrm{q}}{\mathrm{q_{max}}}=\frac{\mathrm{q}}{\mathrm{C_{min}(T_{inlet}-T_{tube})}}$$

$$q=UA\Delta T_{ml}$$

$$\Delta T_{ml} = \frac{\Delta T_1 - \Delta T_2}{ln(\Delta T_1/\Delta T_2)}$$

Where $\vec{V} = u\vec{i} + v\vec{j} + w\vec{k}$ refers to velocity filed (m/s)

Reynolds Number:

$$\mathrm{Re} = \frac{\rho \mathrm{u} \mathrm{D}}{\mu} \qquad \text{III.42}$$

Richardson Number:

$$\mathrm{Ri} = \frac{\mathrm{Gr}}{\mathrm{Re}^2} \qquad \text{III.43}$$

Nusselt Number:

$$Nu_{loc} = \frac{k_{hnf}}{k_{bf}} \frac{\partial T}{\partial y} \qquad \text{III.44}$$

$$Nu_{avg} = \frac{1}{L} \int_0^L Nu_{loc} dL \qquad \text{III.45}$$

Nanofluid:

$$\varphi = \varphi_{Fe_3O_4} + \varphi_{MWCNT}$$

$$\rho_{np} = \frac{\varphi_{Fe_3O_4}\rho_{Fe_3O_4} + \varphi_{MWCNT}\rho_{MWCNT}}{\varphi}$$

$$\left(C_p\right)_{np} = \frac{\varphi_{Fe_3O_4}(C_p)_{Fe_3O_4} + \varphi_{MWCNT}(C_p)_{MWCNT}}{\varphi} \qquad \text{II.46}$$

$$\beta_{np} = \frac{\varphi_{Fe_3O_4}\beta_{Fe_3O_4} + \varphi_{MWCNT}\beta_{MWCNT}}{\varphi}$$

$$k_{np} = \frac{\varphi_{Fe_3O_4}k_{Fe_3O_4} + \varphi_{MWCNT}k_{MWCNT}}{\varphi}$$

$$\sigma_{\boldsymbol{np}} = \frac{\varphi_{Fe_3O_4}\sigma_{Fe_3O_4} + \varphi_{MWCNT}\sigma_{MWCNT}}{\varphi}$$

Hybrid Nanofluid :

$$\sigma_{hnf} = (1-\varphi)\sigma_{bf} + \varphi\sigma_{np}$$

$$\rho_{hnf} = (1-\varphi)\rho_{bf} + \varphi\rho_{np}$$

$$(\rho\beta)_{hnf} = (1-\varphi)(\rho\beta)_{bf} + \varphi(\rho\beta)_{np}$$

$$\left(\rho C_p\right)_{hnf} = (1-\ \varphi)\left(\rho C_p\right)_{bf} + \varphi\left(\rho C_p\right)_{np}$$

$$\alpha_{hnf} = \frac{k_{hnf}}{\left(\rho C_p\right)_{hnf}}$$

$$\frac{k_{hnf}}{k_{bf}} = \frac{k_{np} + (n-1)k_{bf} - (n-1)\left(k_{bf} - k_{np}\right)\varphi}{k_{np} + (n-1)k_{bf} + \left(k_{bf} - k_{np}\right)\varphi}$$

$$\mu_{hnf} = \frac{\mu_{bf}}{(1-\varphi)^{2.5}}$$

$$\frac{\sigma_{hnf}}{\sigma_{bf}} = 1 + \frac{3(\sigma_{np} - \sigma_{bf})\varphi}{\left(\sigma_{np} + 2\sigma_{bf}\right) - \left(\sigma_{np} - \sigma_{bf}\right)\varphi}$$

III.6. CONCLUSION:

We have attempted to present the two geometric configurations (2-D) and (3-D) shell/ tube heat exchanger, respectively, that have been investigated with these related presumptions within this section. Our goal is to present a comprehensive understanding of the mathematical formulation utilized and the creation of the physical domain mesh, followed by an examination of the various numerical resolution techniques applied.

CHAPTER Ⅳ:

RESULTS AND DISCUSSION

Ⅳ.1. Introduction:

Over the years, the development of computers has encouraged scientists to solve increasingly complex problems for which analytical solutions cannot be found. These types of problems are generally modeled by non-linear partial differential equations. This chapter is dedicated to the modeling of flow and heat transfer in geometries. The study of these geometries is dealt with mainly using COMSOL Multiphysics software, which is specially designed for computational fluid dynamics (CFD). CFD is a collection of numerical techniques for solving heat transfer and fluid dynamics problems roughly.

In this chapter of our study, we are interested in the numerical results acquired for the evolution of dynamic and thermal convection flow in the geometries mentioned above. (Chapter Ⅳ) representation of streamline, isotherms, and entropy generation for the different cases studied.

Ⅳ.2. Validation:

A validation study based on Roy and Mondal's published work [166] is carried out following the mesh structure's finalization. Using the isotherms, Figure Ⅳ.1 compares the current findings with the published work of Roy and Mondal [166]. The two outcomes are nearly identical, according to the comparison [166].

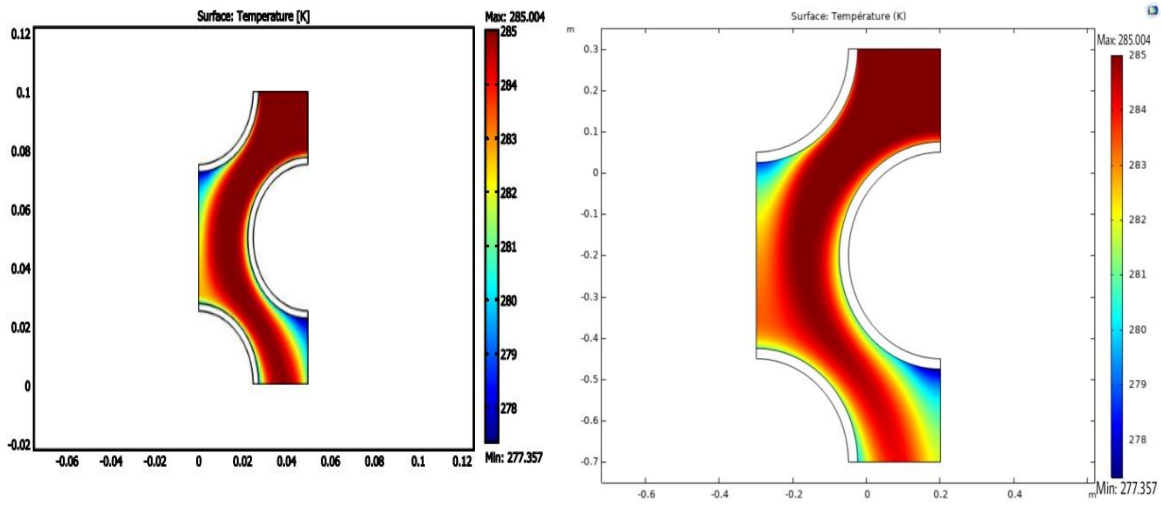

(a) (b)

Figure (Ⅳ.1): Validation of our results with ref.[166]. (**a**) Results of ref.[166]; (**b**) our results.

Ⅳ.3. CONFIGURATION 2-D:

Ⅳ.3.Case 1: 2D Shell / Tube Heat Exchanger

Ⅳ.3.1. Geometries 1:

The current study focuses on enhancing the tube/shell heat exchanger to increase efficiency, either by adding nanoparticles to the heat transfer fluid or by changing the tube's geometrical shape. This heat transfer fluid uses a water-based Al_2O_3-MWCNT hybrid nanofluid. The fluid flows at a steady speed and high temperature, while the tubes of different forms are kept at a low temperature. The finite-element-based computational tool solves the related transport equations numerically. The results are displayed using Nusselt number profiles for varied nanoparticle volume fractions of $0.01 \leq \phi \leq 0.04$ and Reynolds numbers $2400 \leq Re \leq 2700$ for the variously shaped heat exchanger tubes, as well as streamlines, isotherms, and entropy generation contours.

Ⅳ.3.1.1. Grid Test:

Prior to carrying out the thorough examination of the current issue, Taking into account the circular tube bundle, a thorough grid independence analysis is conducted. In this case, six distinct mesh sizes, extra coarse, very coarse, coarse, normal, fine, and very fine, are utilized with number elements of 1398, 3501, 5487, 13,108, 32,128 and 42,948. The average Nusselt number which is displayed in Figure Ⅳ.2 and Table Ⅳ.1 is used to compare the two. The middle value (with a fine mesh structure) is used to save computational time and produce the proper results since Figure Ⅳ.2and Table Ⅳ.1 show that the average Nusselt's last three values are near to one another.

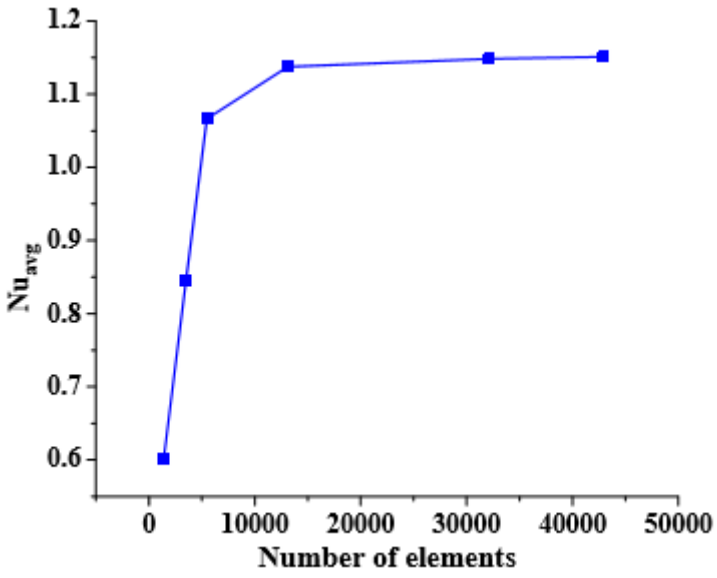

Figure (Ⅳ.2): Grid test, variation of the average via element number.

Mesh	Element Number	Average Nusselt Number
Extra coarse	1398	0.6011
Very coarse	3501	0.84613

Coarse	5487	1.0666
Normal	13108	1.13758
Fine	32128	1.14863
Very fine	42948	1.15084

Table (Ⅳ.1): Mesh comparison

Ⅳ.3.1.2. RESULTS AND DISCUSSION:

The goal of the current study is to optimize the efficiency of the tube/shell heat exchanger by changing the tubes' geometrical shape and/or by including nanoparticles into the fluid used for heat transfer. Here, a water-based hybrid nanofluid for heat transfer called Al_2O_3-MWCNT is used. The streamline, isotherms, entropy contours, and average Nusselt number for the two primary parameters are used to present the results: the volume fraction ($0.01 \leq \varphi \leq 0.04$) and the Reynolds number ($2400 \leq Re \leq 2700$) in order to analyze the heat exchanger's heat transfer efficiency. To get the optimal shape, the heat exchanger tube's shape which might be square, rectangular, diamond, or round is altered from a standard circular shape.

Ⅳ.3.1.2.1. Effect of Nanofluid Volume Fraction:

Figure Ⅳ.3, for Re = 2600, illustrates the impact of the rising hybrid nanofluid volume fraction ($0.01 \leq \varphi < 0.04$) on the heat transmission for each of the four tube bundle shapes. According to the illustration, the Nu_{avg} for the circular, rectangular, and diamond-shaped tubes rises monotonically with increasing φ, whereas the Nu_{avg} for the square-shaped tubes stays constant. The increase in φ signifies a rise in the heat transfer fluid's effective thermal conductivity relative to the base fluid, hence improving the heat transfer rate. It should be noted that these characteristics lead to an improvement in the working fluid's thermal conducting qualities [156–167]. As a result, the average Nu correlates with the concentrations of the nanoparticles, and this relationship enhances convective transfer. Because of the altered tube form, which permits more heat to be removed from the tube bundles, the Nu_{avg} has improved even further. All other shapes of tubes are inferior in heat transfer when compared to the performance of a diamond-shaped tube.

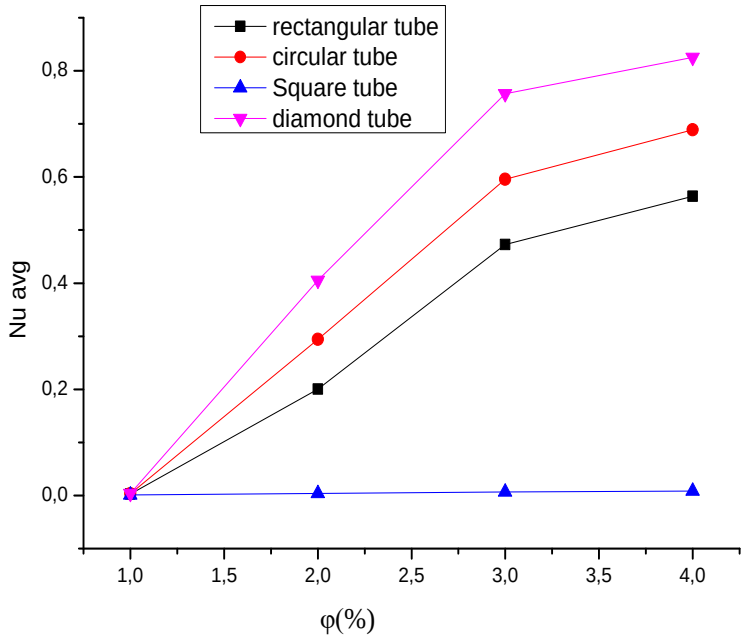

Figure (Ⅳ.3): Variation of the Nu avg with the increasing φ(%) for Re=2600.

Ⅳ.3.1.2.2. Reynolds Number Effect:

As demonstrated in Figures Ⅳ.4 and Ⅳ.5, the isotherm and streamline contours provide insight into the cause of the Nu_{avg}'s improvement, For the various time intervals (t = 0 to 100 s), the Al_2O_3-MWCNT/water hybrid nanofluid at Re = 2600 and φ = 0.02 was used, respectively. This analysis also includes the impact of the Reynolds number (2400 ≤ Re < 2700) on the formation of entropy, streamlines, and isotherms.

Because of the thermal buoyancy brought on by the temperature differential between the shell/tube heat exchanger's intake and exit walls, the fluid moves through the narrow gaps in the convoluted path. It is important to note that the flows initially start at the intake of the flow route and proceed to the next intricate and constricted path between the tube bundle gaps. The temperature and other thermal parameters within the chamber are replicated by the isotherms. The concentration of isotherm lines is concentrated at the bottom of the fluid as it is heated from below, and it gradually diminishes as it moves upwards in the direction of the flow passage's outlet. When time passes, heat is taken up from the bottom by the working

fluid and eventually dissipated as it rises to an exit. The convection fluxes are very modest at the lower flow regime (Re = 2600), and the domain is filled with uniformly distributed temperature lines. Consequently, the thermal behavior is determined by the thermal conduction modes. As one moves from the hot wall to the cold wall, the isothermal line values progressively rise. Heat transport is facilitated by thermal diffusion in this topology, known as thermal stratification. The isotherm contours spread evenly along the flow passage over time, and the diamond-shaped tube bundle exhibits this uniformity more than any other tube shape. It is evident from the streamline contours (Figure Ⅳ.5) that the flow channel contains multi-cellular vortices.

As time passes, these vortices' positions, sizes, and shapes alter. In reality, the flow via the very thin gaps is the reason for the results, which show a linear rise in the flow functions over time. Figure Ⅳ.5 illustrates how the eddies at the entry wall grow stronger and larger over time before heading upward and enabling significant free convection, which increases the flow velocity and quickens the fluid flow. The isotherms were blown to the edge by the growing Re as the flow passed through the entrance at increased Re values. Furthermore, because the intake and outflow of the flow domain have shaped corners, the fluid in rectangular and square tubes encounters greater resistance in its flow path. The circular and diamond fluids, on the other hand, encounter less resistance, which raises the rate of heat evacuation.

Circular tube

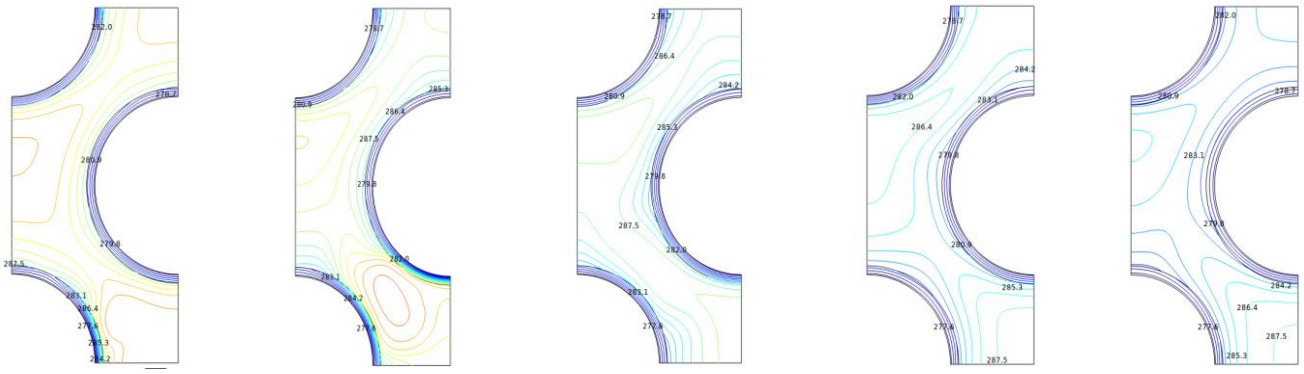

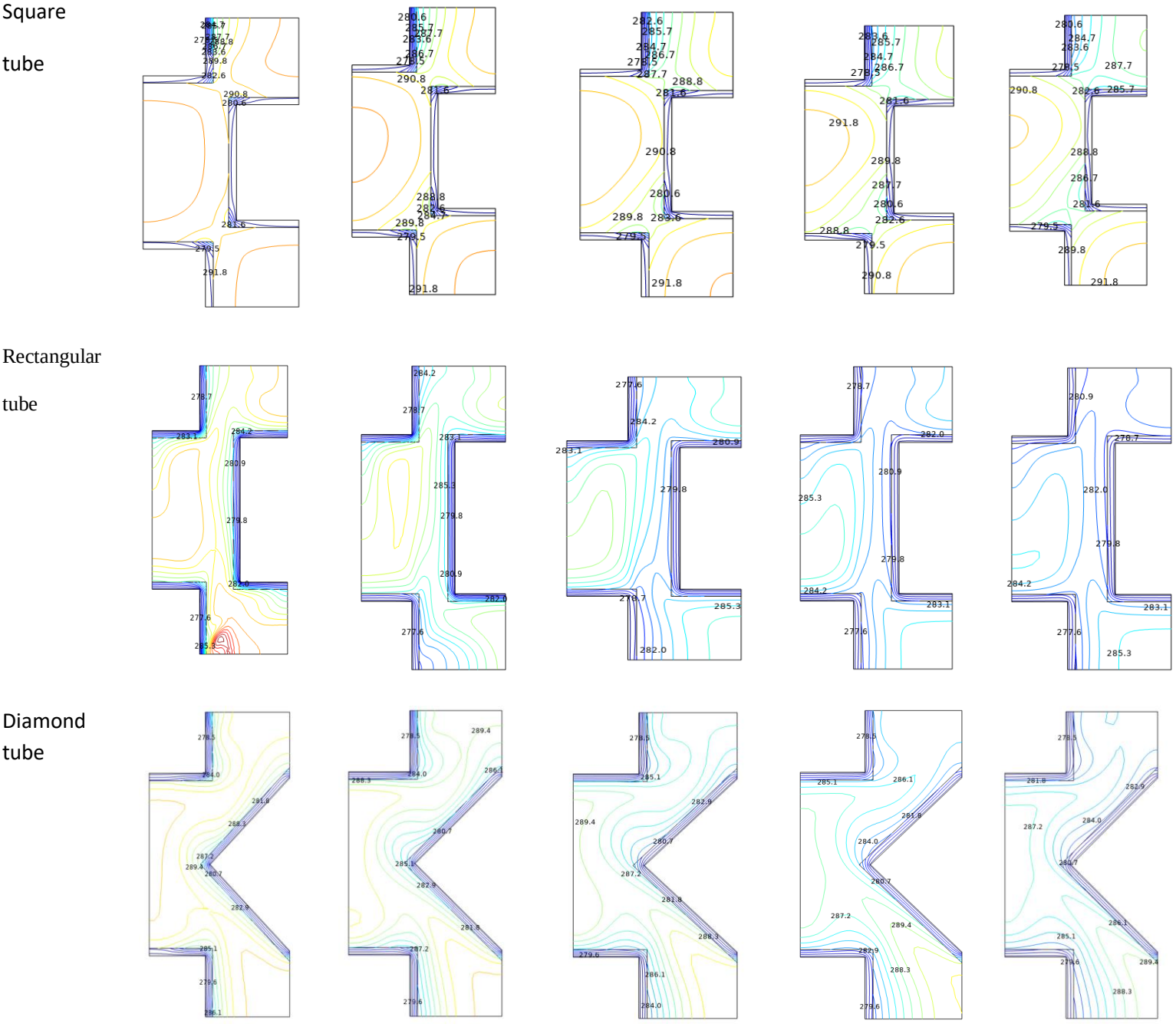

Figure (Ⅳ.4): Isotherms in a tube/shell heat exchanger with different shape of manufacturing tubes for Re = 2600, φ = 0.02

CHAPTER Ⅳ: RESULTS AND DISCUSSION

Circular tube

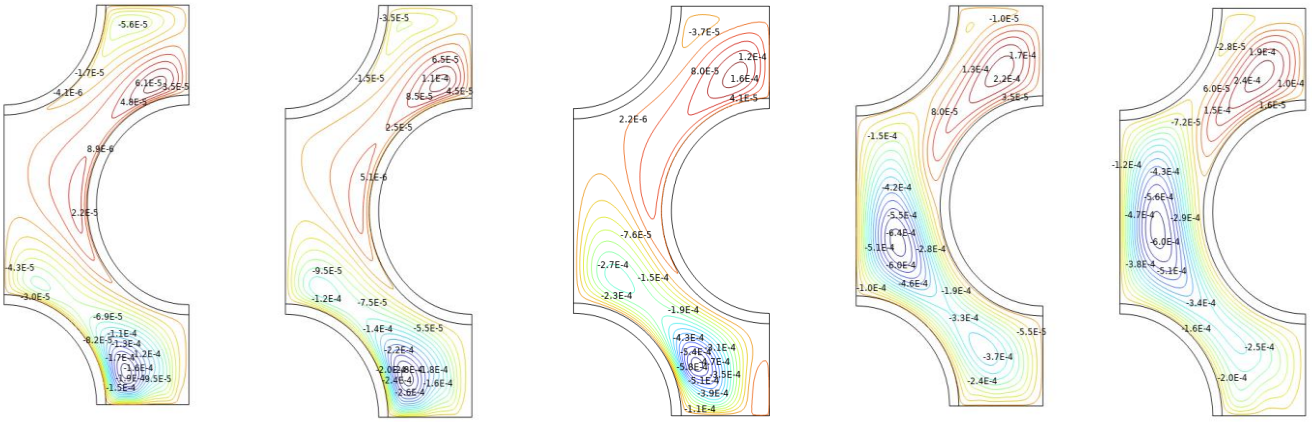

Square tube

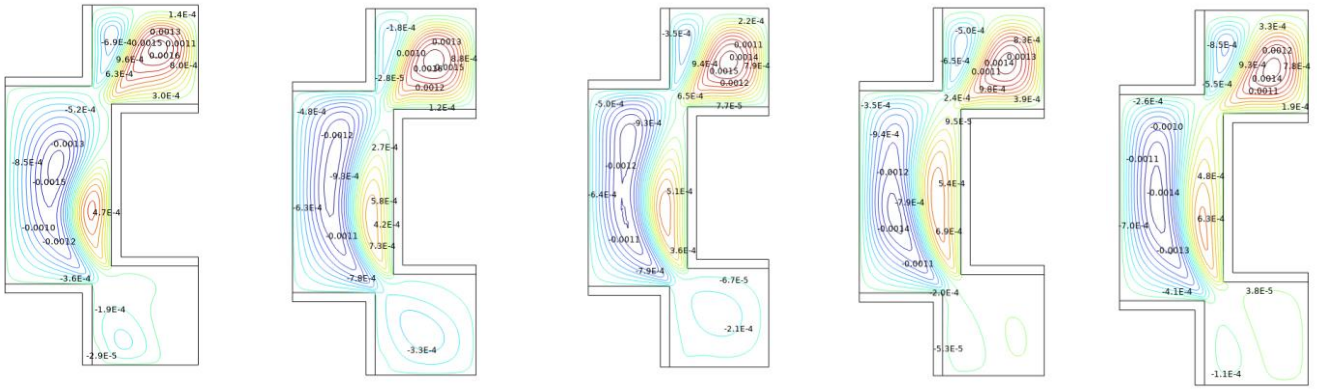

Rectangular tube

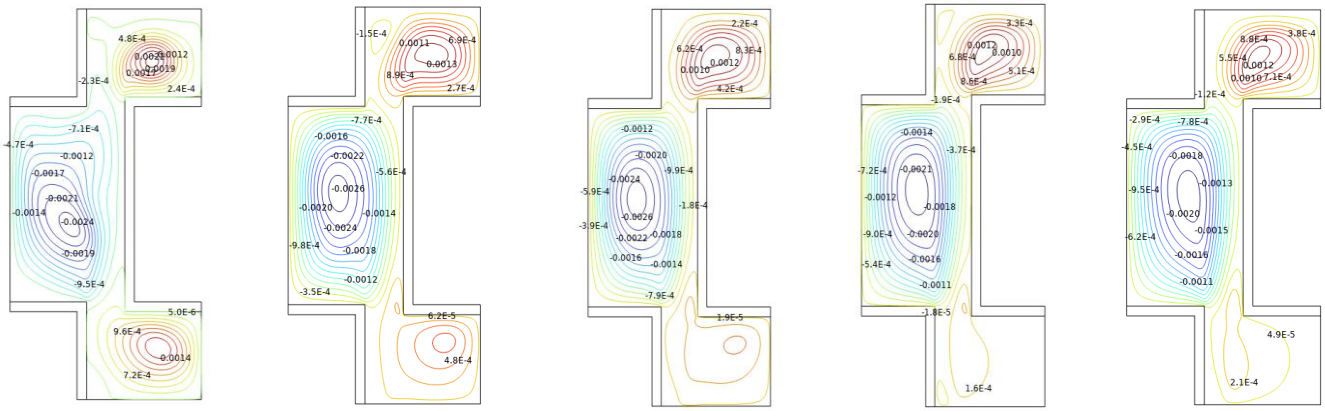

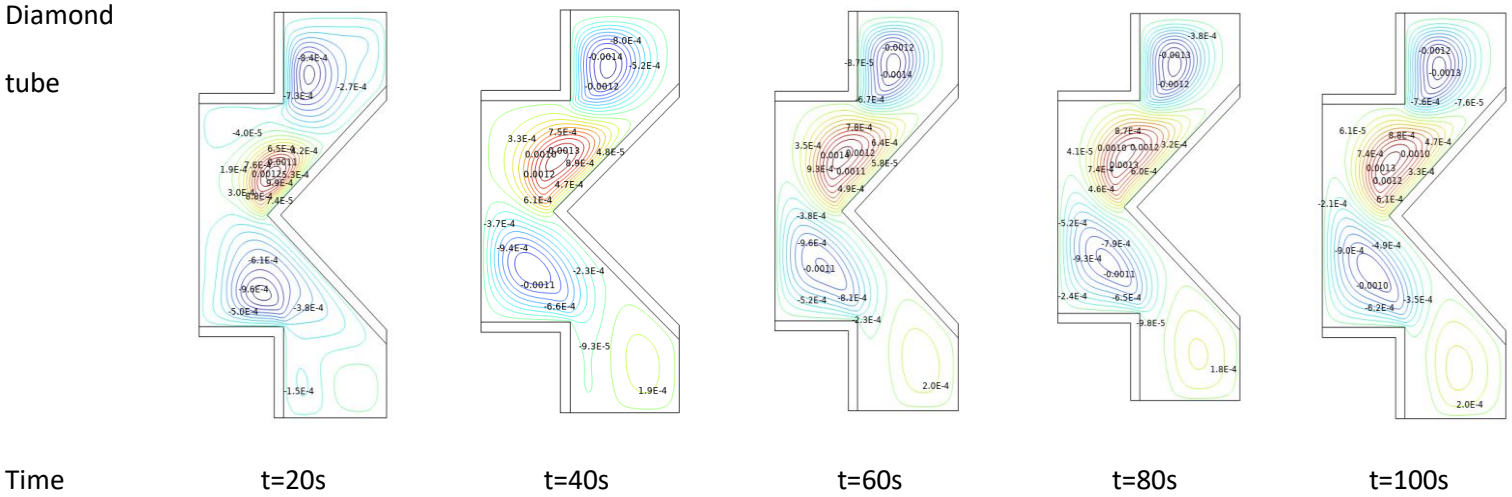

Figure (Ⅳ.5): Streamlines in a tube/shell heat exchanger with different shape of manufacturing tubes for Re = 2600, φ = 0.02

The Nu_{avg} is plotted for the varied Re in Figure Ⅳ.6 to help comprehend the overall effect of the various shaped tube bundles on the overall heat transfer. When the flow velocity of the Al_2O_3-MWCNT/water hybrid nanofluid increases, the heat transmission efficiency improves as well, amplifying the thermal convection effect. A higher heat transfer is correlated with a higher fluid Re. Additionally, for all Re values, the greater heat transmission is correlated with the diamond-shaped tube bundles.

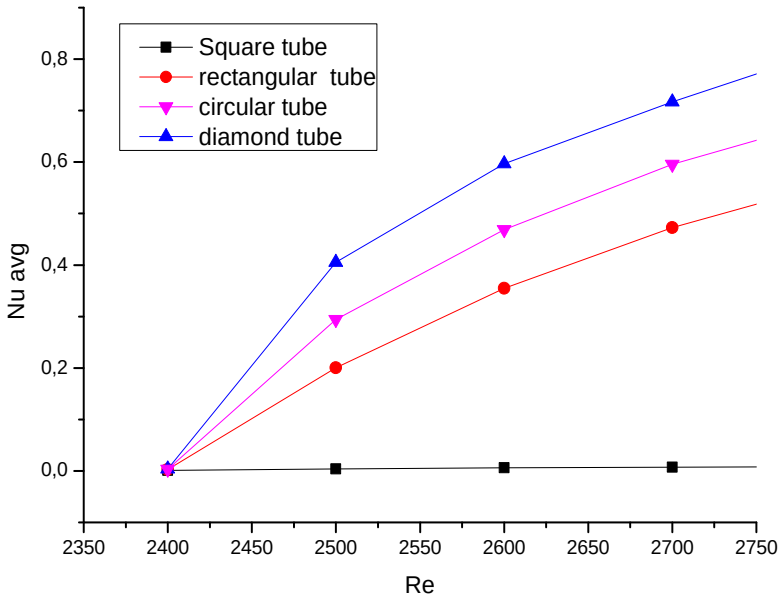

Figure (Ⅳ.6): Variation of the Nu_{avg} as a function of change in the Re at φ = 0.02.

Ⅳ.3.1.2.3. The Effect of Tube Shape:

Through the analysis of streamlines and isotherms, as depicted in Figure Ⅳ.4 and Figure Ⅳ.5, Compared to diamond-shaped tubes, the flow velocity is reduced in square, circular, and rectangular-shaped tubes because of the flow separation, This, since it offers the biggest flow function values, promotes the transfer of heat. The vortex is actually dispersed between the outlet and input walls, giving the moving fluid a larger surface area and accelerating the rate of heat transfer. Additionally, temperature change greatly enhances buoyant forces, which promote natural convection. Furthermore, the pipe's diamond form enhances heat transfer, as seen by Figures Ⅳ.3 and Ⅳ.6, which display the largest peak of average Nu values when compared to the other shapes. Moreover, the diamond's geometric properties and the homogeneous region surrounding it permit hybrid nanofluid dispersion. By doing this, heat convection and the Nu_{avg} number are both improved.

Ⅳ.3.1.2.4. Entropy Generation:

Inthissection, When entropy generation is computed (Figure Ⅳ.8), weaker isotherms near the hot wall cones are the reason for the low entropy that is shown there.More fluid circulation is therefore necessary. With the exception of the circulating cells' oval form, the distribution is likewise bicellular. This suggests a stronger induced flow. The isotherms show that thermal convection is dominant as a result. The latter suggests increased convection, supporting the convection mechanism over the conduction process. Furthermore, Figure Ⅳ.7 demonstrates how the diamond tube shape outperforms the other shapes in terms of heat exchanger efficacy by displaying the largest entropy drops.

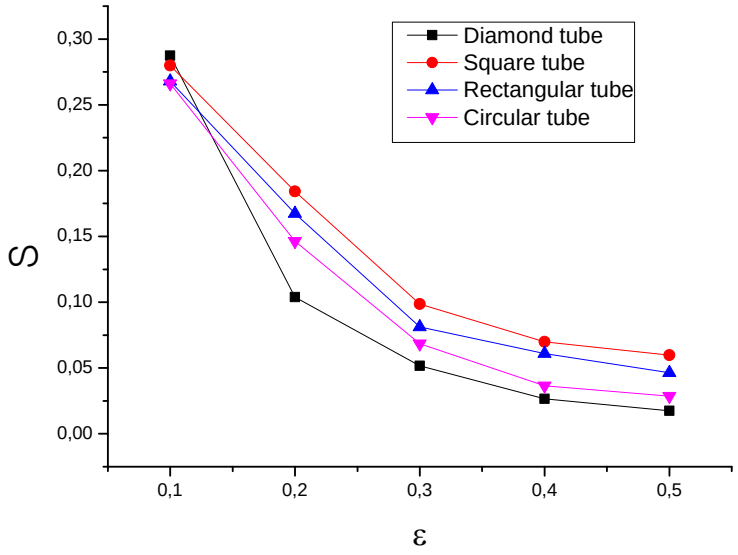

Figure (Ⅳ.7): Entropy generation (S) variation as a function of effectiveness of the heat exchanger (ε_p) for Re = 2600 and φ = 0.02

Circular Tube

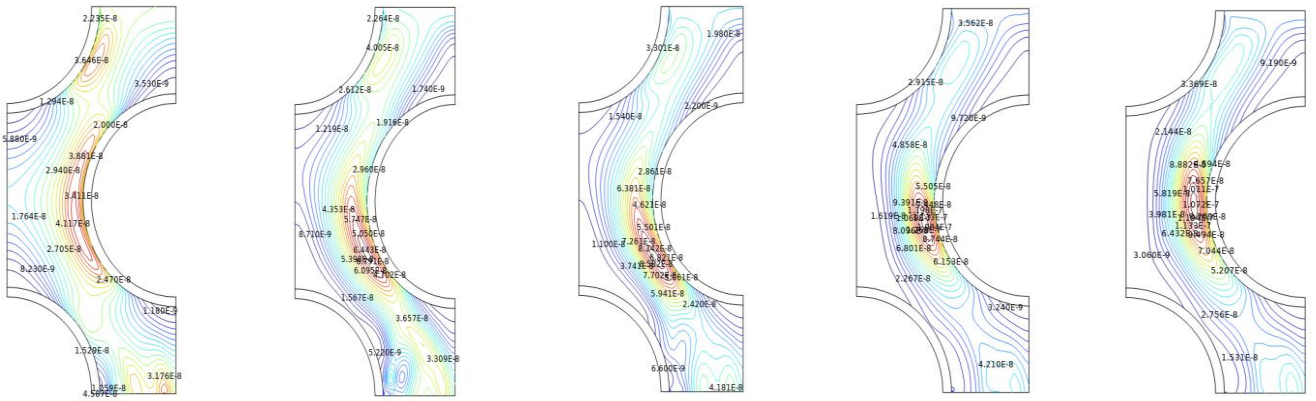

Square Tube

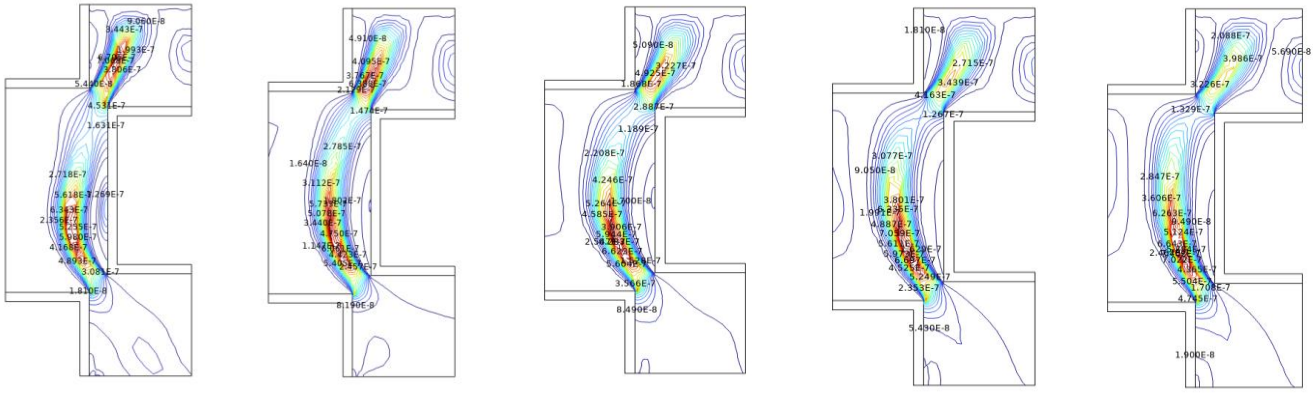

Rectangular tube

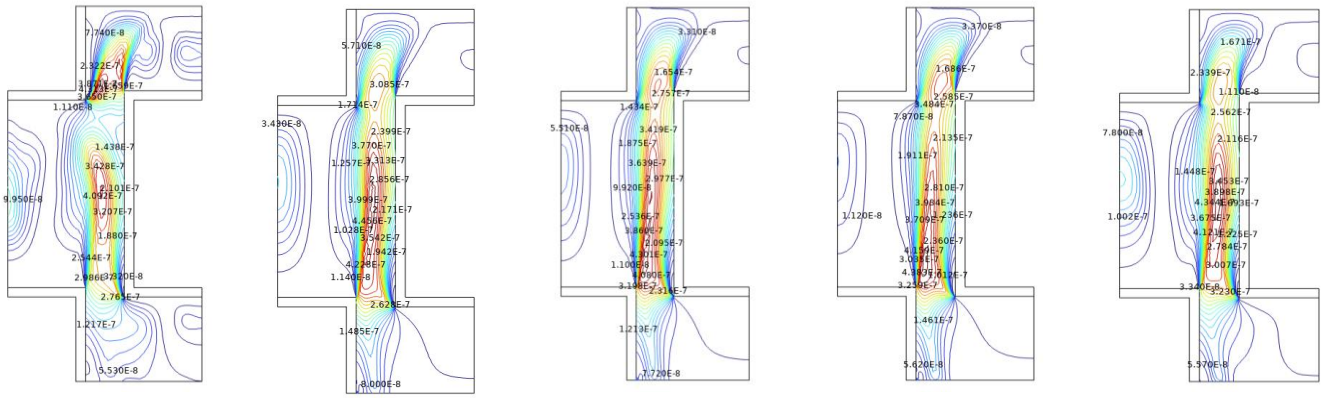

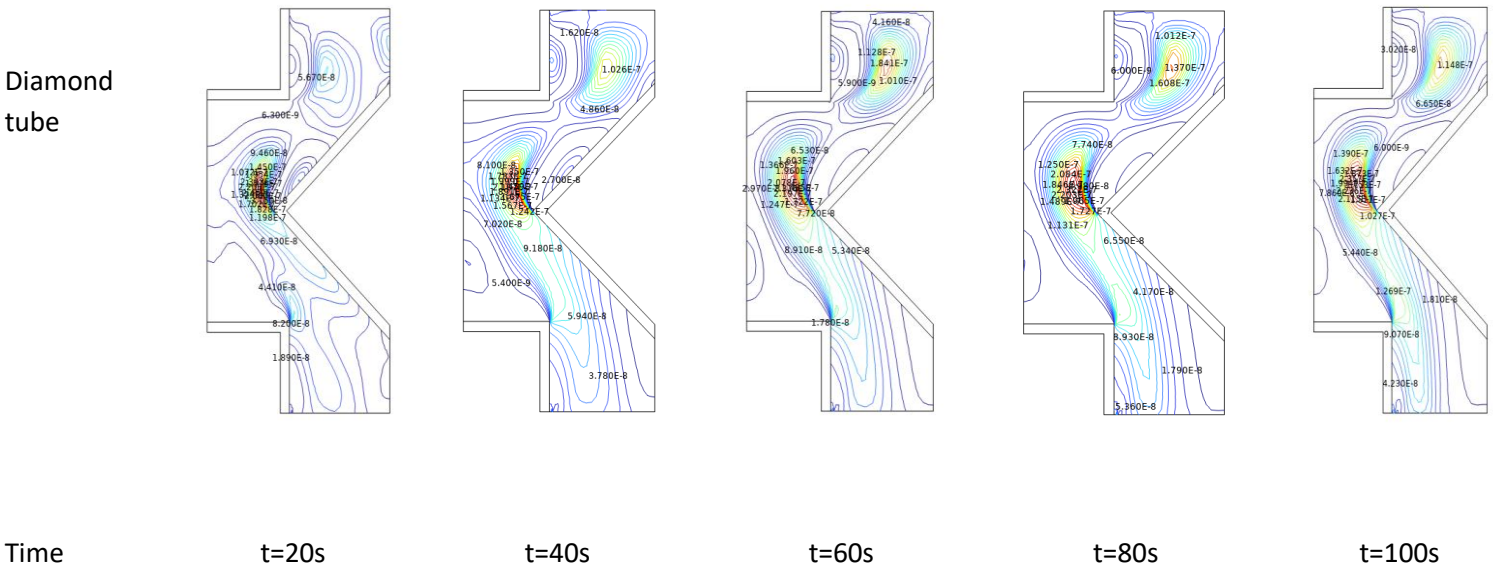

Figure (Ⅳ.8): Entropy in a tube/Shell heat exchanger with different shape of manufacturing tubes for Re = 2600 and φ = 0.02.

Ⅳ.3.2. Geometries 2:

The impacts of φ, Re, and nanofluid types on heat transfer rate are the main topics of this work. We have reported and gone into further detail on the results of a numerical simulation of 2D turbulent forced convection in a shell/tube heat exchanger loaded with three different types of hybrid nanofluids (Cu-Fe_3O_4-MWCNT/water; Fe_3O_4-MWCNT/water; and MWCNT/water). The study focused on convective heat transfer in the turbulent regime, examining the relationship between heat transfer efficiency by the volume fraction of the hybrid nanofluid with a value between 0.02 and 0.04 and heat transfer efficiency by Reynolds number change. The outcomes were displayed as entropy contours, streamlines, and isotherms. in addition to the mean Nusselt number for the two primary parameters: Reynolds number and volume fraction and different tube radius.

Ⅳ.3.2.1. Mesh test:

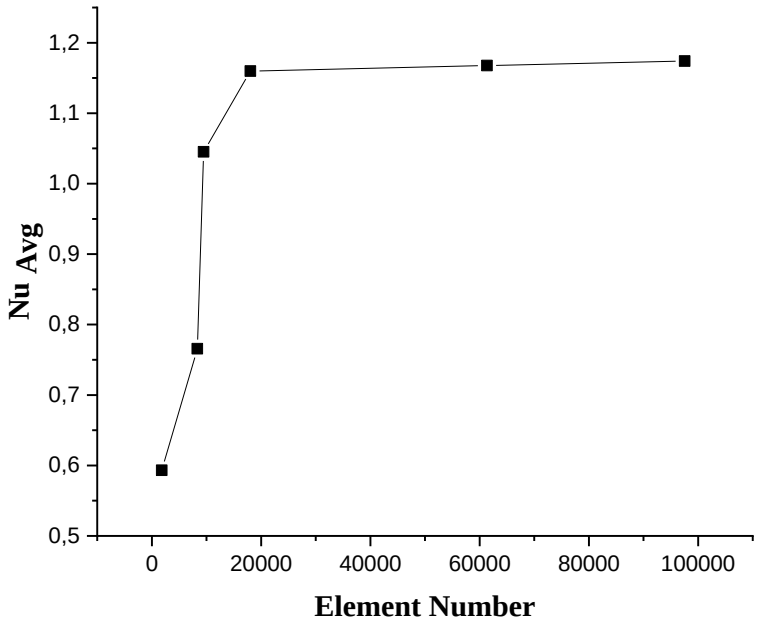

Figure (Ⅳ.9): variation in average Nu number as a function of element number

Mesh	Element Number	Average Nusselt Number
Extra coarse	1828	0,5932
Very coarse	8329	0,7956
Coarse	9481	1,0452
Normal	18053	1,15983
Fine	61350	1,16764
Very fine	97562	1,17392

Table (Ⅳ.2): Mesh comparison

Ⅳ.3.2.2. Effect of Nanofluid Volume Fraction:

The mean Nu_{avg} values for three types of nanofluids parameterized by Re and φ are shown in Figure Ⅳ.10 and Figure Ⅳ.14. For the same nanofluid, and throughout the range of Re values, the average nude increases monotonously with the increase φ. For the same nanofluid, at a fixed φ = 0.02, Nu_{avg} increases as Re increases, as expected.

Figure Ⅳ.8 and Figure Ⅳ.14 display the average Nu values for the heat exchanger using three different types of nanofluids that are parameterized by Re and φ. As φ increases, Nu avg rises monotonically. We now want to introduce the situation Re = 2600, which forms the basis of the current investigation because the Nu results exhibit intriguing patterns. Nu increases observably for MWCNT, Fe_3O_4, and Cu as φ increases, with a little peak emerging at φ = 0.04.

A Re = 2600 Figure Ⅳ.10 provides further comparisons for the variation in the number of Nusselt due to the addition of different nanofluids. In all three cases, we recorded an increase in the average number of Nusselt. Nu_{avg} seems to increase with the volume fraction, but we notice that when three nanoparticles (Cu, Fe_3O_4, and MWCNT) are added, it increases more. These findings corroborate the precision attained using the numerical approach presented in this work.

An increase in the hybrid nanofluid's concentration is correlated with an increase in nanoparticle presence, both Fe_3O_4 and MWCNT and Cu, which have improved thermo-physical characteristics compared to conventional fluids, as shown in Table (III.2), especially the way they conduct heat. It is important to note that these characteristics raise the hybrid nanofluid's surface area and enhance its thermal conductivity.

It can be observed that the values of the average number of Nusselts increase with the increase in volume fraction. Sound also increases with the increase of particles. We note that when adding Fe_3O_4 and Cu to the nanofluid MWCNT/water.

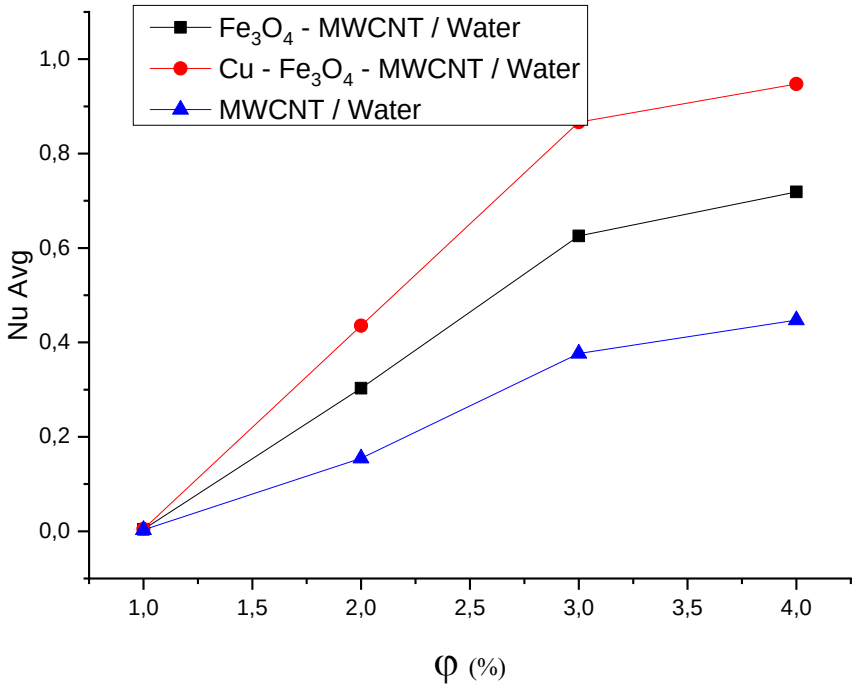

Figure (Ⅳ.10): Variation of the average Nusselt number based on fraction φ(%) for three types of nanofluids, Re = 2600

Figure Ⅳ.11, Figure Ⅳ.12, and Figure Ⅳ.13, respectively, illustrate the isotherm, streamlines, and entropy for the various time intervals (t = 0 to 100 s) utilizing the nanofluids MWCNT/water, Fe_3O_4-MWCNT/water, and Cu-Fe_3O_4-MWCNT/water at Re = 2600.

The distribution of streamlines, isotherms, and entropic lines for various nanofluid for φ = 0,02 and Re = 2600 is displayed in Figure Ⅳ.11, Figure Ⅳ.12, and Figure Ⅳ.13. The rationalizations expand downward with increasing time, as Figure Ⅳ.11, Figure Ⅳ.12, and Figure Ⅳ.13 illustrate. Multicellular patterns start to show up at the top and bottom of the wall as time goes on. as a result of the chilly surroundings. At high temperatures and speed gradients, the irreversibility of heat transfer and the irreversiality of nanofluid flow form the entropy zones. The isentropic lines show a development of concentrated entropy near three locations: the tube's surface, the top and bottom right corners of the enclosure, and these three

areas. For isentropic lines at a shorter time, no change was seen. But when the lines started to form on the wall's sloping surfaces and the tube, they somewhat altered the isentropic lines. Furthermore, Figure Ⅳ.11, Figure Ⅳ.12, and Figure Ⅳ.13 demonstrate how the windshields close to the entrance wall grow stronger and larger over time, moving quickly upward to permit strong free convection, which quickens and enhances the fluid's flow. The isotherms blew up as Re grew, and the flow passed past the input for higher Re values. Because of the thermal floatability brought on by the temperature differential between the tube/candy heat exchanger's input and output walls, the fluid flows through the narrow gaps in the complicated path. It is important to note that the flows first leave the input (flow passage) and proceed to the next intricately designed tiny route between the tube beam spaces. Isotherms replicate the chamber's overall thermal conditions, or temperature. As the fluid heats up from the bottom, the concentration of the isothermal lines gathers at the bottom and decreases as it stretches vertically towards the flow passage's output.

As the heat spreads upward over time, It is dispersed as it ascends to an exit after being absorbed by the working fluid from the bottom. Convection flows are very low at the lowest flow regime (Re = 2600), and the entire range is occupied by uniformly distributed temperature lines. Thermal behavior is therefore determined by thermal conduction modes. The isothermal lines values progressively rise from the hot wall to the cold wall. Heat transport is caused by thermal diffusion in this topology, which is known as thermal stratification.

Isothermal

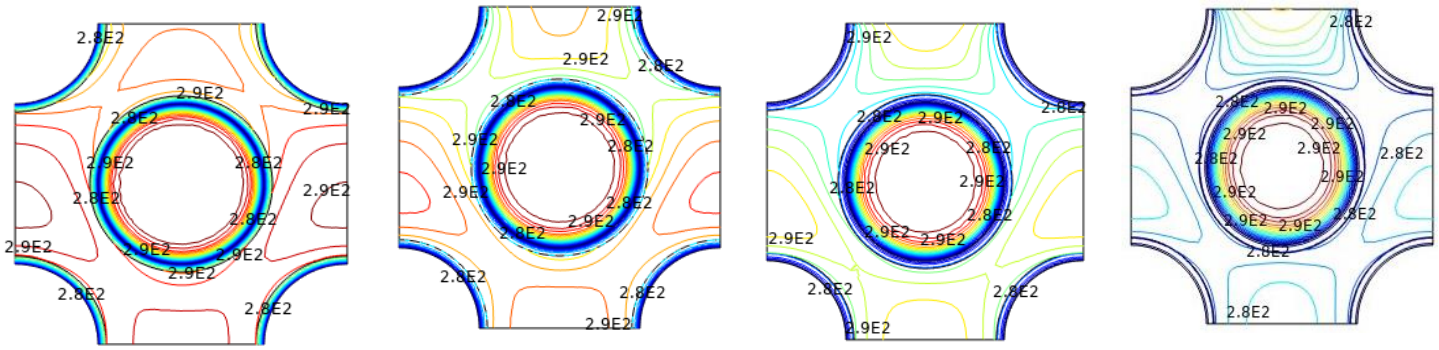

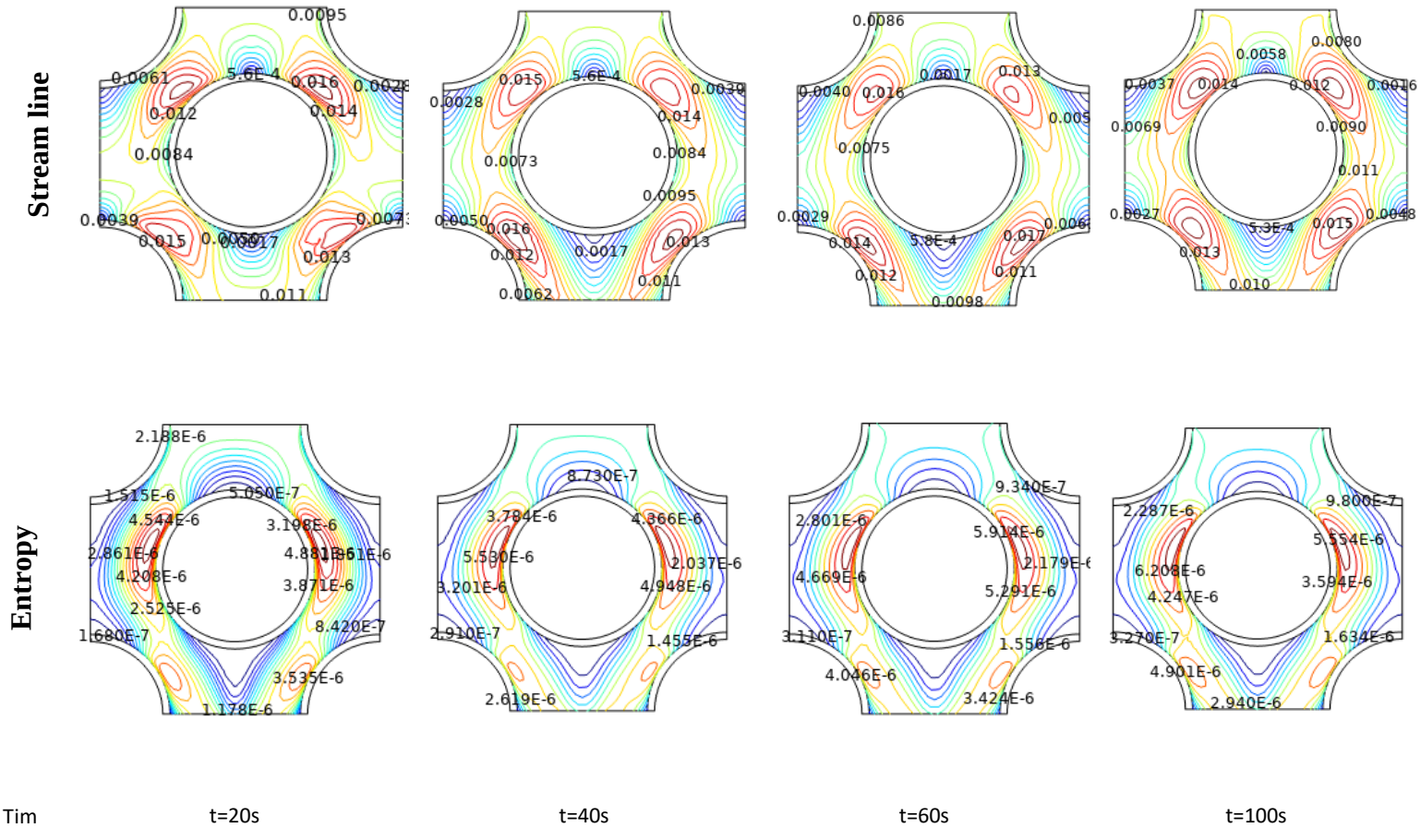

Figure (Ⅳ.11): Isothermal, Stream line, Entropy in a Shell/ Tube Heat Exchanger for this Nanofluid MWCNT/water φ = 0,02, Re = 2600

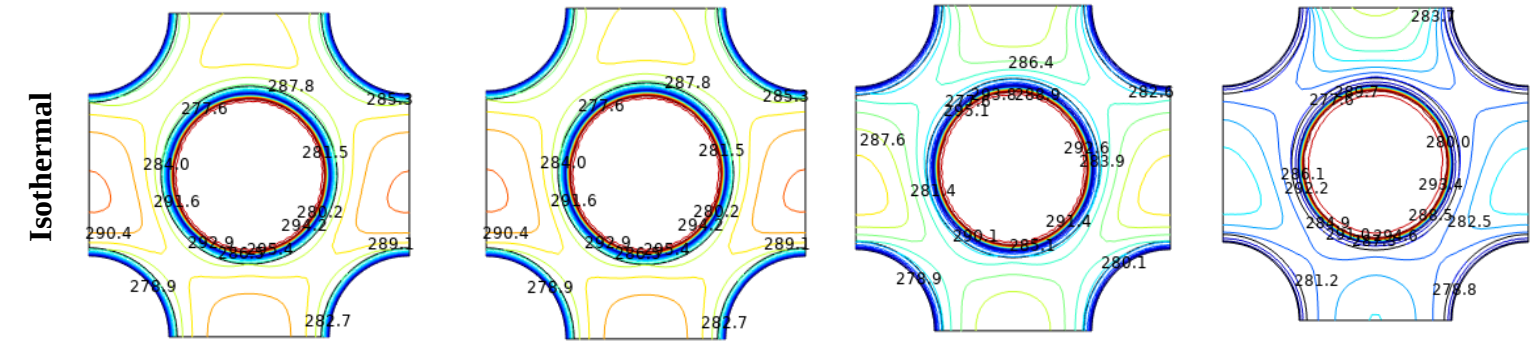

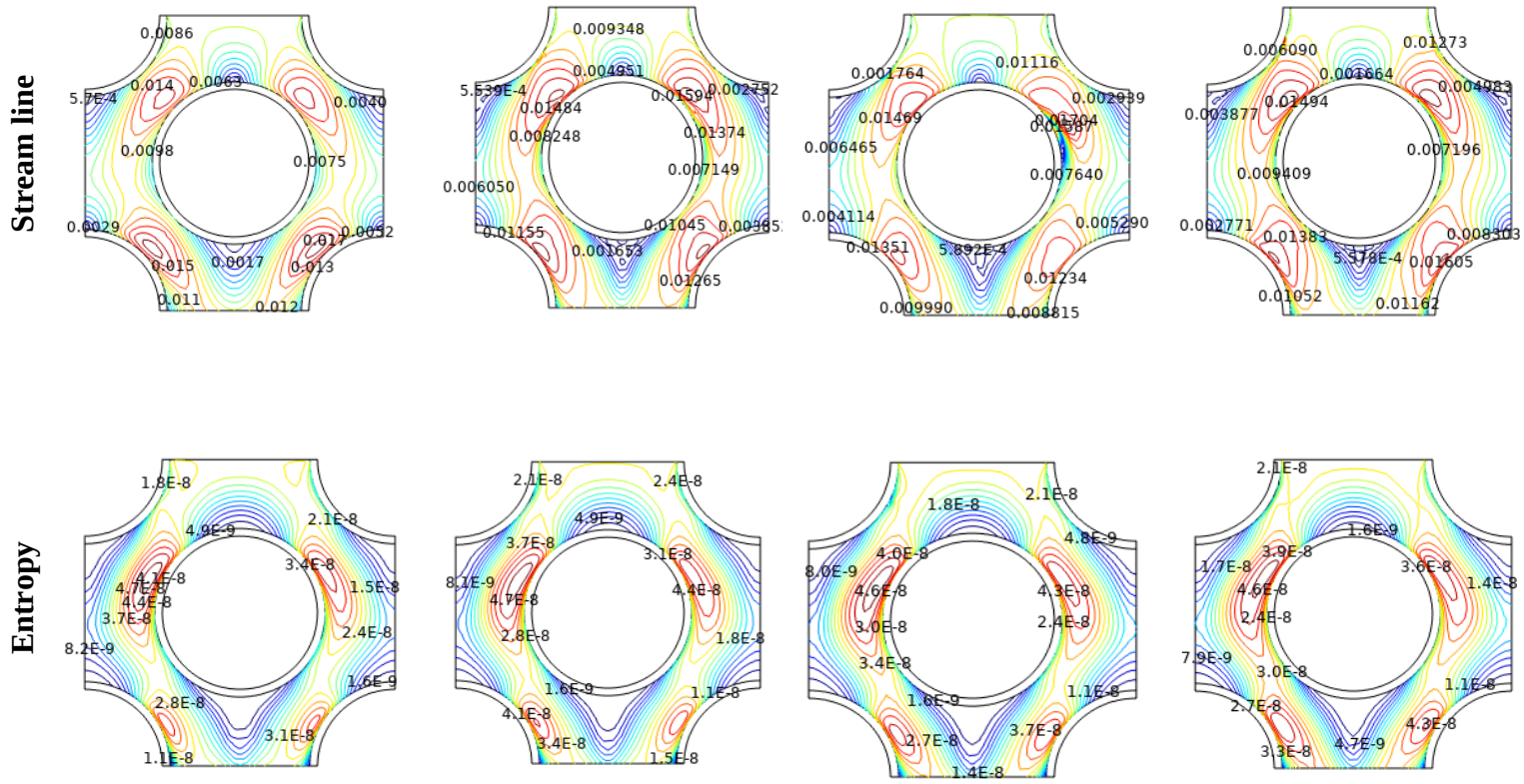

Figure (Ⅳ.12): Isothermal, Stream line, Entropy in a Shell/ Tube Heat Exchanger for this Hybrid Nanofluid $Fe_3O_4 - MWCNT/water$ φ = 0,02; Re = 2600

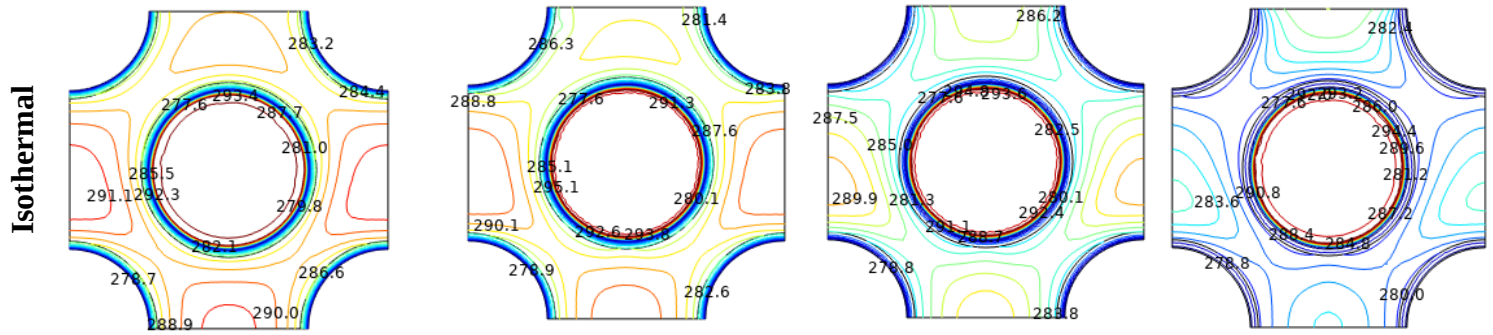

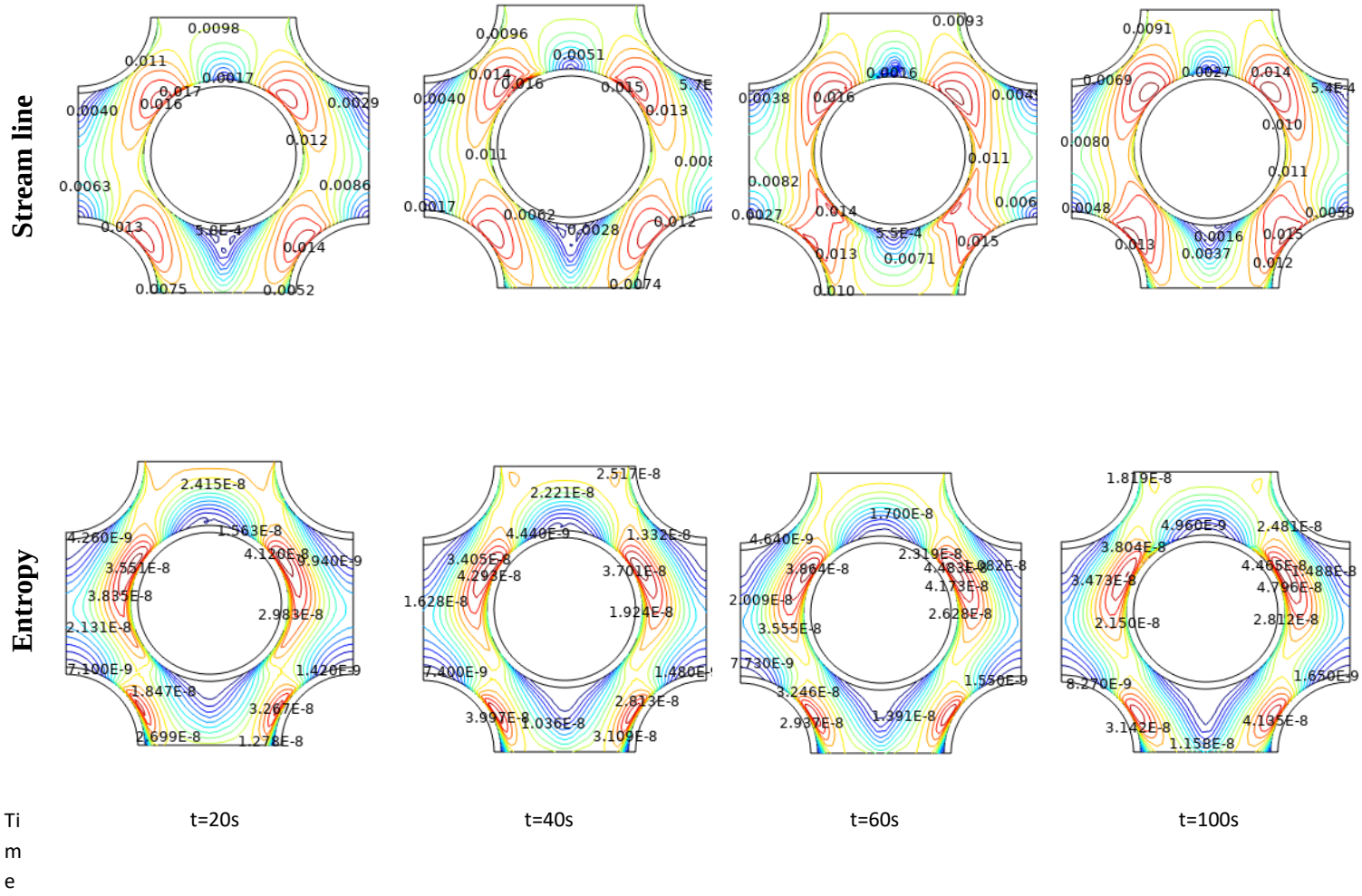

Figure (Ⅳ.13): Isothermal, Streamlines, Entropy in a Shell/ Tube Heat Exchanger for this Hybrid Nanofluid $Cu - Fe_3O_4 - MWCNT/water$, φ = 0,02; Re = 2600

Ⅳ.3.2.3. Reynolds Number Effect:

A variation in the average number of Nusselts depending on the number of Reynolds for different nanofluids on the shell/tube heat exchanger for the three configurations studied above is represented in Figure Ⅳ.14.

Figure Ⅳ.14 illustrates the effect of the Reynolds number on the average Nusselt number. As Re increases, the average number of Nusselt also increases for any fluid nano. It was noticed

that the better performance of the average Nusselt number was at higher nanoparticles (Cu, Fe_3O_4, and MWCNT). A higher volume fraction of nanoparticles produced the optimal entropy production outcomes in contrast to a lower volume fraction of nanoparticles (Figure Ⅳ.15).

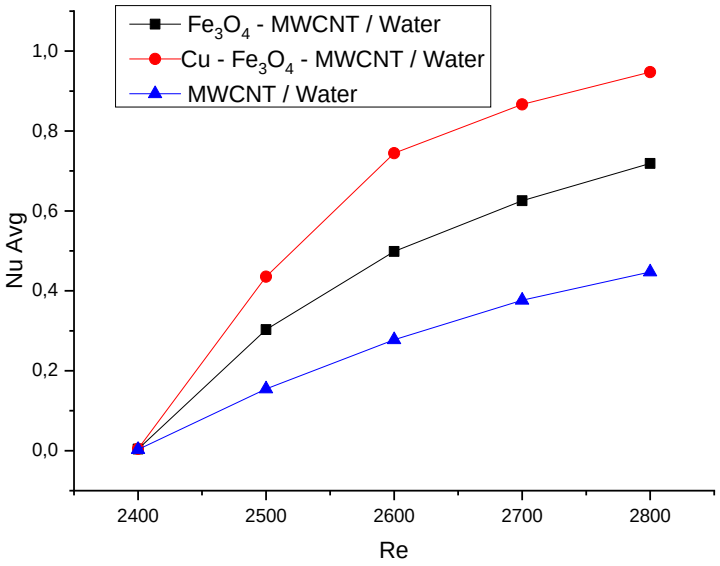

Figure (Ⅳ.14): Variation of the average Nusselt number on the change of the Reynolds number Re, φ = 0,02

Ⅳ.3.2.4. Entropy Generation:

The frictional entropy generation characteristics of the Shell/Tube heat exchanger with the ε_p efficiency at a Reynolds number of Re = 2600 are presented in Figure Ⅳ.15. As you can see, the viscous entropy generation decreases slightly by increasing the efficiency of the heat exchanger. When the nanoparticle increases from 1 to 3, entropy generation decreases slightly. But to a lesser extent than the other two cases, where the particles are less than 3 nanoparticles, The high volume fraction of nanoparticles increases entropy generation and improves heat transfer performance. This is because concentration related changes in viscosity exacerbate the production of friction entropy and pressure decrease. Variations in the creation of frictional entropy and pressure drop are mostly determined by the contribution of the developing area.

.

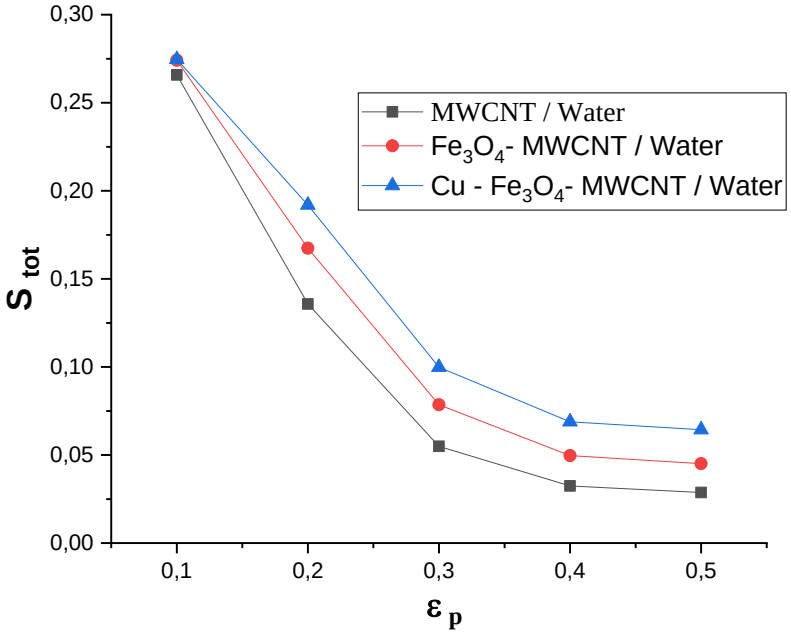

Figure (Ⅳ.15): Entropy generation S_{tot} variation as a function of effectiveness of the heat exchanger (εp) for Re = 2600 and φ = 0.02.

Ⅳ.3.2.5. Different Tube Radius Effect:

Figure Ⅳ.16 with Re = 2600 and φ = 0.02. As the tube radius increases, the passage width between the tube and the top and bottom walls decreases. Consequently, cell size decreases as tube radius increases. Consequently, extending the tube revealed highly intense isothermal lines at the cavity's top and bottom.

It was also shown that changes in tube radius size affected the average number of Nusselt as shown in Figure Ⅳ.17. The average Nusselt number increased as the radio tube size increased. Moreover, All radius sizes have high Nusselt numbers.

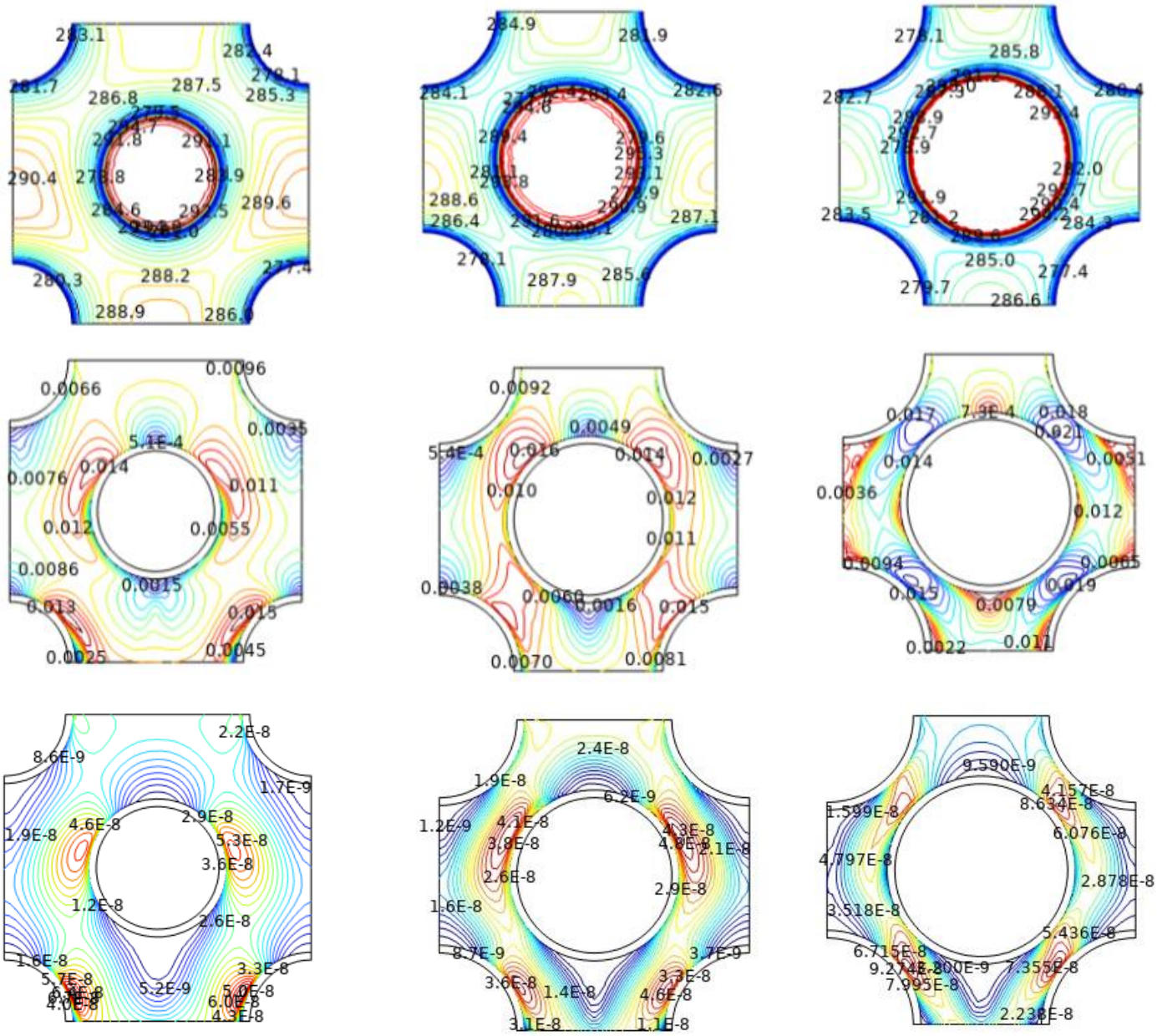

Figure (Ⅳ.16): Isothermal, Streamlines, Entropy in a Shell/ Tube Heat Exchanger for this Hybrid Nanofluid $Cu - Fe_3O_4 - MWCNT/eau$ and different Tube Radius, φ = 0,02, Re = 2600

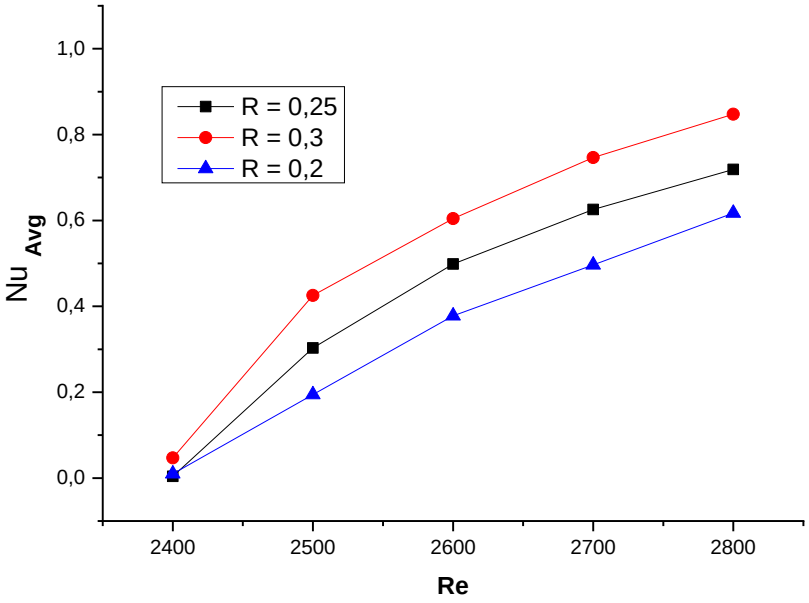

Figure (Ⅳ.17): Variation of the average Nusselt number with changing Reynolds number Re, and different Tube radius R ; φ = 0,02

Ⅳ.4.Case 2: Zigzage walled cavity

In this chapter, a numerical study has been carried out for natural convection heat transfer in a zigzag-walled enclosure with a cylinder occupied by a MgO-SWCNT/water hybrid nanofluid. The current study uses COMSOL multi-physics software. The governing equations are verified using the Galerkin finite element method (GFEM). The effect of many factors is detailed, including Rayleigh number ($104 \leq Ra \leq 106$), nano-fluid volume percentage ($0.01 \leq \varphi \leq 0.04$) and ripple number $1 \leq N \leq 8$. Our numerical conclusions are expressed in terms of isotherm distributions, the Nusselt number, and the all-important rationalizations of the control parameters for heat convection and flow in the enclosure. The results show that Nu avg increases with increasing Ra and N, and the best cylinder shape is the diamond shape.

Ⅳ.4.1.Mesh test:

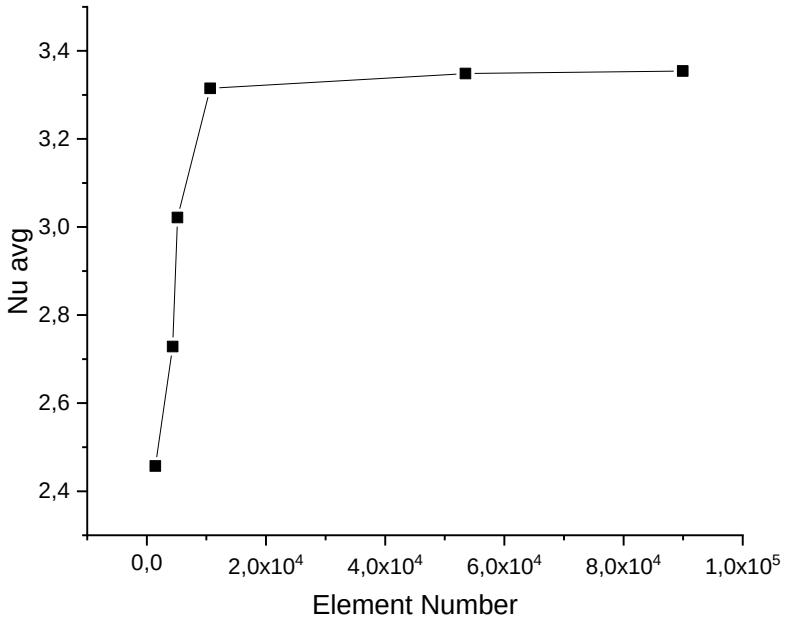

Figure (Ⅳ.18): variation in average Nu number as a function of element number

Mesh	Element Number	Average Nusselt Number
Extra coarse	1446	2.4573
Very coarse	4358	2.7284
Coarse	5139	3.0215
Normal	10634	3.3151
Fine	53481	3.3487
Very fine	89938	3.3542

Table (Ⅳ.3): Mesh comparison

Ⅳ.4.2.Rayleigh Number Effect:

Figure Ⅳ.19 shows the current lines, isotherms and entropy at different Ra, N= 2, φ = 0.02. A primary recirculation cell revolving clockwise may be seen. As Ra increases, the vortex intensity increases and the current lines move closer together. The isothermal lines become less congested as the volume fraction of nanoparticles increases. Isothermal lines are packed around isothermal walls, indicating that temperature gradients are particularly substantial in these places.

In order to evaluate fluid flow behavior, it (Figure Ⅳ.19) displays schematics of the water-based MgO-SWCNT at Ra 10^4, 10^5, and 10^6. Heat transfer occurs at the heated surface, where fluid at the higher surfaces decreases and fluid at the hot surface increases. In addition, the streamlines' density is far from the core, and the two vortices' size and amplitude are increased when Ra is raised to 10^5. However, the number of vortices increases for Rayleigh number 10^6. In the fluid domain, there is a large clockwise vortex on the right side, two vortices: one in the lower right corner and one on the left side, both rather small counterclockwise vortices. shows how the Ra impact affects isotherms where the nanofluid volume fraction (φ = 0.02) is varied. For comparatively.

Concentrated entropy creation inside the hollow and surrounding the solid cylinder is indicated by isentropic lines. The irreversibility of heat transmission and the irreversibility of the nanofluid resulting from buoyancy and shear forces cause these zones of entropy. The isentropic lines become less intense as Ra rises, especially in the vicinity of the solid cylinder. Because of the dominating shear force at the top of the wall, which increased with Ra, Only at Ra = 10^6 do isentropic lines begin to form at the top and bottom of the wall.

The influence of φ and Ra on Nu avg is explained in Figure Ⅳ.20 as it can be understood. Nu average will rise with rising φ and Ra. this is due to the fact that adding nanoparticles to the fluid will increase both the temperature and viscosity of the nanofluid. Figure Ⅳ.20 shows how Ra affects the rate of heat transmission. Because of the higher buoyancy forces, it is evident that increasing the volume fraction of MgO and SWCNT raises Nu avg. Heat transmission is subsequently improved by the addition of nanoparticles, which also increase

the nanofluid's characteristics. Actually, increasing the MgO-SWCNT volume fractions from 0.01 to 0.04 nearly doubles the Nu average.

It was shown that at increasing nanoparticle volume fractions, the average Nusselt number performed best. the irreversibility of the heat transfer was dominant over the irreversibility of the nanofluid in the system. The value of Ra was shown at folds for the entire volume fraction of nanoparticle above is shown in Figure Ⅳ.20.

Figure Ⅳ.20 shows how Ra affects the rate of heat transmission. Because of the higher buoyancy forces, it is evident that increasing the volume fraction of MgO and SWCNT raises Nu avg. Heat transmission is subsequently improved by the addition of nanoparticles, which also increase the nanofluid's characteristics. Actually, increasing the MgO-SWCNT volume fractions from 0.01 to 0.04 nearly doubles the Nu average.

Isotherme Stream line Entropy

Ra = 10^4

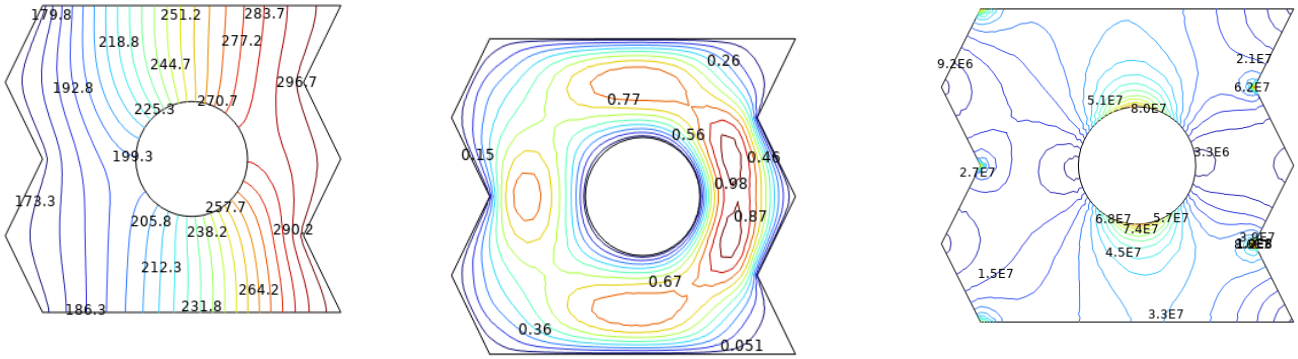

Ra = 10^5

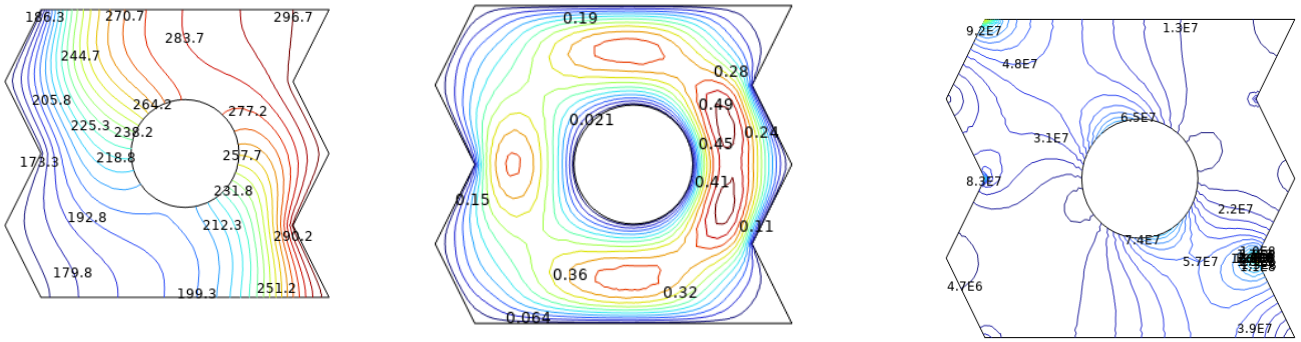

Ra = 10^6

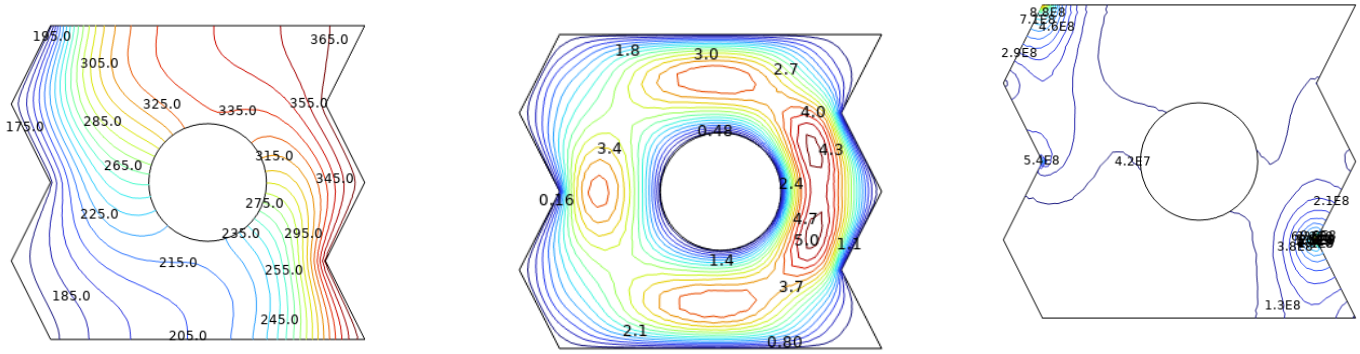

Figure (Ⅳ.19): isotherms, Streamlines and Entropy evaluated by Ra number for φ = 0.02, N = 2.

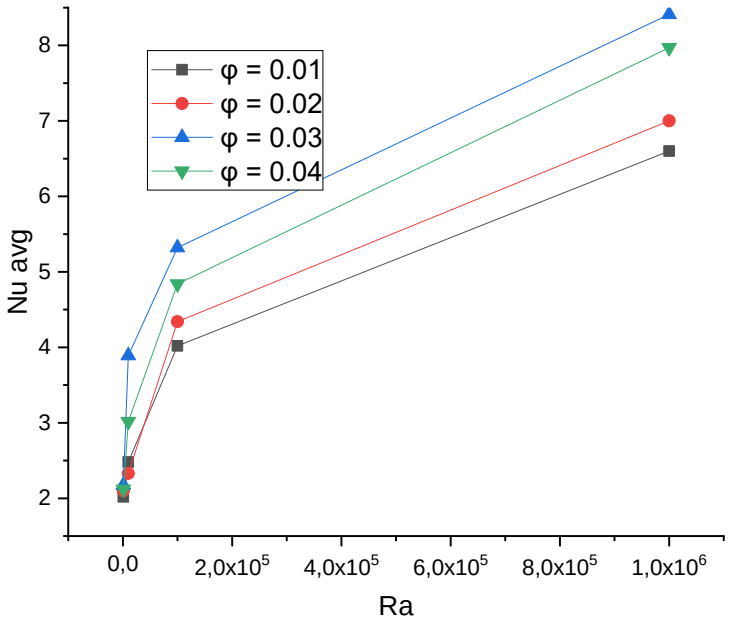

Figure (Ⅳ.20): Variation of the Nu_{avg} with the increasing Ra for different φ .

Ⅳ.4.3. The effect of the various undulations (N):

To investigate the impact of N oscillations (ranging from 1 to 8) on the thermal and dynamic properties within the enclosure, we provide the rationalisms, solid phase isotherms, and nanofluid phase isotherms at φ = 0.02, Ra = 10^5 in Figure Ⅳ.21.

The distribution of isotherms close to corrugated walls and the geometric structure of flow cells are both impacted by the presence of corrugations on vertical walls, as this image illustrates. Fluid accelerates in these regions when current lines are applied to wave crests.

Furthermore, a considerable rate of heat transfer happens close to cold vertical walls because as the number of oscillations grows, the temperature gradient rises as well, especially in the upper portion of these walls.

Figure Ⅳ.21 shows Streamline and Isotherm contours for N at Ra = 10^5 and at fixed values of φ = 0.02. Different waveforms result in different temperature distributions and flux function patterns inside the cavity. Increasing Ra thus contributes to both enhancement and free convection, improving the flux function. For Ra = 10^5, as N increases from 1 to 4, while an

increase in (N) leads to an increase in convection flow. It was noted that the increasing number of waves decreases both the strength of heat and fluid flow.

in Figure Ⅳ.22, at φ = 0.02 and N = (1, 2, 3, 4 and 8). The impact of N also improves with increasing Ra. Ra rises with increasing wave number, and heat transfer rises as well. (Figure Ⅳ.22), where we observe a direct correlation between the mean Nu and the number of ripples for low Ra (Ra = 10^4), However, at higher Ra (Ra = 10^6), where N = 4 is the optimal choice, this link breaks off.

Isotherme Stream line Entropy

N = 1

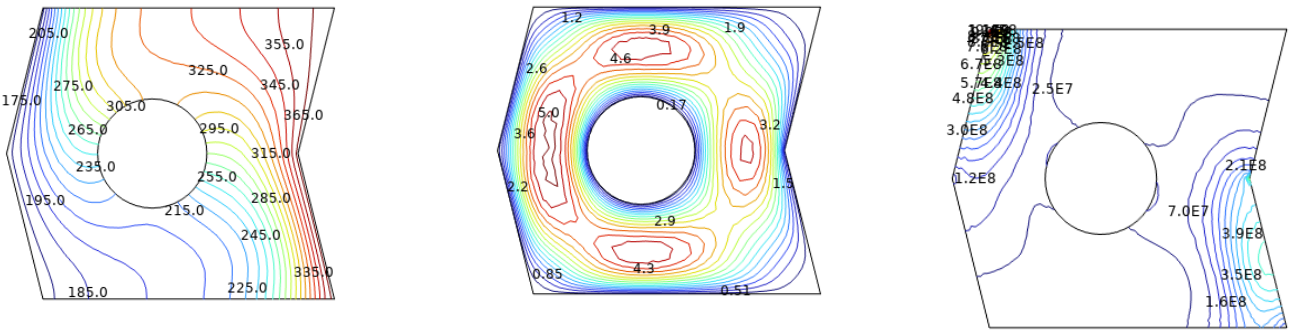

N = 2

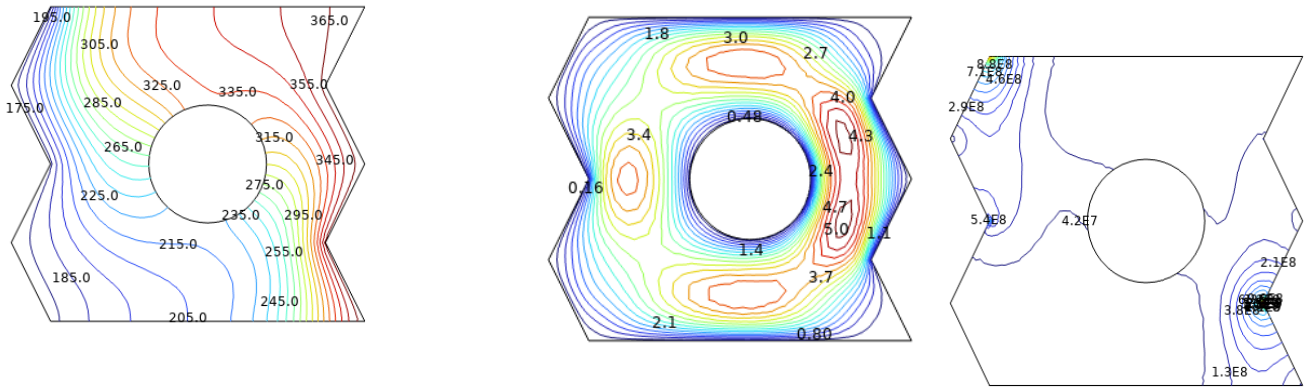

N = 3

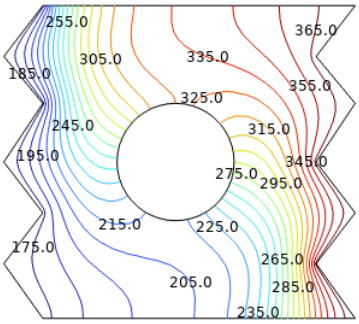

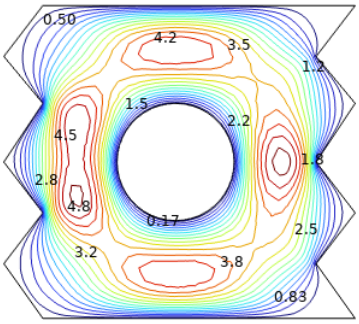

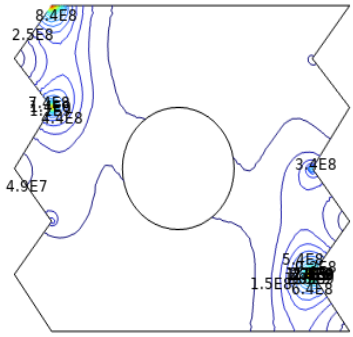

N = 4

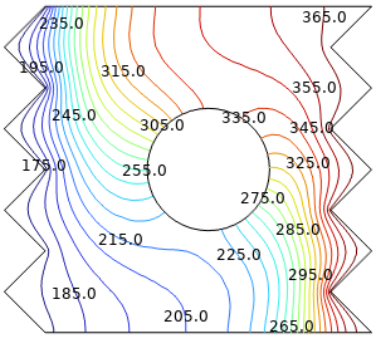

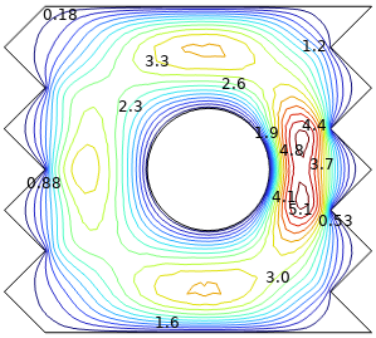

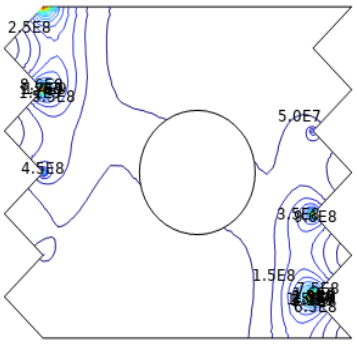

N = 8

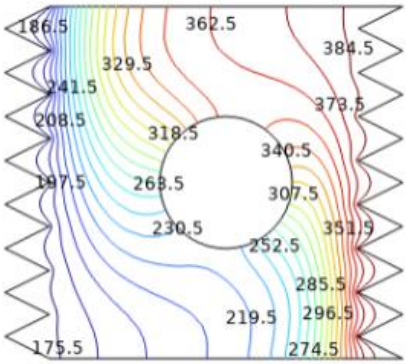

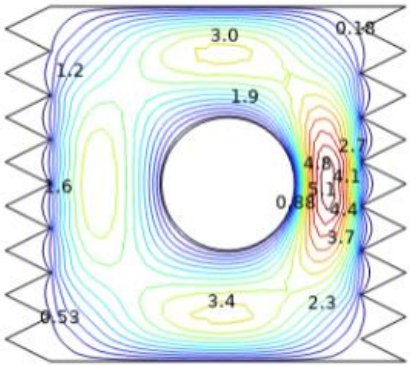

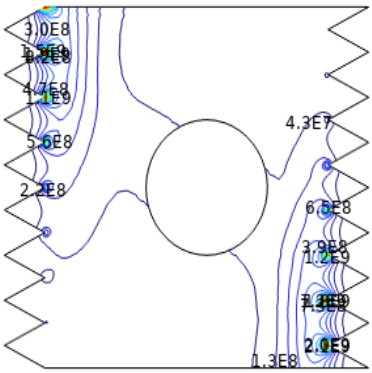

Figure (Ⅳ.21): Streamlines, isotherms and Entropy evaluated by undulations number (N) for $Ra = 10^5$, $\varphi = 0.02$.

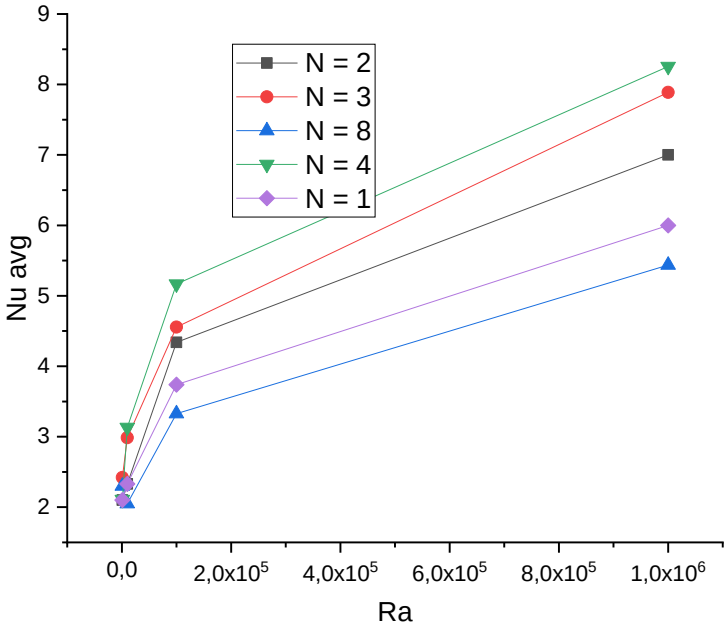

Figure (Ⅳ.22): Variation of the Nu_{avg} with the increasing Ra for different N.

Ⅳ.4.4.The effect of Different Obstacles:

The rationalizations, isotherms, and entropy created and depicted in Figure Ⅳ.23 examine the impact of various impediments on the flow distribution in the geometry under consideration. The results show that the square and rectangular obstructions appear to slow the flow by producing small vortices compared to the diamond obstacle, which increases heat transfer since it provides the largest flux function values. This cylinder is surrounded by both vortices, which increases the area available for the flux distribution and improves heat transfer. Changes in temperature also have a major impact on the increased buoyant forces that propel and encourage natural convection.

	Isotherme	Streamline	Entropy
Square	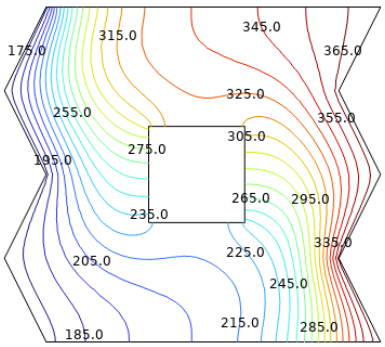	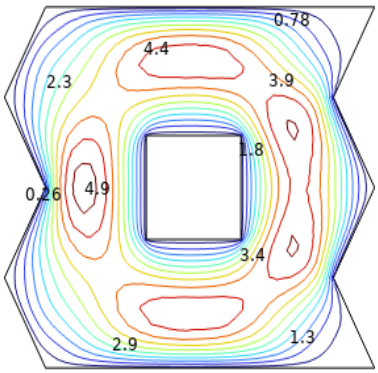	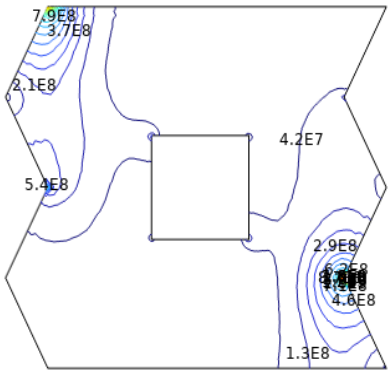
Rectangular	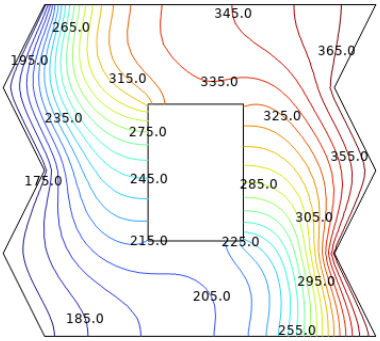	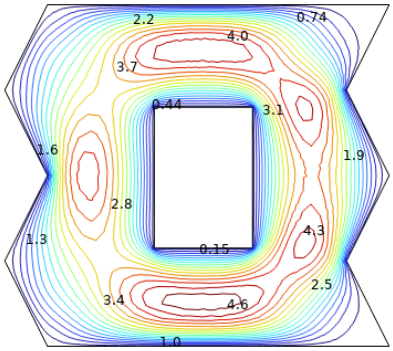	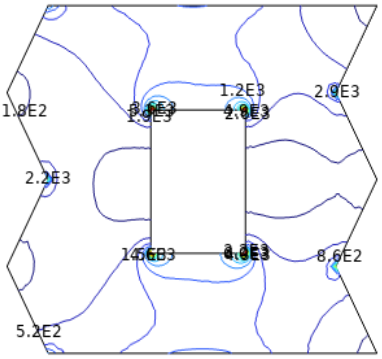
Circular	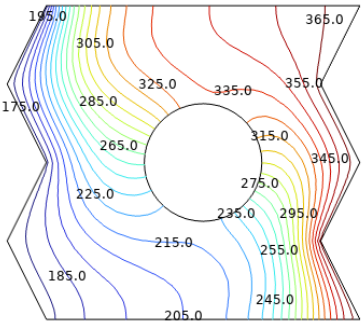	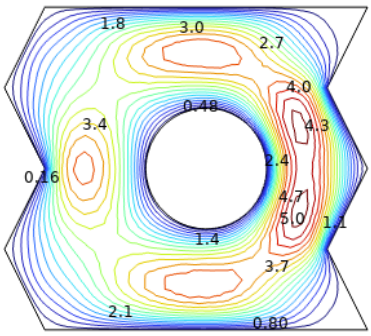	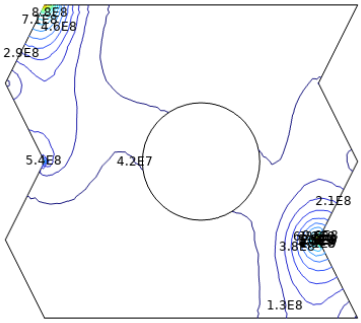

Diamond

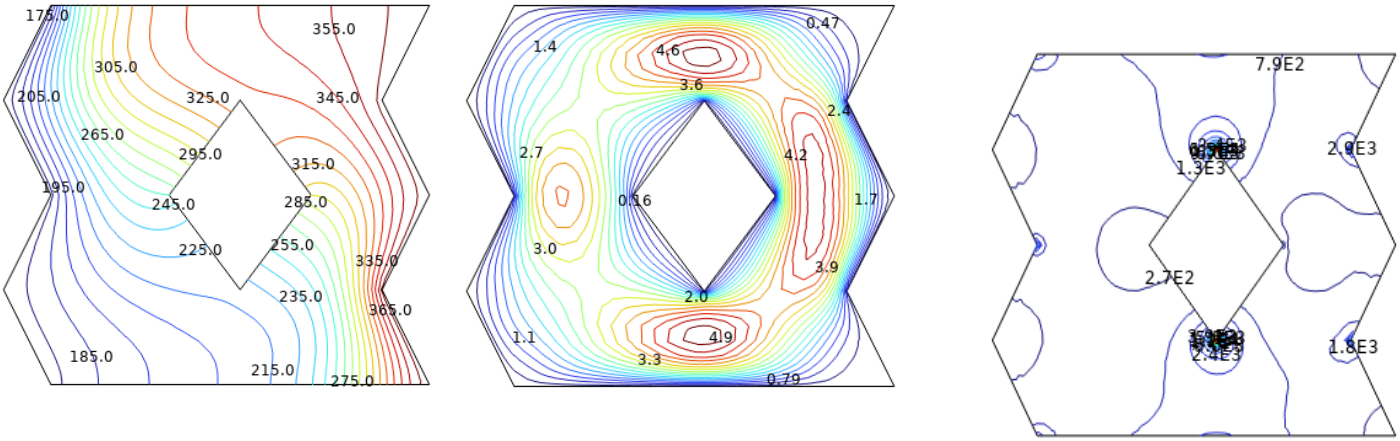

Figure (Ⅳ.23): Streamlines, isotherms and Entropy evaluated by Different Obstacles for Ra = 10^5, φ = 0.02.

Figure Ⅳ.24 shows that the diamond barrier improves heat transfer efficiency by exhibiting greatest peak Nu average in relation to other cylinders. The diamond's geometric properties and the even area surrounding it make it easier for the hybrid nanofluid to disperse, This can influence convective transfer by amplifying and changing the average Nu number.

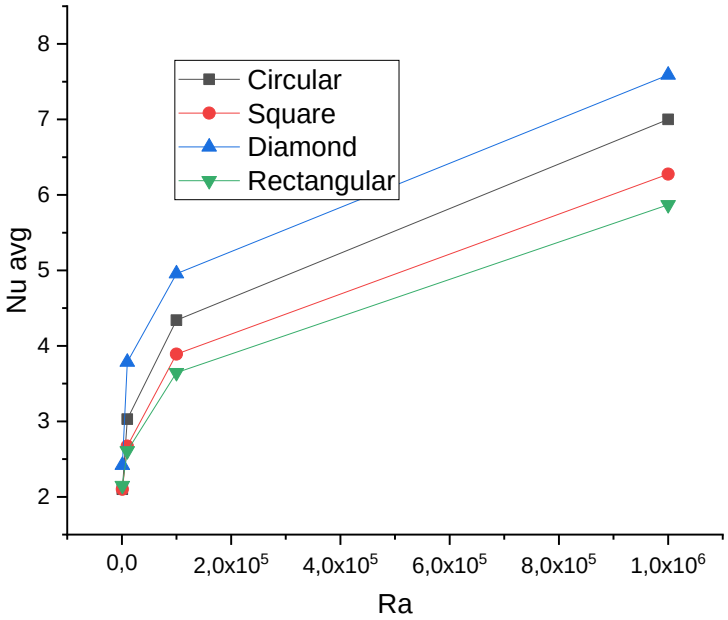

Figure (Ⅳ.24): Average Nusselt values for different Obstacles ; Ra = 10^5, and φ = 0.02.

Ⅳ.4.5.Entropy Generation:

Figure Ⅳ.25 shows how different nanoparticle volume fractions affect the average Nusselt number, or the total entropy generation with Rayleigh number.

The mean generation for all nanoparticle volume fractions rises with Ra. An increase in entropy generation was noted. The best overall entropy generation results were obtained with a bigger nanoparticle volume percentage compared to a smaller one. This is because as concentration rises, viscosity rises as well, causing a greater production of frictional entropy and pressure drop. Variations in the creation of frictional entropy and pressure drop are mostly determined by the contribution of the developing area.

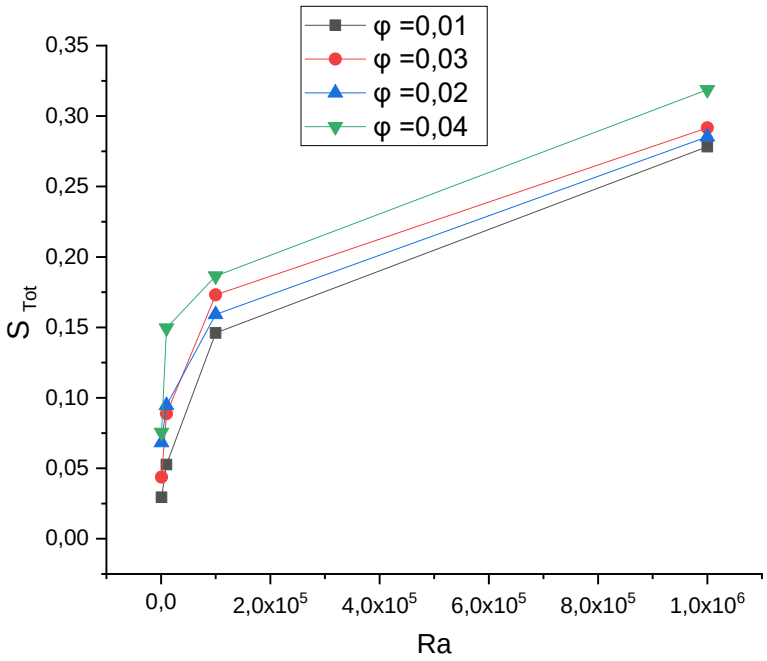

Figure (Ⅳ.25): Variation of the S_{Tot} with the increasing Ra for different φ.

Ⅳ.4. CONFIGURATION 3-D: 3D Shell / Tube Heat Exchanger

In this section, we examine in detail the outcomes of the computational simulations carried out in this work. The results obtained from the numerical simulation of three-dimensional laminar mixed convection in a shell/tube heat exchanger filled with Tri hybrid nanofluid Ag-Fe_3O_4-MWCNT/water have been presented and discussed in more detail. The results were given in terms of streamlines, isotherms and entropy, as well as the average Nusselt number Given the two primary variables, the volume fraction and the Reynolds number, to examine the convective heat transfer in the laminar regime, to study the relationship between the heat transfer efficiency by the volume fraction of the hybrid nanofluid with a value between 0.02 and 0.04 and the heat transfer efficiency by Reynolds number change in the range 10 and 100, and to evaluate the presence of nanoparticles in heat exchangers and study their efficiency.

Ⅳ.4. 1.Mesh test :

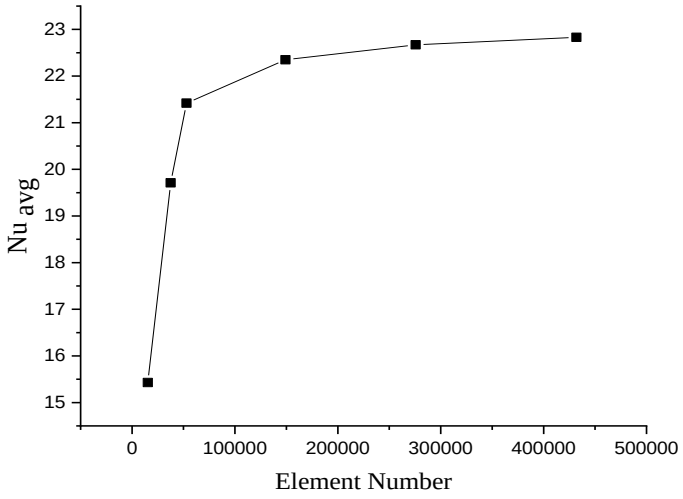

Figure (Ⅳ.26): variation in average Nu number as a function of element number

Mesh	Element Number	Average Nusselt Number
Extra coarse	15349	15,43
Coarser	37491	19,71
Coarse	52983	21,42

Normal	149074	22,349
Fine	275631	22,67
Finer	431892	22,83

Table (Ⅳ.4): Mesh comparison

Ⅳ.4. 2. The impact of the volume fraction of nanofluid:

The use of a tri hybrid nanofluid Ag-Fe_3O_4-MWCNT/water in a heat exchanger was considered in order to examine the impact of tri hybrid nanofluid on flux natural convection and heat transfer. Numerous studies have discussed the effect of additional nanoparticles in detail, and almost all have concluded that a high the concentration of nanoparticles increases the host's heat conductivity [168-172].

The simulation of three-dimensional flux and heat transfer of nanofluids occurs within the range of 10 to 100 Reynolds numbers, while the volume fractions of nanoparticles, denoted as φ, range from 2% to 4%.

The mean number of Nu appears to rise with the volume fraction at Re = 100 (Figure Ⅳ.27), when natural convection predominates. The presence of nanoparticles, both Ag, Fe_3O_4 and MWCNT, increases with increasing concentrations of tri hybrid nanofluide. These nanoparticles have better thermo-physical properties than the classic fluids, as shown in Table III.2, especially their thermal conductivity. Noteworthy is the fact that these characteristics raise the surface area of the nanoparticles and enhance the thermal conductivity of the tri hybrid nanofluid. As a result, Nu average is correlated with the volume fraction and presence of tri hybrid nanofluid, demonstrating the relationship between the volume fraction and the mean number of Nusselt in the heat exchanger for a range of values. We can observe that the values of as the volume fraction increases, so does the average Nusselt number. It’s also increases with the increase of the particles we note that when adding Fe_3O_4 and MWCNT to nanofluid Ag /water.

By providing the solid particle concentration and aspect ratio in a tri hybrid nanofluid, one can ascertain the fluid's physical characteristics and the unique scale of the channel.

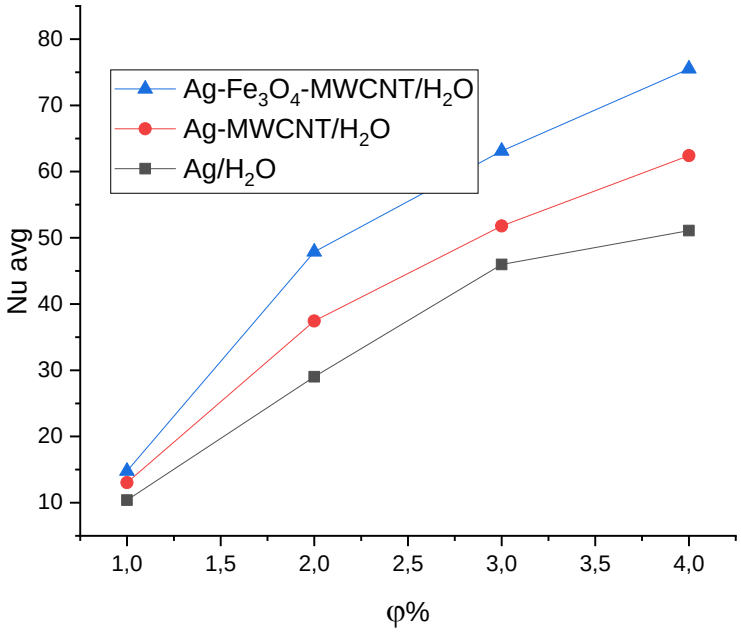

Figure (Ⅳ.27): Variation of the average Nusselt number as a function of volume fraction φ (%); Re = 100

Figure Ⅳ.28 illustrates how heat transfer properties, isotherms, and current lines are affected by the tri hybrid concentration of nanoparticules. With a small shift in the value of the observed flux function, it is demonstrated that increasing there is no effect from the volume proportion of nanoparticles. On the streamlines and isotherms. Increasing the volume fraction results in improved heat transfer qualities, however, it also raises the formation of entropy, which lowers the rate of heat transmission and decrements flow function values. The goal of the presence of nanofluid is to promote convection, but as their concentration rises, so does the development of entropy. As a result, when raising φ, balance needs to be considered.

Isotherm Streamline Entropy

φ=1 %

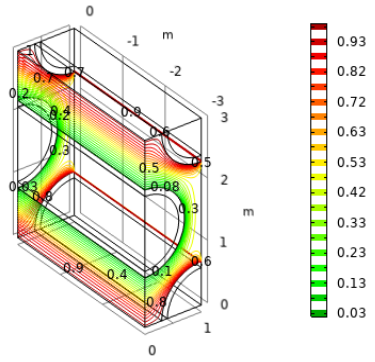

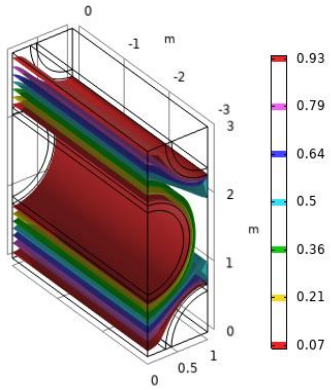

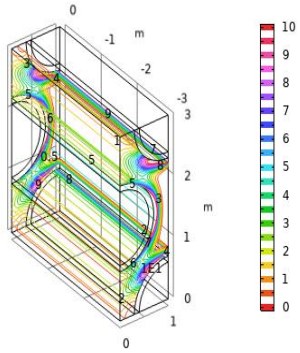

φ=2 %

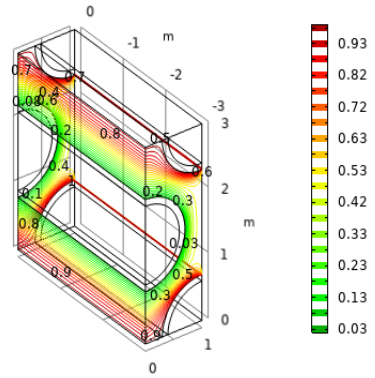

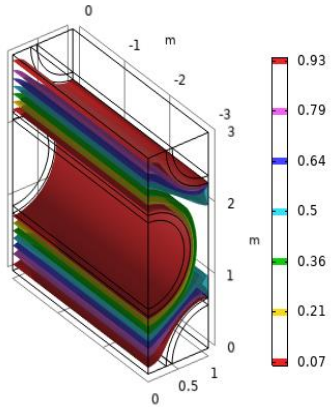

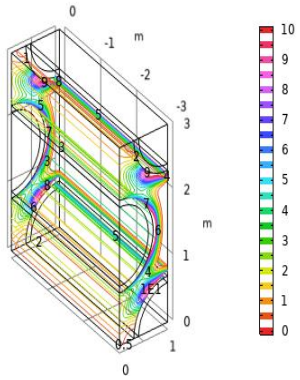

φ=3 %

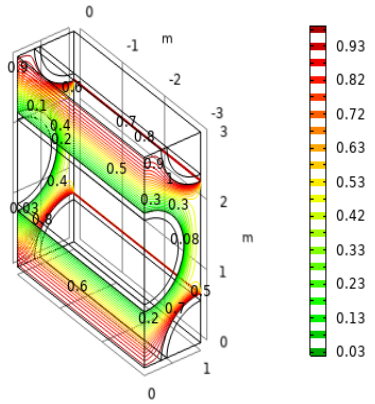

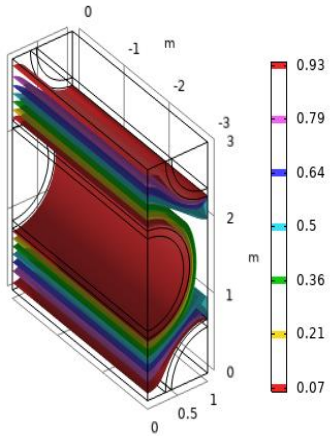

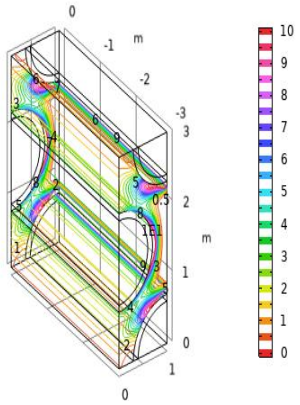

φ=4 %

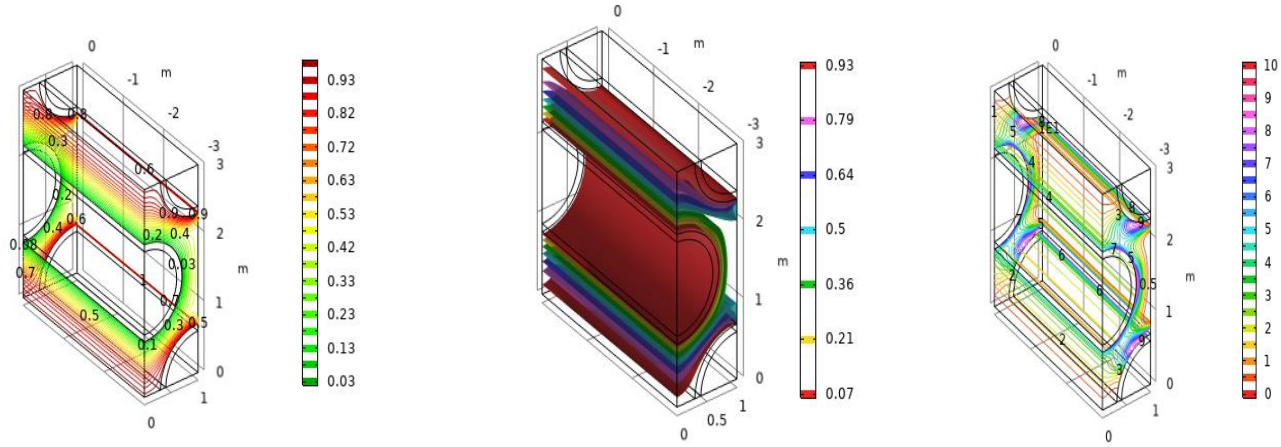

Figure (Ⅳ.28): Three-dimensional surface plot to show the effect of volume fraction on Isotherms and Streamline and Entropy.

Ⅳ.4. 3. Reynolds number effect:

We studied the effects of Reynolds number on streamlines, isotherms and entropy production. The results of this review are presented in Figure Ⅳ.31. In such structures, the flow force inside the cavity occurs due to the thermal push brought on by the shell/tube heat exchanger's temperature gradient between the inlet and output walls.

For 2% of the tri hybrid nanofluid, Figure Ⅳ.29 shows how the number of Re affects the current lines. The findings show that the flow functions grow linearly as Re increases. Figure Ⅳ.29 illustrates how the vortices around the cylinder get bigger and stronger as the number of Re increases. This greatly increases the ability to take advantage of free convection, which quickens and increases flow velocity. Consequently, buoyancy forces are able to mount the tri hybrid nanofluid and concentrate the flow as a result of the tri hybrid nanofluid heating and becoming less dense. Heat transfer is consequently a trend in Reynolds number since a higher number indicates better heat transport.

Figure Ⅳ.29 illustrates the flow behavior and thermal aspects in the schematic chamber for the Reynolds number (Re) across the current lines and isotherms (T) of the tri hybrid nanofluid Ag-Fe_3O_4-MWCNT/water, respectively. The new shape on the father side for

higher Re values was aided by the flows for lower flows starting to travel closer to the entrance and deeper into the chamber. Within the chamber, isotherms replicate the temperature. The heat concentration is most noticeable at the bottom, where it is heated from below, and it diminishes as it rises vertically to an outlet. The isotherm acts as a perfect duplicate of the thermal stresses inside the chamber. The image shows how the vortices are created in the hollow and how they congregate in the left corner as Re increases. As the Reynolds number rises, the heat transfer increases along the channel's whole length, although, as the figures illustrate, the increase is greater for the channel's area than for the cavity.

When heated from below, heat builds up at the bottom and releases as it rises to an outlet. The isotherms were blown towards the edge due to Reynolds number affects as the flow goes through the entrance for the higher Re values. The rate of heat transfer by the number of Nusselt (Nu) in Figure Ⅳ.33 was used to quantify the number of Nusselt tracked for Re and Ri. For larger concentrations of Re and Ri, the Ag-Fe_3O_4-MWCNT/water tri hybrid nanofluid enhanced heat transmission efficiency results in increased flow and convection rate, respectively.

The effects of Reynolds number (Re), fractional volume (φ), and Richardson number (Ri) on the rate of heat transfer are displayed in Figure Ⅳ.30 and Figure Ⅳ.31 of the document. The tri hybrid nanofluid Ag-Fe_3O_4-MWCNT/water thermal transfer efficiency increased with particle fraction; however, with higher Reynolds numbers (Re), the heat transfer rate is subject to variation based on the Richardson number (Ri). The Reynolds number, which shows how the flow rate improves as Re increases, has a major impact on improving heat transmission.

Isotherm Streamline Entropy

Re=10

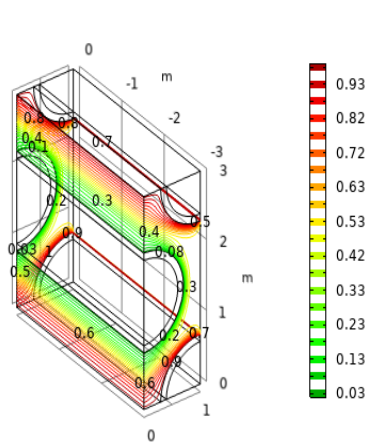
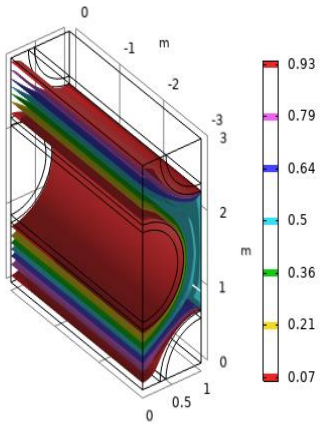
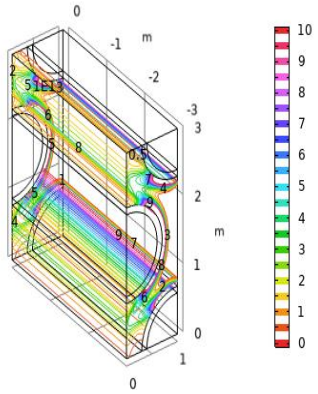

Re=50

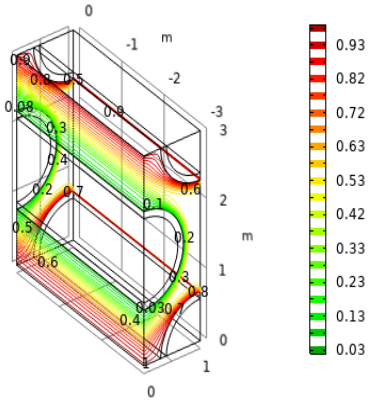
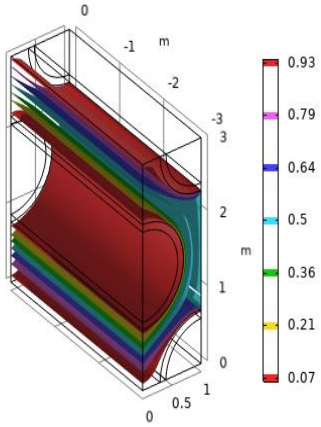
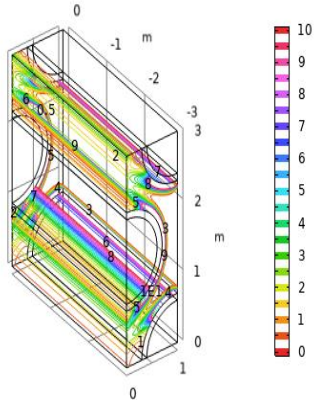

Re=70

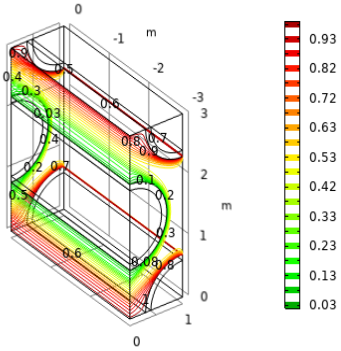
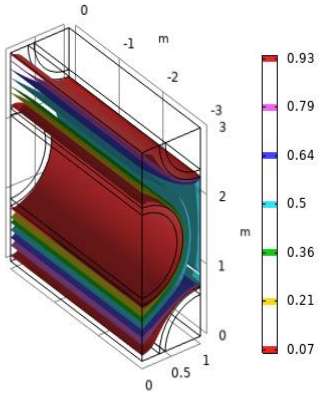
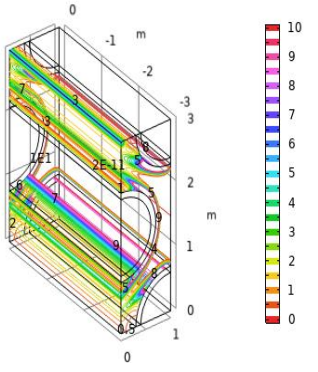

Re=100

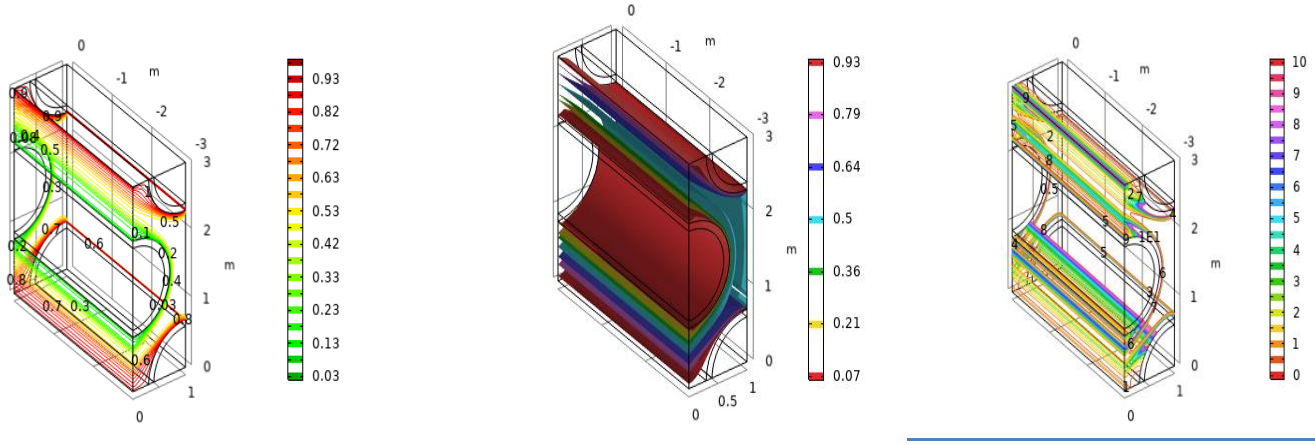

Figure (Ⅳ.29): Three-dimensional surface plot to show the effect of Reynolds number on Isotherms and Streamline and Entropy.

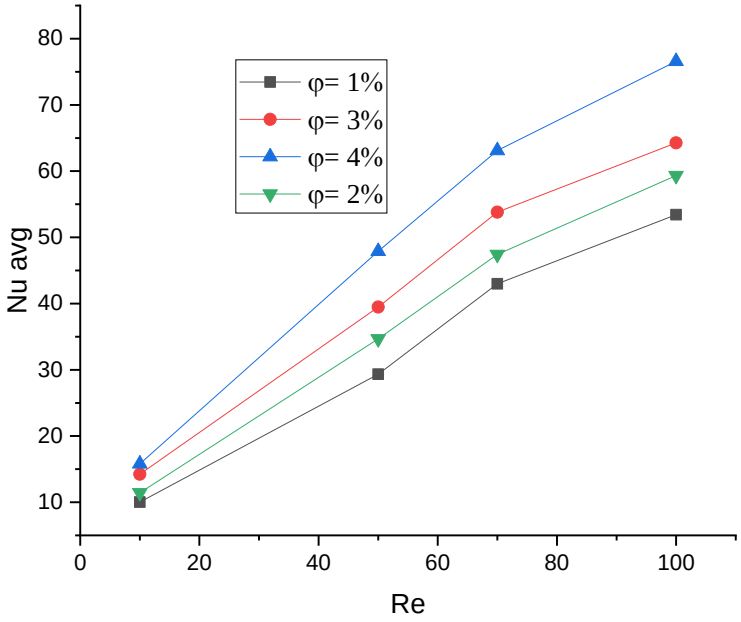

Figure (Ⅳ.30): Variation of average Nusselt number versus Reynolds Re number with different volume fraction (Tri Hybrid Nanofluid $Ag - Fe_3O_4 - MWCNT/water$)

Ⅳ.4. 4. The effect of Richardson's number:

Figure (Ⅳ.31) and Figure (Ⅳ.32) represent variation of Nusselt average on function of Richardson number with different Renolds number , We noticed that as the Richardson number increases , Nusselt average increases.

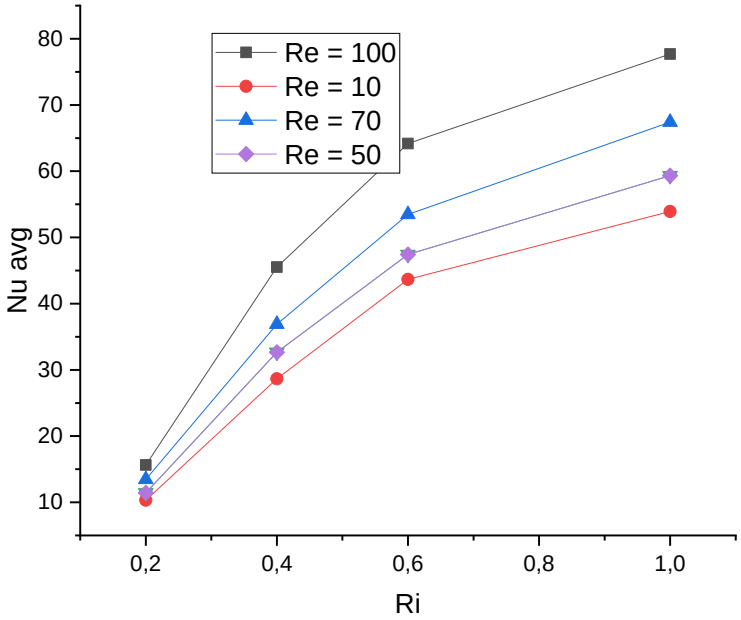

Figure (Ⅳ.31): Variation of the average Nusselt number as a function of volume fraction Richardson number Ri with different Reynolds number (Tri Hybrid Nanofluid $Ag - Fe_3O_4 - MWCNT/water$) φ = 2%

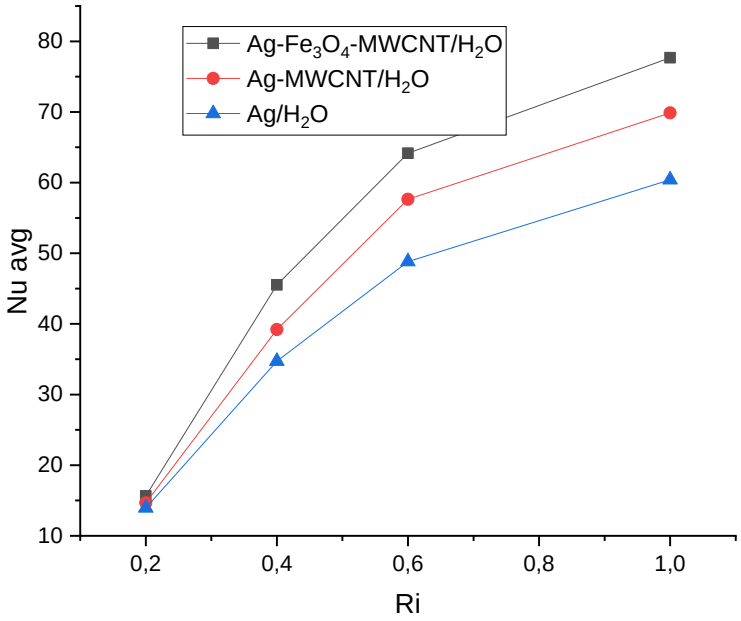

Figure (Ⅳ.32): Variation of the Nusselt number as a function of Richardson number Ri with different nanofluids φ = 2%

Removal aim this endeavour is to examine the convective mixed facets of Ag-Fe_3O_4-MWCNT/water tri hybrid nanofluid. The Richardson number (Ri) plays a vital part in the manipulation of the convection characteristics of the flux. Isothermal curves and variations (T) for the Richardson number (Ri) have been shown in Figure Ⅳ.32, the currents in the chamber reach two contours, one dominating the other to propagate wider and narrowing the outer contour, This could be due to crucial changes in buoyancy across (Ri) in the tri hybrid nanofluid Ag-Fe_3O_4-MWCNT/water. These coiled flows tend to sweep the chamber temperature which is evident through the spiral isotherms at the furthest end of the chamber. Initially, for lower Ri values, the isotherms were raised vertically towards the outlet.

Isotherm Streamline Entropy

Ri=0.2

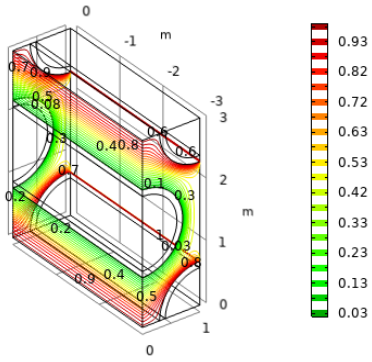
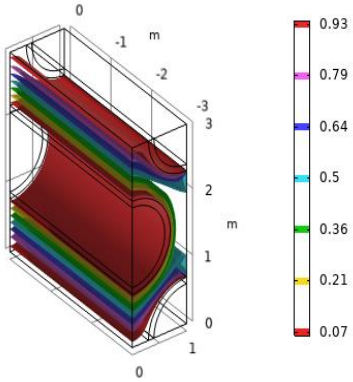
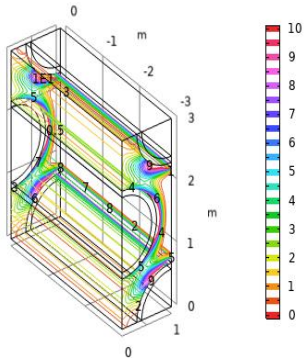

Ri=0.4

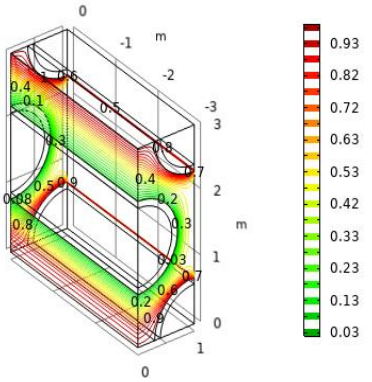
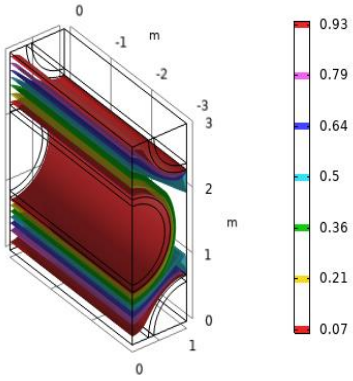
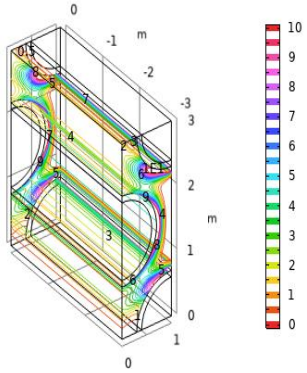

Ri=0.6

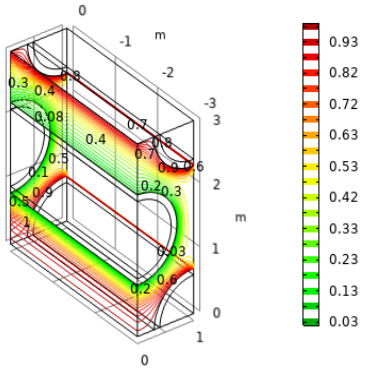
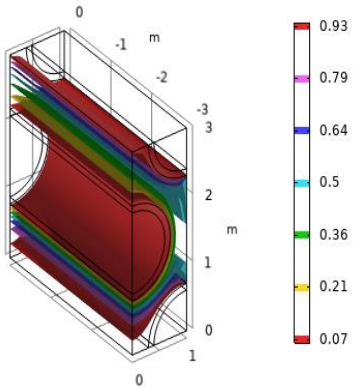
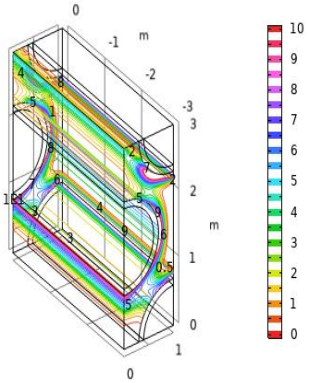

Ri=1

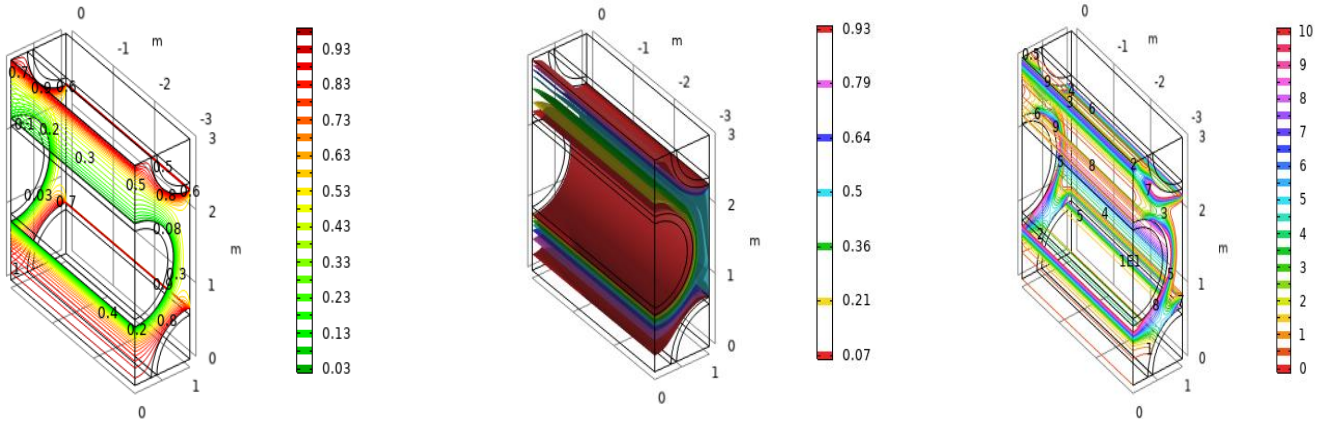

Figure (Ⅳ.33): Three-dimensional surface plot to show the effect of Richardson number on Isothermal and Streamline and Entropy.

Ⅳ.4. 5. The entropy effect:

Figure Ⅳ.34 represents Entropy variation S as a function of heat exchanger efficiency $\mathcal{E}_p$ (Tri Hybrid Nanofluid Ag-Fe_3O_4-MWCNT/water) Re =100, φ = 0.02.

It is noted that with the increase in heat exchanger efficiency $\mathcal{E}_p$ entropy decreases, and Figure Ⅳ.28 shows that the Entropy is produced in proportion to an increase in their concentration. As a result, when raising φ, balance needs to be taken into account.

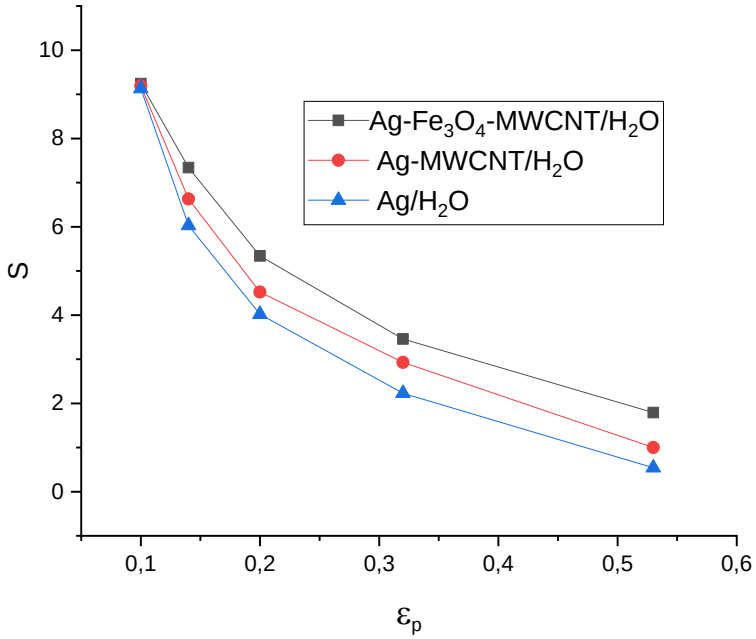

Figure (Ⅳ.34): S entropy variation as a function of heat exchanger efficiency $\mathcal{E}_p$ (Tri Hybrid Nanofluid $Ag - Fe_3O_4 - MWCNT/water$) Re =100, φ = 0.02.

Ⅳ.5. Conclusion:

In this chapter, a 2-D and 3-D numerical study of heat transfer by forced and natural convection of a heat exchanger filled with different hybrid nanofluid (Ag,Cu, Fe_3O_4, MgO, Al_2O_3, MWCNT, and SWCNT) base fluid waterwith different volume fractions was performed $0.01 \leq \varphi \leq .0.04$ A thorough analysis was performed in which the equations of mass, motion, energy conservation, and entropy generation were solved using the COMSOL Multiphysics calculation code.

The effects of Reynolds number, The effects of Rayleigh number, The effects of Richardson number, volume fraction of nanoparticles and nanofluid type on fluid flow, thermal performance and entropy generation are studied in detail. The results lead to the following conclusions:

- We notice that the heat transfer rate increases with the increase of the solid volume fraction of the nanoparticles and the increase of the Reynolds number.
- Entropy generation increases with increasing Reynolds number and decreases with increasing values of the volume fraction of the nanofluids
- The nano fluide volume fraction increases the mean Nusselt number and increases the overall rate of entropy generation.
- Increased tube radius promotes increased heat transfer

GENERAL CONCLUSION

GENERAL CONCLUSION

The present thesis work consists of a numerical characterization of the dynamic and thermal flow by natural, forced convection of a nanofluid immersed in a shell/tube heat exchanger. The numerical simulation is implemented using the COMSOL Multiphysics finite element code.

To compute the flow and temperature fields, the Nusselt number, and the entropy production, a COMSOL Multiphysics algorithm has been built. In-depth research is done on the effects of Rayleigh and Reynolds numbers, the nanofluid type and volume percentage, the various tube radius effects, the average Nusselt number, and entropy generation.

In the first part, we studied the turbulent flow of nanofluid hybrid water- (Al_2O_3/MWCNT) in a 2D shell/tube heat exchanger. The results of the numerical simulation allowed us to make several observations on the effects of the presence of nanoparticles in the base fluid. The main results are summarized as follows:

- ✓ As fluid velocity increases, so does the heat transmission (function of Re).
- ✓ As the concentration of nanoparticles increases, so does the heat transfer. At a particle concentration of 2%, the heat transfer enhancement increases to 103.07% in comparison to the circular tubes.
- ✓ When it comes to heat transfer, the diamond-shaped tube outperforms all other tube shapes.
- ✓ Out of all the shapes, the diamond tube shape shows the greatest decreases in entropy, which enhances heat exchanger performance.

In the second part, we studied the turbulent flow of different hybrid nanofluids (Cu, Fe_3O_4, and MWCNT) - water in 2D shell/tube heat exchanger flow. The results of the numerical simulation allowed us to make several observations on the effects of the presence of nanoparticles in the base fluid. The main results are summarized as follows:

- ✓ Convective thermal energy is increasing with the rise Re, φ higher Reynolds number values improve fluid flow, temperature distribution, and heat transfer and minimize the contribution of heat transfer to total entropy production.

GENERAL CONCLUSION

- ✓ Heat transport is facilitated by an increase in volume fraction φ, but entropy production is also increased by an increase in their concentration. As a result, when raising φ, balance needs to be taken into account.
- ✓ The increase of nanoparticles promotes an increase in heat transfer; Cu-Fe_3O_4-MWCNT/water is the best nanofluid.
- ✓ An increased tube radius promotes increased heat transfer.

In the third part, we studied the laminaire flow of hybrid nanofluid (MgO/SWCNT)-water in a 2D zigzag cavity. The results of the numerical simulation allowed us to make several observations on the effects of the presence of nanoparticles in the base fluid. The main results are summarized as follows:

- ✓ Nanofluid flow circulation intensity increases with amplitude or number of ripples.
- ✓ In convection modulation, the Rayleigh number and the volume percentage of nanoparticles are important parameters.
- ✓ Using diamond obstacles can increase thermal transmission.
- ✓ The nanofluid volume fraction increases the mean Nusselt number and increases the overall rate of entropy generation.

In the fourth part, we studied the laminaire flow of hybrid nanofluid (Ag-Fe_3O_4- MWCNT / water) in 3D shell/tube heat exchanger. The results of the numerical simulation allowed us to make several observations on the effects of the presence of nanoparticles in the base fluid. The main results are summarized as follows:

- ✓ Convective thermal energy is enhanced with rising Re, Ri, and φ.
- ✓ It has been observed that whenever a high volume of nanoparticle fractions is associated with a high Reynolds number, maximum improvements in heat transfer occur.
- ✓ Higher Reynolds number values improve fluid flow, temperature distribution, and heat transfer and minimize the contribution of heat transfer to total entropy production.
- ✓ The increase in volume fraction φ promotes an increase in heat transfer, however the increase in their concentration also boosts entropy production. As a result, when raising φ, balance needs to be taken into account.

BIBLIOGRAPHIC REFERENCES

REFERENCES

[1] Bontemps, A. ; Garrigue, A. ; Goubier, C. ; Huetz, J. ; Marvillet, C. ; Mercier, P. ; Vidil,R. 1994.Echangeursde Chaleur.In *Définitions et Architecture Générale.France: Techniques de l'Ingénieur, Traité Génie Energétique*. p.B2340.Available online: https://www.techniques-ingenieur.fr/base-documentaire/archives-th12/archives-thermique-industrielle-tiabec/archive-1/echangeurs-de-chaleur-b2340/architecture-generale-de-l-echangeur-b2340niv10002.html(accessed on 15 May 2023).

[2] Finkbeiner, F. ; Gonard, T. ; Filiol, B. 1993.*Echangeurs Thermiques : Enjeux, Marchés, Technologie et Politique d'Innovation* ; Editions Eu-ropéennes Thermique et Industrie (EETI) : Paris, France.

[3] Labbadlia, O., Laribi, B., Chetti, B., & Hendrick, P. (2017). Numerical study of the influence of tube arrangement on the flow distribution in the header of shell and tube heat exchangers. *Applied Thermal Engineering*, *126*, 315–321. https://doi.org/10.1016/j.applthermaleng.2017.07.184

[4] He, Z.; Fang, X.; Zhang, Z.; Gao,X.Numerical investigation on performance comparison of non-Newtonian fluid flow invertical heat exchangers combined helical baffle with elliptic and circular tubes. *Appl.Therm.Eng.*2016,*100*,84–97.

[5] Qiu, Y., Li, M., Wang, W., Du, B., & Wang, K. (2018). An experimental study on the heat transfer performance of a prototype molten-salt rod baffle heat exchanger for concentrated solar power. *Energy*, *156*, 63–72. https://doi.org/10.1016/j.energy.2018.05.040

[6] Yang, J., Zeng, M., & Wang, Q. (2014). Numerical investigation on shell-side performances of combined parallel and serial two shell-pass shell-and-tube heat exchangers with continuous helical baffles. *Applied Energy*, *139*, 163–174. https://doi.org/10.1016/j.apenergy.2014.11.029

[7] Zeyons, O. (2008, September 25). *Etudes des interactions physicochimiques et biologiques entre des nanoparticules manufacturées et des bactéries de l'environnement.* https://hal.archives-ouvertes.fr/tel-00331931/

[8] Bang, I. C., & Chang, S. H. (2005). Boiling heat transfer performance and phenomena of Al2O3–water nano-fluids from a plain surface in a pool. *International Journal of Heat and Mass Transfer/International Journal of Heat and Mass Transfer*, *48*(12), 2407–2419. https://doi.org/10.1016/j.ijheatmasstransfer.2004.12.047

[9] Buzea, C., Pacheco, I. I., & Robbie, K. (2007). Nanomaterials and nanoparticles: Sources and toxicity. *Biointerphases*, *2*(4), MR17–MR71. https://doi.org/10.1116/1.2815690

REFERENCES

[10] Ostiguy C., Roberge B., Woods C. Brigitte, Soucy B., 2010. Les nanoparticules de synthèse : Connaissances actuelles sur les risques et les mesures de prévention en SST 2e édition. *Rapport R-646*.

[11] Witharana, S., Palabiyik, I., Musina, Z., & Ding, Y. (2013). Stability of glycol nanofluids The theory and experiment. *Powder Technology*, *239*, 72–77. https://doi.org/10.1016/j.powtec.2013.01.039

[12] Jailani, S., Franks, G. V., & Healy, T. W. (2008). Z Potential of Nanoparticle Suspensions : Effect of Electrolyte Concentration, Particle Size, and Volume Fraction. *Journal of the American Ceramic Society*, *91*(4), 1141–1147. https://doi.org/10.1111/j.1551-2916.2008.02277.x

[13] Eastman, J. A., Choi, S. U. S., Li, S., Yu, W., & Thompson, L. J. (2001). Anomalously increased effective thermal conductivities of ethylene glycol-based nanofluids containing copper nanoparticles. *Applied Physics Letters*, *78*(6), 718–720. https://doi.org/10.1063/1.1341218

[14] Zhu, H. Zhang, C. Liu S. and Tang, Y. Effects of nanoparticle clustering and alignment on thermal conductivities of aqueous nanofluids. *Appl. Phys*. Lett. 89, 023123, 2006.

[15] Liu, M. S. Lin, M. C. C. Tsai, C. Y and Wang, C. C. Enhancement of thermal conductivity with cu for nanofluids using chemical reduction method. *Int. J. Heat Mass Transf*. 49, 3028-3033, 2006.

[16] Phuoc, T. X., Soong, Y., & Chyu, M. K. (2007). Synthesis of Ag-deionized water nanofluids using multi-beam laser ablation in liquids. *Optics and Lasers in Engineering*, *45*(12), 1099–1106. https://doi.org/10.1016/j.optlaseng.2007.06.005

[17] Kwak, K., & Kim, C. (2005). viscosity and thermal conductivity of copper oxide nanofluid dispersed in ethylene glycol. *17*(2), 35–40. https://www.koreascience.or.kr:443/article/JAKO200504703989169.pdf

[18] Wei, X., & Wang, L. (2010). Synthesis and thermal conductivity of microfluidic copper nanofluids. *Particuology*, *8*(3), 262–271. https://doi.org/10.1016/j.partic.2010.03.001

[19] Zhu, H. T., Zhang, C. Y., Tang, Y. M., & Wang, J. X. (2007). Novel Synthesis and Thermal Conductivity of CuO Nanofluid. *Journal of Physical Chemistry. C./Journal of Physical Chemistry. C*, *111*(4), 1646–1650. https://doi.org/10.1021/jp065926t

[20] Chen, Y., & Wang, X. (2008). Novel phase-transfer preparation of monodisperse silver and gold nanoparticles at room temperature. *Materials Letters*, *62*(15), 2215–2218. https://doi.org/10.1016/j.matlet.2007.11.050

[21] Feng, X., Ma, H., Huang, S., Pan, W., Zhang, X., Tian, F., Gao, C., Cheng, Y., & Luo, J. (2006). Aqueous−Organic Phase-Transfer of Highly Stable Gold, Silver, and Platinum Nanoparticles and New Route for Fabrication of Gold Nanofilms at the Oil/Water

REFERENCES

Interface and on Solid Supports. ˜the œJournal of Physical Chemistry. B, *110*(25), 12311–12317. https://doi.org/10.1021/jp0609885

[22] Yu, W., Xie, H., Chen, L., & Li, Y. (2010). Enhancement of thermal conductivity of kerosene-based Fe3O4 nanofluids prepared via phase-transfer method. *Colloids and Surfaces. A, Physicochemical and Engineering Aspects*, *355*(1–3), 109–113. https://doi.org/10.1016/j.colsurfa.2009.11.044

[23] Wang, L., & Fan, J. (2010). Nanofluids Research: Key Issues. *Nanoscale Research Letters*, *5*(8), 1241–1252. https://doi.org/10.1007/s11671-010-9638-6

[24] Chopkar, M., Das, P. K., & Manna, I. (2006). Synthesis and characterization of nanofluid for advanced heat transfer applications. *Scripta Materialia*, *55*(6), 549–552. https://doi.org/10.1016/j.scriptamat.2006.05.030

[25] Wong, K. V., & De Leon, O. (2010). Applications of Nanofluids: Current and Future. *Advances in Mechanical Engineering/Advances in Mechanical Engineering*, *2*, 519659. https://doi.org/10.1155/2010/519659

[26] Prasad, A. R. Singh, S. Nagar, H. A review on Nanofluids:Properties and applications, International journal of advanced research and innovative ideas in Education, Vol-3, no. 3,pp.70-76, 2017

[27] Choi, S. U. S. and Eastman, J. A. Enhancing Thermal Conductivity of Fluids with Nanoparticles. ASME International Mechanical Engineering Congress & Exposition, pages 99–106, 1995.

[28] Jana, S., Salehi-Khojin, A., & Zhong, W. H. (2007). Enhancement of fluid thermal conductivity by the addition of single and hybrid nano-additives. *Thermochimica Acta*, *462*(1–2), 45–55. https://doi.org/10.1016/j.tca.2007.06.009

[29] Otanicar, T. P., Phelan, P. E., Prasher, R. S., Rosengarten, G., & Taylor, R. A. (2010). Nanofluid-based direct absorption solar collector. *Journal of Renewable and Sustainable Energy*, *2*(3). https://doi.org/10.1063/1.3429737

[30] Yu, W., France, D. M., Routbort, J. L., & Choi, S. U. S. (2008). Review and Comparison of Nanofluid Thermal Conductivity and Heat Transfer Enhancements. *Heat Transfer Engineering*, *29*(5), 432–460. https://doi.org/10.1080/01457630701850851

[31] Ayub, Z. H., Yang, D., Khan, T. S., Al-Hajri, E., & Ayub, A. H. (2018). Performance characteristics of a novel shell and tube heat exchanger with shell side interstitial twisted tapes for viscous fluids application. *Applied Thermal Engineering*, *134*, 248–255. https://doi.org/10.1016/j.applthermaleng.2018.01.054

[32] Biswas, N.; Manna, N.K.; Chamkha, A.J.; Mandal, D.K. Effect of surface waviness on MHD thermo-gravitational convection of Cu−Al_2O_3−water hybrid nanofluid in a porous oblique enclosure. *Phys. Scr.* 2021,*96*,105002.

REFERENCES

[33] Mandal, D. K., Biswas, N., Manna, N. K., Gorla, R. S. R., & Chamkha, A. J. (2022). Hybrid nanofluid magnetohydrodynamic mixed convection in a novel W-shaped porous system. *International Journal of Numerical Methods for Heat &Amp Fluid Flow*, *33*(2), 510–544. https://doi.org/10.1108/hff-03-2022-0163

[34] Horvat, A., Leskovar, M., & Mavko, B. (2005). Comparison of heat transfer conditions in tube bundle cross-flow for different tube shapes. *International Journal of Heat and Mass Transfer*, *49*(5–6), 1027–1038. https://doi.org/10.1016/j.ijheatmasstransfer.2005.09.030

[35] Mebarek-Oudina, F.; Preeti; Sabu, A.S.; Vaidya, H.; Lewis, R.W.; Areekara, S.; Mathew, A.; Ismail, A.I. Hydromagnetic flow of magnetite-water nano-fluid utilizing adapted Buongiorno model. *Int. J.Mod. Phys. B*2023, *2450003*.

[36] Fazelpour, F., Ansarirad, P., Vafaeipour, M., & Rahbari, O. (2013). CFD simulation of hydrodynamics of gas-solid two-phase flow for different geometries of solid particles. *In Proceedings of the 5th International Congress on Energy and Environment Engineering and Management, Lisbon, Portugal.*

[37] Skoglund, T., Årzén, K., & Dejmek, P. (2006). Dynamic object-oriented heat exchanger models for simulation of fluid property transitions. *International Journal of Heat and Mass Transfer*, *49*(13–14), 2291–2303. https://doi.org/10.1016/j.ijheatmasstransfer.2005.12.005

[38] Raza, J., Mebarek-Oudina, F., & Lund, L. A. (2022). The flow of magnetised convective Casson liquid via a porous channel with shrinking and stationary walls. *Pramana*, *96*(4). https://doi.org/10.1007/s12043-022-02465-1

[39] Zaversky, F., Sánchez, M., & Astrain, D. (2013). Object-oriented modeling for the transient response simulation of multi-pass shell-and-tube heat exchangers as applied in active indirect thermal energy storage systems for concentrated solar power. *Energy*, *65*, 647–664. https://doi.org/10.1016/j.energy.2013.11.070

[40] Shahdad, I., & Fazelpour, F. (2018). Numerical analysis of the surface and geometry of plate fin heat exchangers for increasing heat transfer rate. *International Journal of Energy and Environmental Engineering*, *9*(2), 155–167. https://doi.org/10.1007/s40095-018-0270-z

[41] Xie, S., Liang, Z., Zhang, L., & Wang, Y. (2018). A numerical study on heat transfer enhancement and flow structure in enhanced tube with cross ellipsoidal dimples.

International Journal of Heat and Mass Transfer, *125*, 434–444. https://doi.org/10.1016/j.ijheatmasstransfer.2018.04.106

[42] Matos, R., Laursen, T., Vargas, J., & Bejan, A. (2004). Three-dimensional optimization of staggered finned circular and elliptic tubes in forced convection. *International Journal of Thermal Sciences*, *43*(5), 477–487. https://doi.org/10.1016/j.ijthermalsci.2003.10.003

[43] Matos, R., Vargas, J., Laursen, T., & Saboya, F. (2001). Optimization study and heat transfer comparison of staggered circular and elliptic tubes in forced convection. *International Journal of Heat and Mass Transfer*, *44*(20), 3953–3961. https://doi.org/10.1016/s0017-9310(01)00006-0

[44] Nouri-Borujerdi, A., & Lavasani, A. (2007). Experimental study of forced convection heat transfer from a cam shaped tube in cross flows. *International Journal of Heat and Mass Transfer*, *50*(13–14), 2605–2611. https://doi.org/10.1016/j.ijheatmasstransfer.2006.11.028

[45] Nouri-Borujerdi, A., & Lavasani, A. M. (2008). Pressure loss and heat transfer characterization of a Cam-Shaped cylinder at different orientations. *Journal of Heat Transfer*, *130*(12). https://doi.org/10.1115/1.2969259

[46] Mohanty, R. L., Swain, A., & Das, M. K. (2018). Thermal performance of mixed tube bundle composed of circular and elliptical tubes. *Thermal Science and Engineering Progress*, *5*, 492–505. https://doi.org/10.1016/j.tsep.2018.02.009

[47] Dharmaiah, G.; Mebarek-Oudina, F.; Balamurugan, K.S.; Vedavathi, N. Numerical Analysis of the Magnetic Dipole Effect on a Radiative Ferro magnetic Liquid Flowing over a Porous Stretched Sheet. *Fluid Dyn. Mater. Process*. 2023.

[48] Li, B., Feng, B., He, Y., & Tao, W. (2006). Experimental study on friction factor and numerical simulation on flow and heat transfer in an alternating elliptical axis tube. *Applied Thermal Engineering*, *26*(17–18), 2336–2344. https://doi.org/10.1016/j.applthermaleng.2006.03.001

[49] Bouris,D.;Papadakis,G.;Bergeles,G.Numerical evaluation of alternate tube configurations for particle deposition rate reduction in heat exchanger tube bundles. Int. J. Heat Fluid Flow 2001, 22, 525–536.

[50] Moawed, M. (2010). Experimental study of forced convection from helical coiled tubes with different parameters. *Energy Conversion and Management*, *52*(2), 1150–1156. https://doi.org/10.1016/j.enconman.2010.09.009

REFERENCES

[51] Rosen, M., & Dincer, I. (2003). Exergy methods for assessing and comparing thermal storage systems. *International Journal of Energy Research*, *27*(4), 415–430. https://doi.org/10.1002/er.885

[52] Khan, M.G.; Fartaj, A.; Ting, D.S.-K. An experimental characterization of cross-flow cooling of air via an in-line elliptical tube array. Int. J. Heat Fluid Flow 2004, 25, 636–648.

[53] Harris, D.K.; Goldschmidt, V.W. Measurements of the overall heat transfer from combustion gases confined within elliptical tube heat exchangers. Exp. Therm. Fluid Sci. 2002, 26, 33–37.

[54] Tao, Y.; He, Y.; Wu, Z.; Tao, W. Three-dimensional numerical study and field synergy principle analysis of wavy fin heat exchangers with elliptic tubes. Int. J. Heat Fluid Flow 2007, 28, 1531–1544.

[55] Li, Z., Davidson, J. H., & Mantell, S. C. (2005). Numerical simulation of flow field and heat transfer of streamlined cylinders in cross flow. *Journal of Heat Transfer*, *128*(6), 564–570. https://doi.org/10.1115/1.2188463

[56] Kumar, N., & Jhinge, P. K. (2014). Effect of segmental baffles at different orientation on the performances of single pass shell and tube heat exchanger. *International Journal of Engineering Trends and Technology*, *15*(9), 423–428. https://doi.org/10.14445/22315381/ijett-v15p281

[57] Raj, K., & Ganne, S. (2011). Shell side numerical analysis of a shell and tube heat exchanger considering the effects of baffle inclination angle on fluid flow using CFD. *Thermal Science*, *16*(4), 1165–1174. https://doi.org/10.2298/tsci110330118r

[58] Zhang, J., He, Y., & Tao, W. (2009). 3D numerical simulation on shell-and-tube heat exchangers with middle-overlapped helical baffles and continuous baffles – Part I: Numerical model and results of whole heat exchanger with middle-overlapped helical baffles. *International Journal of Heat and Mass Transfer*, *52*(23–24), 5371–5380. https://doi.org/10.1016/j.ijheatmasstransfer.2009.07.006

[59] Sivarajan, C.; Rajasekaran, B.; Krishnamohan, N. Comparision of numerical heat transfer in conventional and helically baffled heat exchanger. *IJERA*2012,*2*,1278–1282.

[60] Kwon, Y. H., Kim, D., Li, C. G., Lee, J. K., Hong, D. S., Lee, J. G., Lee, S. H., Cho, Y. H., & Kim, S. H. (2011). Heat transfer and pressure drop characteristics of nanofluids in a plate heat exchanger. *Journal of Nanoscience and Nanotechnology*, *11*(7), 5769–5774. https://doi.org/10.1166/jnn.2011.4399

REFERENCES

[61] Albadr, J., Tayal, S., & Alasadi, M. (2013). Heat transfer through heat exchanger using Al2O3 nanofluid at different concentrations. *Case Studies in Thermal Engineering*, *1*(1), 38–44. https://doi.org/10.1016/j.csite.2013.08.004

[62] Asadi, A.; Asadi, M.; Rezaniakolaei, A.; Rosendahl, L.A.; Afrand, M.; Wongwises, S. Heat transfer efficiency of Al_2O_3- MWCNT/ thermal oil hybrid nanofluid as acooling fluid in thermal and energy management applications:An experimental and theoretical investigation.*Int.J.HeatMassTransf.*2018,*117*,474–486.

[63] Ghazanfari, V., Imani, M., Shadman, M. M., Amini, Y., & Zahakifar, F. (2022). Numerical study on the thermal performance of the shell and tube heat exchanger using twisted tubes and Al2O3 nanoparticles. *Progress in Nuclear Energy*, *155*, 104526. https://doi.org/10.1016/j.pnucene.2022.104526

[64] Multiphysics,C.*Comsol Multiphysics User Guide,Version4.3a*; COMSOL, AB: Stockholm, Sweden, 2012; pp.39–40.

[65] Gourari, S., Mebarek-Oudina, F., Makinde, O. D., & Rabhi, M. (2021). Numerical investigation of Gas-Liquid Two-Phase flows in a cylindrical channel. *Defect and Diffusion Forum/Diffusion and Defect Data, Solid State Data. Part a, Defect and Diffusion Forum*, *409*, 39–48. https://doi.org/10.4028/www.scientific.net/ddf.409.39

[66] Salari, M., Malekshah, E. H., & Malekshah, M. H. (2017). Natural convection in a rectangular enclosure filled by two immiscible fluids of air and Al2O3-water nanofluid heated partially from side walls. *Alexandria Engineering Journal*, *57*(3), 1401–1412. https://doi.org/10.1016/j.aej.2017.07.004

[67] Mebarek-Oudina, F, Redouane, F., & Rajashekhar, C. (2020). Convection Heat Transfer of MgO-Ag /Water Magneto-Hybrid Nanoliquid Flow into a Special Porous Enclosure. *Algerian Journal of Renewable Energy and Sustainable Development*, *2*(2), 84–95. https://doi.org/10.46657/ajresd.2020.2.2.1

[68] Mourad, A., Aissa, A., Mebarek-Oudina, F., Jamshed, W., Ahmed, W., Ali, H. M., & Rashad, A. (2021). Galerkin finite element analysis of thermal aspects of FeO-MWCNT/water hybrid nanofluid filled in wavy enclosure with uniform magnetic field effect. *International Communications in Heat and Mass Transfer*, *126*, 105461. https://doi.org/10.1016/j.icheatmasstransfer.2021.105461

[69] Mebarek-Oudina, F., Hussein, A. K., Younis, O., Rostami, S., & Nikbakhti, R. (2021). Natural Convection Enhancement in the Annuli Between Two Homocentric Cylinders by Using Ethylene Glycol / Water Based Titania Nanofluid. *Journal of Advanced Research in Fluid Mechanics and Thermal Sciences*, *80*(2), 56–73. https://doi.org/10.37934/arfmts.80.2.5673

REFERENCES

[70] Swain, K., Mebarek-Oudina, F., & Abo-Dahab, S. M. (2021). Influence of MWCNT/Fe3O4 hybrid nanoparticles on an exponentially porous shrinking sheet with chemical reaction and slip boundary conditions. *Journal of Thermal Analysis and Calorimetry*, *147*(2), 1561–1570. https://doi.org/10.1007/s10973-020-10432-4

[71] Mebarek-Oudina, F. (2018b). Convective heat transfer of Titania nanofluids of different base fluids in cylindrical annulus with discrete heat source. *Heat Transfer—Asian Research*, *48*(1), 135–147. https://doi.org/10.1002/htj.21375

[72] Abu-Libdeh, N., Redouane, F., Aissa, A., Mebarek-Oudina, F., Almuhtady, A., Jamshed, W., & Al-Kouz, W. (2021). Hydrothermal and Entropy Investigation of Ag/MgO/H2O Hybrid Nanofluid Natural Convection in a Novel Shape of Porous Cavity. *Applied Sciences*, *11*(4), 1722. https://doi.org/10.3390/app11041722

[73] Mebarek-Oudina, F., Fares, R., Aissa, A., Lewis, R., & H. Abu-Hamdeh, N. (2021). Entropy and convection effect on magnetized hybrid nano-liquid flow inside a trapezoidal cavity with zigzagged wall. *International Communications in Heat and Mass Transfer*, *125*, 105279. https://doi.org/10.1016/j.icheatmasstransfer.2021.105279

[74] Marzougui, S., Mebarek-Oudina, F., Magherbi, M., & Mchirgui, A. (2021). Entropy generation and heat transport of Cu–water nanoliquid in porous lid-driven cavity through magnetic field. *International Journal of Numerical Methods for Heat & Fluid Flow*, *32*(6), 2047–2069. https://doi.org/10.1108/hff-04-2021-0288

[75] Mebarek-Oudina, F., & Bessaïh, R. (2019). Numerical simulation of natural convection heat transfer of copper-water nanofluid in a vertical cylindrical annulus with heat sources. *Thermophysics and Aeromechanics*, *26*(3), 325–334. https://doi.org/10.1134/s0869864319030028

[76] Zaydan, M., Riahi, M., Mebarek-Oudina, F., & Sehaqui, R. (2021). Mixed Convection in a Two-Sided Lid-Driven Square Cavity Filled with Different Types of Nanoparticles: A Comparative Study Assuming Nanoparticles with Different Shapes. *Fluid Dynamics & Materials Processing*, *17*(4), 789–819. https://doi.org/10.32604/fdmp.2021.015422

[77] Raza, J., Mebarek-Oudina, F., & Chamkha, A. (2019). Magnetohydrodynamic flow of molybdenum disulfide nanofluid in a channel with shape effects. *Multidiscipline Modeling in Materials and Structures*, *15*(4), 737–757. https://doi.org/10.1108/mmms-07-2018-0133

[78] Mourad, A., Aissa, A., Mebarek-Oudina, F., Al-Kouz, W., & Sahnoun, M. (2021). Natural convection of nanoliquid from elliptic cylinder in wavy enclosure under the effect of uniform magnetic field: numerical investigation. *The European Physical Journal Plus*, *136*(4). https://doi.org/10.1140/epjp/s13360-021-01432-w

[79] Pushpa, B. V., Sankar, M., & Mebarek-Oudina, F. (2021). Buoyant Convective Flow and Heat Dissipation of Cu–H2O Nanoliquids in an Annulus Through a Thin Baffle. *Journal of Nanofluids*, *10*(2), 292–304. https://doi.org/10.1166/jon.2021.1782

REFERENCES

[80] Alomari, M. A., Hassan, A. M., Alajmi, A., Salho, A. K., Sadeq, A. M., Alqurashi, F., & Flayyih, M. A. (2025b). Analysis of Double-Diffusive transport and entropy generation in a wavy cylindrical enclosure with inner heated core: Effects of MHD and radiation on Casson CU─H2O nanofluid. *Energy Science & Engineering*. https://doi.org/10.1002/ese3.70069

[81] Bouchoucha, A. M., Mebarek-Oudina, F., Azizi, M. W., & Sankar, M. (2023b). Natural Convection and Entropy Generation in a Nanofluid Filled Cavity with a Hanged Fin and Heated from the Bottom. *Journal of Nanofluids*, *12*(8), 2370–2380. https://doi.org/10.1166/jon.2023.2106

[82] Mebarek-Oudina, F., Bouselsal, M., Djebali, R., Vaidya, H., Biswas, N., & Ramesh, K. (2025b). Thermal performance of MgO-SWCNT/water hybrid nanofluids in a zigzag walled cavity with differently shaped obstacles. *Modern Physics Letters B*. https://doi.org/10.1142/s0217984925501635

[83] Rashidi, M. M., Sadri, M., & Sheremet, M. A. (2021). Numerical Simulation of Hybrid Nanofluid Mixed Convection in a Lid-Driven Square Cavity with Magnetic Field Using High-Order Compact Scheme. *Nanomaterials*, *11*(9), 2250. https://doi.org/10.3390/nano11092250

[84] Asogwa, K. K., Mebarek-Oudina, F., & Animasaun, I. L. (2022). Comparative Investigation of Water-Based Al2O3 Nanoparticles Through Water-Based CuO Nanoparticles Over an Exponentially Accelerated Radiative Riga Plate Surface via Heat Transport. *Arabian Journal for Science and Engineering*, *47*(7), 8721–8738. https://doi.org/10.1007/s13369-021-06355-3

[85] Said, B. O., Mebarek-Oudina, F., & Medebber, M. A. (2024). Magneto-Hydro-Convective nanofluid flow in porous square enclosure. *Frontiers in Heat and Mass Transfer*, *0*(0), 1–10. https://doi.org/10.32604/fhmt.2024.054164

[86] Hussam, W. K., Khanafer, K., Salem, H. J., & Sheard, G. J. (2019). Natural convection heat transfer utilizing nanofluid in a cavity with a periodic side-wall temperature in the presence of a magnetic field. *International Communications in Heat and Mass Transfer*, *104*, 127–135. https://doi.org/10.1016/j.icheatmasstransfer.2019.02.018

[87] Alhashash, A., & Saleh, H. (2021). Impact of Surface Undulation on Flow and Heat Transfer Characteristics in an Enclosure Filled with Nanoencapsulated Phase Change Materials (NEPCMs). *Mathematical Problems in Engineering*, *2021*, 1–13. https://doi.org/10.1155/2021/8899995

[88] Asmadi,M.S., Kasmani, R. M., Siri, Z., Saleh, H., & Ghani, N. C. (2023). Buoyancy-driven heat transfer performance, vorticity and fluid flow analysis of hybrid nanofluid within a U-shaped lid with heated corrugated wall. *Alexandria Engineering Journal*, *71*, 21–38. https://doi.org/10.1016/j.aej.2023.03.029

[89] Fares, R., Mebarek-Oudina, F., Aissa, A., Bilal, S. M., & Öztop, H. F. (2021). Optimal entropy generation in Darcy-Forchheimer magnetized flow in a square enclosure filled

with silver based water nanoliquid. *Journal of Thermal Analysis and Calorimetry*, *147*(2), 1571–1581. https://doi.org/10.1007/s10973-020-10518-z

[90] Hazarika, S., AHMED, S., & CHAMKHA, A. J. (2021). Analysis of Platelet Shape Al2O3 and TiO2 on Heat Generative Hydromagnetic Nanofluids for the Base Fluid C2H6O2 in a Vertical Channel of Porous Medium. *Walailak Journal of Science and Technology (WJST)*, *18*(14). https://doi.org/10.48048/wjst.2021.21424

[91] Afridi, M. I., Alkanhal, T. A., Qasim, M., & Tlili, I. (2019). Entropy Generation in Cu-Al2O3-H2O Hybrid Nanofluid Flow over a Curved Surface with Thermal Dissipation. *Entropy*, *21*(10), 941. https://doi.org/10.3390/e21100941

[92] Shah, Z., Saeed, A., Khan, I., M. Selim, M., Ikramullah, & Kumam, P. (2021). Numerical modeling on hybrid nanofluid (Fe3O4+MWCNT/H2O) migration considering MHD effect over a porous cylinder. *PLOS ONE*, *16*(7), e0251744. https://doi.org/10.1371/journal.pone.0251744

[93] Abu Bakar, S., Md Arifin, N., Bachok, N., & Md Ali, F. (2021). Effect of thermal radiation and MHD on hybrid Ag–TiO2/H2O nanofluid past a permeable porous medium with heat generation. *Case Studies in Thermal Engineering*, *28*, 101681. https://doi.org/10.1016/j.csite.2021.101681

[94] Wahid, N. S., Md Arifin, N., Khashi'ie, N. S., Pop, I., Bachok, N., & Hafidzuddin, M. E. H. (2022). MHD mixed convection flow of a hybrid nanofluid past a permeable vertical flat plate with thermal radiation effect. *Alexandria Engineering Journal*, *61*(4), 3323–3333. https://doi.org/10.1016/j.aej.2021.08.059

[95] Wahid, N. S, Norihan Md Arifin, Najiyah Safwa Khashi'ie, Rusya Iryanti Yahaya, Ioan Pop, Norfifah Bachok, & Mohd Ezad Hafidz Hafidzuddin. (2021). Three-Dimensional Radiative Flow of Hybrid Nanofluid Past a Shrinking Plate with Suction. *Journal of Advanced Research in Fluid Mechanics and Thermal Sciences*, *85*(1), 54–70. https://doi.org/10.37934/arfmts.85.1.5470

[96] Khashi'ie, N. S., Md Arifin, N., Pop, I., Nazar, R., Hafidzuddin, E. H., & Wahi, N. (2020). Thermal Marangoni Flow Past a Permeable Stretching/Shrinking Sheet in a Hybrid Cu-Al2O3/Water Nanofluid. *Sains Malaysiana*, *49*(1), 211–222. https://doi.org/10.17576/jsm-2020-4901-25

[97] Mourad, A., Abderrahmane, A., Younis, O., Marzouki, R., & Alazzam, A. (2022b). Numerical Simulations of Magnetohydrodynamics Natural Convection and Entropy Production in a Porous Annulus Bounded by Wavy Cylinder and Koch Snowflake Loaded with Cu–Water Nanofluid. *Micromachines*, *13*(2), 182. https://doi.org/10.3390/mi13020182

[98] Gul, T., Nasir, S., Berrouk, A. S., Raizah, Z., Alghamdi, W., Ali, I., & Bariq, A. (2023). Simulation of the water-based hybrid nanofluids flow through a porous cavity for the applications of the heat transfer. *Scientific Reports*, *13*(1). https://doi.org/10.1038/s41598-023-33650-w

REFERENCES

[99] Saeed, A., Jawad, M., Alghamdi, W., Nasir, S., Gul, T., & Kumam, P. (2021). Hybrid nanofluid flow through a spinning Darcy–Forchheimer porous space with thermal radiation. *Scientific Reports*, *11*(1). https://doi.org/10.1038/s41598-021-95989-2

[100] Ahmadian, A., Bilal, M., Khan, M. A., & Asjad, M. I. (2020). Numerical analysis of thermal conductive hybrid nanofluid flow over the surface of a wavy spinning disk. *Scientific Reports*, *10*(1). https://doi.org/10.1038/s41598-020-75905-w

[101] Alrabaiah, H., Bilal, M., Khan, M. A., Muhammad, T., & Legas, E. Y. (2022). Parametric estimation of gyrotactic microorganism hybrid nanofluid flow between the conical gap of spinning disk-cone apparatus. *Scientific Reports*, *12*(1). https://doi.org/10.1038/s41598-021-03077-2

[102] Dinarvand, S., Rostami, M. N., & Pop, I. (2019). A novel hybridity model for TiO2-CuO/water hybrid nanofluid flow over a static/moving wedge or corner. *Scientific Reports*, *9*(1). https://doi.org/10.1038/s41598-019-52720-6

[103] Gul, T., Khan, A., Bilal, M., Alreshidi, N. A., Mukhtar, S., Shah, Z., & Kumam, P. (2020). Magnetic Dipole Impact on the Hybrid Nanofluid Flow over an Extending Surface. *Scientific Reports*, *10*(1). https://doi.org/10.1038/s41598-020-65298-1

[104] Tlili, I., Nabwey, H. A., Samrat, S. P., & Sandeep, N. (2020). 3D MHD nonlinear radiative flow of CuO-MgO/methanol hybrid nanofluid beyond an irregular dimension surface with slip effect. *Scientific Reports*, *10*(1). https://doi.org/10.1038/s41598-020-66102-w

[105] Waini, I., Ishak, A., & Pop, I. (2020). Hybrid nanofluid flow towards a stagnation point on a stretching/shrinking cylinder. *Scientific Reports*, *10*(1). https://doi.org/10.1038/s41598-020-66126-2

[106] Abid, N., Ramzan, M., Chung, J. D., Kadry, S., & Chu, Y. M. (2020). Comparative analysis of magnetized partially ionized copper, copper oxide–water and kerosene oil nanofluid flow with Cattaneo–Christov heat flux. *Scientific Reports*, *10*(1). https://doi.org/10.1038/s41598-020-74865-5

[107] Ramzan, M., Shahmir, N., Ghazwani, H. a. S., Nisar, K. S., Alharbi, F. M., & Yahia, I. S. (2022). Hydrodynamic and heat transfer analysis of dissimilar shaped nanoparticles-based hybrid nanofluids in a rotating frame with convective boundary condition. *Scientific Reports*, *12*(1). https://doi.org/10.1038/s41598-021-04173-z

[108] Jawad, M., Saeed, A., Tassaddiq, A., Khan, A., Gul, T., Kumam, P., & Shah, Z. (2021). Insight into the dynamics of second grade hybrid radiative nanofluid flow within the boundary layer subject to Lorentz force. *Scientific Reports*, *11*(1). https://doi.org/10.1038/s41598-021-84144-6

[109] Bilal, M., Arshad, H., Ramzan, M., Shah, Z., & Kumam, P. (2021). Unsteady hybrid-nanofluid flow comprising ferrousoxide and CNTs through porous horizontal channel with dilating/squeezing walls. *Scientific Reports*, *11*(1). https://doi.org/10.1038/s41598-021-91188-1

REFERENCES

[110] Saeed, A., Alsubie, A., Kumam, P., Nasir, S., Gul, T., & Kumam, W. (2021). Blood based hybrid nanofluid flow together with electromagnetic field and couple stresses. *Scientific Reports*, *11*(1). https://doi.org/10.1038/s41598-021-92186-z

[111] Jamshed, W., Prakash, M., Devi, S. S. U., Ibrahim, R. W., Shahzad, F., Nisar, K. S., Eid, M. R., Abdel-Aty, A., Khashan, M. M., & Yahia, I. S. (2023). Retraction Note: A brief comparative examination of tangent hyperbolic hybrid nanofluid through a extending surface: numerical Keller–Box scheme. *Scientific Reports*, *13*(1). https://doi.org/10.1038/s41598-023-33083-5

[112] Riaz, A., Bobescu, E., Ramesh, K., & Ellahi, R. (2021). Entropy Analysis for Cilia-Generated Motion of Cu-Blood Flow of Nanofluid in an Annulus. *Symmetry*, *13*(12), 2358. https://doi.org/10.3390/sym13122358

[113] Albqmi, N. M., & Sivanandam, S. (2024). Entropy Generation and Thermal Radiation Impact on Magneto-Convective Flow of Heat-Generating Hybrid Nano-Liquid in a Non-Darcy Porous Medium with Non-Uniform Heat Flux. *Computation*, *12*(3), 43. https://doi.org/10.3390/computation12030043

[114] Alhashash, A. (2023). Free Convection Heat Transfer in Composite Enclosures with Porous and Nanofluid Layers. *Advances in Mathematical Physics*, *2023*, 1–16. https://doi.org/10.1155/2023/2088607

[115] Barik, D., Chandran, S. S. R., Dennison, M. S., Raj, T. G. A., & Roy, K. E. R. (2023). Investigation on Fluid Flow Heat Transfer and Frictional Properties of Al2O3 Nanofluids Used in Shell and Tube Heat Exchanger. *International Journal of Photoenergy*, *2023*, 1–12. https://doi.org/10.1155/2023/6838533

[116] Kadhim, H. T., Al-Manea, A., Al-Shamani, A. N., & Yusaf, T. (2022). Numerical analysis of hybrid nanofluid natural convection in a wavy walled porous enclosure: Local thermal non-equilibrium model. *International Journal of Thermofluids*, *15*, 100190. https://doi.org/10.1016/j.ijft.2022.100190

[117] Alsabery, A. I., Ismael, M. A., Chamkha, A. J., & Hashim, I. (2020). Impact of finite wavy wall thickness on entropy generation and natural convection of nanofluid in cavity partially filled with non-Darcy porous layer. *Neural Computing and Applications*, *32*(17), 13679–13699. https://doi.org/10.1007/s00521-020-04776-z

[118] Maneengam, A., Bouzennada, T., Abderrahmane, A., Ghachem, K., Kolsi, L., Younis, O., Guedri, K., & Weera, W. (2022). Numerical Study of 3D MHD Mixed Convection and Entropy Generation in Trapezoidal Porous Enclosure Filled with a Hybrid Nanofluid: Effect of Zigzag Wall and Spinning Inner Cylinder. *Nanomaterials*, *12*(12), 1974. https://doi.org/10.3390/nano12121974

[119] Gumir, F. J., Al-Farhany, K., Jamshed, W., Tag El Din, E. S. M., & Abd-Elmonem, A. (2022). Natural convection in a porous cavity filled (35%MWCNT-65% Fe3O4)/water hybrid nanofluid with a solid wavy wall via Galerkin finite-element process. *Scientific Reports*, *12*(1). https://doi.org/10.1038/s41598-022-22782-0

REFERENCES

[120] Barman, P., Rao, P. S., & Chowdhury, S. (2023). Numerical Computation of Natural Convection of Nanofluid in an Open Wavy Porous Cavity Heated Partially. *Journal of Nanofluids*, *12*(7), 1773–1781. https://doi.org/10.1166/jon.2023.2050

[121] Khan, Z. H., Khan, W. A., Qasim, M., Alharbi, S. O., Hamid, M., & Du, M. (2022). Hybrid nanofluid flow around a triangular-shaped obstacle inside a split lid-driven trapezoidal cavity. *The European Physical Journal Special Topics*, *231*(13–14), 2749–2759. https://doi.org/10.1140/epjs/s11734-022-00607-5

[122] Muhamad Hasif Mohd Hashim, N Md Arifin, Ahmad Nazri Mohamad Som, Nazihah Mohamed Ali, Aniza Ab Ghani, & Safaa Jawad Ali. (2023). Natural Convection in Trapezoidal Cavity containing Hybrid Nanofluid. *Journal of Advanced Research in Micro and Nano Engieering*, *13*(1), 18–30. https://doi.org/10.37934/armne.13.1.1830

[123] Ferhi, M., Djebali, R., Mebarek-Oudina, F., Abu-Hamdeh, N. H., & Abboudi, S. (2022). Magnetohydrodynamic Free Convection Through Entropy Generation Scrutiny of Eco-Friendly Nanoliquid in a Divided L-Shaped Heat Exchanger with Lattice Boltzmann Method Simulation. *Journal of Nanofluids*, *11*(1), 99–112. https://doi.org/10.1166/jon.2022.1819

[124] Aneja, M., & Sharma, S. (2022). Analysis of Heat Transfer Characteristics of a Al2O3 - SiO2/Water Hybrid Nanofluid in a Localized Heated Porous Cavity. *Arabian Journal for Science and Engineering*, *48*(1), 967–983. https://doi.org/10.1007/s13369-022-07257-8

[125] Ahlawat, A., Chaudhary, S., Sharma, M. K., Loganathan, K., Pattanaik, B., & Balaram, A. (2024). Entropy optimization of lid-driven micropolar hybrid nanofluid flow in a partially porous hexagonal-shaped cavity with relevance to energy efficient storage processes. *Scientific Reports*, *14*(1). https://doi.org/10.1038/s41598-024-60483-y

[126] Islam, T., Alam, M. N., Niazai, S., Khan, I., Fayz-Al-Asad, M., & Alqahtani, S. (2023). Heat generation/absorption effect on natural convective heat transfer in a wavy triangular cavity filled with nanofluid. *Scientific Reports*, *13*(1). https://doi.org/10.1038/s41598-023-48704-2

[127] Kadhim, H. T., Al-Manea, A., Al-Shamani, A. N., & Yusaf, T. (2022b). Numerical analysis of hybrid nanofluid natural convection in a wavy walled porous enclosure: Local thermal non-equilibrium model. *International Journal of Thermofluids*, *15*, 100190. https://doi.org/10.1016/j.ijft.2022.100190

[128] Alsabery, A. I., Ismael, M. A., Chamkha, A. J., & Hashim, I. (2020b). Impact of finite wavy wall thickness on entropy generation and natural convection of nanofluid in cavity partially filled with non-Darcy porous layer. *Neural Computing and Applications*, *32*(17), 13679–13699. https://doi.org/10.1007/s00521-020-04776-z

[129] Islam, S., Siddiki, M. N. a. A., & Islam, M. S. (2024). Numerical Simulation and Sensitivity Analysis Using RSM on Natural Convective Heat Exchanger Containing

Hybrid Nanofluids. *Mathematical Problems in Engineering*, *2024*, 1–15. https://doi.org/10.1155/2024/2834556

[130] Ali, F., Loganathan, K., Eswaramoorthi, S., Prabu, K., Zaib, A., & Chaudhary, D. K. (2022). Heat Transfer Analysis on Carboxymethyl Cellulose Water-Based Cross Hybrid Nanofluid Flow with Entropy Generation. *Journal of Nanomaterials*, *2022*(1). https://doi.org/10.1155/2022/5252918

[131] Tayebi, T., & Chamkha, A. J. (2020). Effects of various configurations of an inserted corrugated conductive cylinder on MHD natural convection in a hybrid nanofluid-filled square domain. *Journal of Thermal Analysis and Calorimetry*, *143*(2), 1399–1411. https://doi.org/10.1007/s10973-020-10206-y

[132] Soleimani, A., Sattari, A., & Hanafizadeh, P. (2020). Thermal analysis of a microchannel heat sink cooled by two-phase flow boiling of Al2O3 HFE-7100 nanofluid. *Thermal Science and Engineering Progress*, *20*, 100693. https://doi.org/10.1016/j.tsep.2020.100693

[133] Islam, Z., Azad, A., Hasan, M. J., Hossain, R., & Rahman, M. (2022). Unsteady periodic natural convection in a triangular enclosure heated sinusoidally from the bottom using CNT-water nanofluid. *Results in Engineering*, *14*, 100376. https://doi.org/10.1016/j.rineng.2022.100376

[134] Hamida, M. B. B., & Hatami, M. (2021). Optimization of fins arrangements for the square light emitting diode (LED) cooling through nanofluid-filled microchannel. *Scientific Reports*, *11*(1). https://doi.org/10.1038/s41598-021-91945-2

[135] Ishak, M. S., Alsabery, A. I., Hashim, I., & Chamkha, A. J. (2021). Entropy production and mixed convection within trapezoidal cavity having nanofluids and localised solid cylinder. *Scientific Reports*, *11*(1). https://doi.org/10.1038/s41598-021-94238-w

[136] Hamzah, H. K., Ali, F. H., & Hatami, M. (2022). MHD mixed convection and entropy generation of CNT-water nanofluid in a wavy lid-driven porous enclosure at different boundary conditions. *Scientific Reports*, *12*(1). https://doi.org/10.1038/s41598-022-06957-3

[137] Khan, U., Zaib, A., Abu Bakar, S., & Ishak, A. (2022). Forced convection flow of water conveying AA7072 and AA7075 alloys-nanomaterials on variable thickness object experiencing Dufour and Soret effects. *Scientific Reports*, *12*(1). https://doi.org/10.1038/s41598-022-10901-w

[138] Gal, S., Kolsi, L., Hassen, W., Ben Ali, N., Ben Khedher, N., & Chamkha, A. J. (2022). Three-Dimensional Study of Magnetohydrodynamic Natural Convection, Entropy Generation, and Electromagnetic Variables in a Nanofluid Filled Enclosure Equipped with Inclined Fins. *ACS Omega*, *7*(14), 12365–12373. https://doi.org/10.1021/acsomega.2c00923

[139] Karagiannakis, N. P., Bourantas, G. C., Skouras, E. D., Loukopoulos, V. C., Miller, K., & Burganos, V. N. (2020). Modeling the Natural Convection Flow in a Square Porous

Enclosure Filled with a Micropolar Nanofluid under Magnetohydrodynamic Conditions. *Applied Sciences*, *10*(5), 1633. https://doi.org/10.3390/app10051633

[140] Munawar, S., Saleem, N., Ahmad Khan, W., & Nasir, S. (2021). Mixed Convection of Hybrid Nanofluid in an Inclined Enclosure with a Circular Center Heater under Inclined Magnetic Field. *Coatings*, *11*(5), 506. https://doi.org/10.3390/coatings11050506

[141] Lu, D., Afridi, M. I., Allauddin, U., Farooq, U., & Qasim, M. (2020). Entropy Generation in a Dissipative Nanofluid Flow under the Influence of Magnetic Dissipation and Transpiration. *Energies*, *13*(20), 5506. https://doi.org/10.3390/en13205506

[142] Mukherjee, S., Aljuwayhel, N. F., Bal, S., Mishra, P. C., & Ali, N. (2022). Modelling, Analysis and Entropy Generation Minimization of Al2O3-Ethylene Glycol Nanofluid Convective Flow inside a Tube. *Energies*, *15*(9), 3073. https://doi.org/10.3390/en15093073

[143] Islam, T., Yavuz, M., Parveen, N., & Fayz-Al-Asad, M. (2022). Impact of Non-Uniform Periodic Magnetic Field on Unsteady Natural Convection Flow of Nanofluids in Square Enclosure. *Fractal and Fractional*, *6*(2), 101. https://doi.org/10.3390/fractalfract6020101

[144] Asmadi .M. S, Kasmani .R. Md, Siri1 .Z, Saleh .H. Thermal Enhancement Effects of Buoyancy-Driven Heat Transfer of Hybrid Nanofluid Confined in a Tilted U-Shaped Cavity. (2022). *Journal of Applied Fluid Mechanics*, *15*(2). https://doi.org/10.47176/jafm.15.02.32920

[145] Barhoi, B. L., Borah, R. C., & Singh, S. (2020). Natural Convection in a Nano-Fluid Filled Square Enclosure. *Key Engineering Materials*, *847*, 114–119. https://doi.org/10.4028/www.scientific.net/kem.847.114

[146] Islam, T., Akter, N., & Jahan, N. (2020). MHD Free Convective Heat Transfer in a Triangular Enclosure Filled with Copper-Water Nanofluid. *International Journal of Material and Mathematical Sciences*, 29–38. https://doi.org/10.34104/ijmms.020.029038

[147] Roslan, R., Ali, I. R., Alsabery, A. I., & Bakar, N. (2020). *Mixed Convection in a Lid-Driven Horizontal Rectangular Cavity Filled with Hybrid Nanofluid By Finite Volume Method*. *1*(1), 38–49

[148] Goldanlou, A. S., Badri, M., Heidarshenas, B., Hussein, A. K., Rostami, S., & Shadloo, M. S. (2020). Numerical Investigation on Forced Hybrid Nanofluid Flow and Heat Transfer Inside a Three-Dimensional Annulus Equipped with Hot and Cold Rods: Using Symmetry Simulation. *Symmetry*, *12*(11), 1873. https://doi.org/10.3390/sym12111873

[149] Al-Farhany, K., Al-Muhja, B., Ali, F., Khan, U., Zaib, A., Raizah, Z., & Galal, A. M. (2022). The Baffle Length Effects on the Natural Convection in Nanofluid-Filled

Square Enclosure with Sinusoidal Temperature. *Molecules/Molecules Online/Molecules Annual*, *27*(14), 4445. https://doi.org/10.3390/molecules27144445

[150] Bejan, A. (2013). *Convection Heat Transfer*. https://doi.org/10.1002/9781118671627

[151] Chatri, K. (2003). Etude des phénomènes magnétothermiques dans les dispositifs de Chauffage par induction par la méthode des éléments finis. *Thèse de magister de L'université de Batna.*

[152] Bennecib, N. (2010). Contribution à l'étude d'une machine MHD à conduction en vue de son exploitation sur un réseau électrique, *Thèse de doctorat. Université de Batna.*

[153] Bergoug, N. (2013). Contribution à la modélisation numérique d'une pompe Magnétohydrodynamique (MHD) annulaire à induction, *thèse de doctorat, Université de Batna.*

[154] *Validation of COMSOL Multiphysics® for Magnetohydrodynamics (MHD) Flows in Fusion Applications*. (n.d.). https://www.comsol.fr/paper/validation-of-comsol-multiphysics-for%20magnetohydrodynamics%20%E2%80%93%20mhd%20flows-in-fusion-a-50552.

[155] Waini, I., Ishak, A., & Pop, I. (2019b). Hybrid nanofluid flow and heat transfer over a nonlinear permeable stretching/shrinking surface. *International Journal of Numerical Methods for Heat & Fluid Flow*, *29*(9), 3110–3127. https://doi.org/10.1108/hff-01-2019-0057

[156] Mebarek-Oudina, F., & Chabani, I. (2022b). Review on Nano-Fluids Applications and Heat Transfer Enhancement Techniques in Different Enclosures. *Journal of Nanofluids*, *11*(2), 155–168. https://doi.org/10.1166/jon.2022.1834

[157] Khan, U., Mebarek-Oudina, F., Zaib, A., Ishak, A., Bakar, S. A., Sherif, E. S. M., & Baleanu, D. (2022b). An exact solution of a Casson fluid flow induced by dust particles with hybrid nanofluid over a stretching sheet subject to Lorentz forces. *Waves in Random and Complex Media*, 1–14. https://doi.org/10.1080/17455030.2022.2102689

[158] Mebarek-Oudina, F., & Aissa, A. (2021c). Convective heat transfer of magneto flow of Fe3O4-MWCNT/H2O hybrid nanofluid in a porous space between two concentric cylinders. In *De Gruyter eBooks* (pp. 55–74). https://doi.org/10.1515/9783110696080-003

[159] Mehryan, S., Kashkooli, F. M., Ghalambaz, M., & Chamkha, A. J. (2017c). Free convection of hybrid Al2O3-Cu water nanofluid in a differentially heated porous cavity. *Advanced Powder Technology*, *28*(9), 2295–2305. https://doi.org/10.1016/j.apt.2017.06.011

[160] Bouselsal, M., Mebarek-Oudina, F., Biswas, N., & Ismail, A. a. I. (2023b). Heat Transfer Enhancement Using Al2O3-MWCNT Hybrid-Nanofluid inside a Tube/Shell Heat

Exchanger with Different Tube Shapes. *Micromachines*, *14*(5), 1072. https://doi.org/10.3390/mi14051072

[161] Ma, Y., Mohebbi, R., Rashidi, M., & Yang, Z. (2019b). MHD convective heat transfer of Ag-MgO/water hybrid nanofluid in a channel with active heaters and coolers. *International Journal of Heat and Mass Transfer/International Journal of Heat and Mass Transfer*, *137*, 714–726. https://doi.org/10.1016/j.ijheatmasstransfer.2019.03.169

[162] Mehryan, S., Kashkooli, F. M., Ghalambaz, M., & Chamkha, A. J. (2017d). Free convection of hybrid Al2O3-Cu water nanofluid in a differentially heated porous cavity. *Advanced Powder Technology*, *28*(9), 2295–2305. https://doi.org/10.1016/j.apt.2017.06.011

[163] Yakah, N. (2012). Heat exchanger design for a solar gas-turbine power plant.*Master of Science Thesis, KTH School of Industrial Engineering and Management, Energy Technology EGI-2012-110MSG EKV925, Division of Heat and Power,* SE-100 44 Stockholm.

[164] Rao, S.S. 1988. *The finite element method in engineering*. *Oxford: Pergamon Press*.

[165] Dogonchi, A. S, Nayak, M. K, and N. Karimi, J. (2020). *Therm. Anal. Calorim.*141, 2109

[166] Roy, P.; Mondal, A. Analysis of Shell and Tube heat exchanger design using Comsol Multiphysics. *Int. J. Sci. Appl*. Res. 2016, 3, 70–82.

[167] Mebarek-Oudina, F., & Chabani, I. (2023). Review on Nano Enhanced PCMs: Insight on NEPCM Application in Thermal Management/Storage Systems. *Energies*, *16*(3), 1066. https://doi.org/10.3390/en16031066

[168] Mahian, O.; Kolsi, L.; Amani, M.; Estellé, P.; Ahmadi, G.; Kleinstreuer, C.; Marshall, J.S.; Siavashi, M.; Taylor, R.A.; Niazmand, H. 2018. Recent advances in modeling and simulation of nanofluid flows-Part I: Fundamentals and theory. *Phys. Rep*., 790, 1–48.

[169] Ramasekhar, G., Mebarek-Oudina, F., Suneetha, S., Vaidya, H., & Selvi, P. (2024). Computational simulation of Casson hybrid nanofluid flow with Rosseland approximation and uneven heat source/sink. *International Journal of Thermofluids*, 100893. https://doi.org/10.1016/j.ijft.2024.100893

[170] Mezaache, A., Mebarek-Oudina, F., Vaidya, H., & Fouad, Y. (2024b). Heat transfer analysis of nanofluid flow with entropy generation in a corrugated heat exchanger channel partially filled with porous medium. *Heat Transfer*, *53*(8), 4625–4647. https://doi.org/10.1002/htj.23149

[171] Fayz-Al-Asad, M., Mebarek-Oudina, F., Vaidya, H., Hasan, M. S., Sarker, M. M. A., & Ismail, A. I. (2024b). Finite element Analysis for Magneto-Convection heat transfer

performance in vertical wavy surface enclosure: FIN Size Impact. *Frontiers in Heat and Mass Transfer*, *22*(3), 817–837. https://doi.org/10.32604/fhmt.2024.050814

[172] Mezaache, A., Mebarek-Oudinal, F., Vaidya, H., & Ramesh, K. (2025). Impact of nanofluids and porous structures on the thermal efficiency of wavy channel heat exchanger. *International Journal of Thermal Sciences*, *210*, 109673. https://doi.org/10.1016/j.ijthermalsci.2024.109673